CONTRACT 950137

RANGER TV SUBSYSTEM (BLOCK III) FINAL REPORT

VOLUME 2: SUBSYSTEM ANALYSIS

Prepared For:

JET PROPULSION LABORATORY
CALIFORNIA INSTITUTE OF TECHNOLOGY
PASADENA, CALIFORNIA

By The:

ASTRO-ELECTRONICS DIVISION
DEFENSE ELECTRONIC PRODUCTS
RADIO CORPORATION OF AMERICA
PRINCETON, NEW JERSEY

AED R-2620

Issued: JULY 22, 1965

Preface

This report summarizes the Ranger TV Subsystem program. This work was performed by the Radio Corporation of America, under JPL Contract No. 950137, for the Jet Propulsion Laboratory of the California Institute of Technology, Pasadena, California. The period covered by this, the Final Report on the program, extends from July, 1961 through July, 1965. The report is submitted in five volumes:

Volume 1	Summary
Volume 2	Subsystem Analysis
Volume 3	TV Subsystem Design
Volume 4	Manufacturing, Product Assurance, and Test
Volume 5	Evaluation

This volume, Volume 2, contains

- A description of the mission parameters,
- A development of the TV Subsystem equipment parameters, and
- A description of the TV Subsystem configuration.

Table of Contents

Table of Contents (Continued)

List of Illustrations

List of Illustrations (Continued)

List of Illustrations (Continued)

List of Tables

Section I

Introduction

In order to establish design requirements for space vehicles, manned or unmanned, that are to land and operate on the Moon, it is essential to have detailed information on the composition and topography of the lunar surface. The best Earth-based photographs of the Moon are limited to a resolution of 600 meters, which is not sufficient to evaluate the nature of small-scale surface features.

The Ranger mission was established to fulfill the need for high-resolution pictures of the lunar surface. The possibility of such a mission had been the subject of a joint study by the Jet Propulsion Laboratory (JPL) and RCA. Concepts and equipment designs had been explored since early in 1958. These studies led to the development of a 4.7-pound, half-inch vidicon camera, which was delivered for use in an Explorer lunar flyby mission. Its purpose was to photograph the unseen side of the Moon. Late in 1960, RCA conducted a television camera design study for JPL. This study culminated in a camera design for the Ranger III to V series. Other related space camera studies and designs by RCA were the half-inch vidicon cameras for TIROS and the 1-inch vidicon cameras for Nimbus. A design study, which was directly applicable to the Ranger TV Subsystem, was conducted by RCA for the Surveyor program under contract to North American Aviation Company. These earlier efforts by RCA contributed greatly toward achieving the desired mission goals of the Ranger program within a tight schedule.

Section II of this volume introduces the principal analyses that were performed to arrive at the conceptual design of the Ranger TV Subsystem. The mission goals and constraints, which were the basis for the analyses, are also described. Analyses are presented to describe the fundamental problems of lunar imaging and cislunar communications. The analyses that were made in selecting and evaluating various parameters of the overall TV Subsystem are also included. Some of the analyses are presented in greater mathematical depth than others. This more extensive treatment is given to those analyses that are considered unique and worthy of recording in this Final Report.

The analyses are presented in a logical sequence, beginning with the analysis of the imaging system. The lunar luminances and range of contrasts are developed for various lunar areas that would be viewed from an impacting trajectory. The results of this analysis are used in computing the expected output signal from the camera. The effect of the spectral response of the sensor on camera output is described.

The next topic presented is the analysis of the communications system. The analysis shows the feasibility of retrieving the video data from the cameras at the cislunar distance. The communications constraints are discussed, as well as the analyses that led to the selection of standard frequency-modulation for the communications system. A discussion of preemphasis is included, followed by a discussion of the RF channel and baseband frequency allocation. A link analysis, which gives the expected performance of the communication system, is presented, and the arrangement of the communications components is described.

An analysis of the overall TV Subsystem is the next topic of discussion. The signal-to-noise ratios of the imaging and communications systems are combined to predict the signal-to-noise ratio for the entire Subsystem.

Included is a discussion of automatic versus fixed methods of exposure and gain control. The analysis of the sine-wave response of the system is next presented. This analysis served as the basis for selecting the electrical and optical elements of the system. A parametric analysis of image smear and resolution is included and shows the factors that led to the selection of the lens focal length and the shutter speed.

The development of the vidicon scanning rates is discussed as well as the considerations that led to the selection of the number of cameras and the camera-pointing array. The design of the power supply, thermal control, and the TV Subsystem structure are considered in relation to the overall TV Subsystem configuration.

The third section of this volume is devoted to a description of the TV Subsystem. Included are a description of (1) the Subsystem arrangement; (2) the internal system for controlling and programming of the various operations; and (3) the command and control system, which responds to external commands. This section is concluded with a description of the telemetry system, which monitors the operation of the entire TV Subsystem.

Section II

Subsystem Analysis

A. MISSION GOALS AND CONSTRAINTS

1. Primary Goal

The primary goal of the Ranger TV Subsystem was to obtain high-resolution pictures of the Moon's surface and transmit these pictures back to Earth. Earth-based photography of the lunar surface is limited by atmospheric disturbances to the resolution of objects larger than 2000 feet, but more detailed knowledge of the lunar surface is necessary for the design of lunar-landing vehicles. To achieve the primary goal, the following design objectives were established for the TV Subsystem:

- Capability to provide pictures with a resolution of 0.5 meter per optical line pair when the common optical axis of the TV Subsystem is aligned with the spacecraft velocity vector;
- Capability to provide wide area coverage;
- Capability to provide a set of nested pictures; and
- Capability to provide the high reliability necessary for ensuring success.

2. Subsystem Constraints

The constraints placed on the design of the TV Subsystem dealt primarily with its function as part of the Ranger Spacecraft; therefore, all constraints placed on the spacecraft have either indirect or direct effects on the design of the TV Subsystem.

a. INDIRECT CONSTRAINTS

The primary mission constraint was a result of the decision to plan four flights of the Ranger Spacecraft as repeated attempts at the single mission objective. All equipment for the first flight would be included on subsequent flights; additional scientific experiments would not be considered. This consistency of equipment was associated with the fact that the same type of launch vehicle would be used for all flights.

The selected launch vehicle was the Atlas D/Agena B. This vehicle is capable of projecting a useful weight of about 800 pounds into an Earth-to-Moon trajectory; therefore, the size, shape, and weight of the spacecraft were dictated by this constraint.

Additional mission constraints were introduced to ensure the return of information in the event of a nonstandard mission. Further constraints were developed as functions of the average luminance of expected lunar impact regions, the expected direction of approach to the lunar surface, the expected distance from the point of impact to the lunar terminator, the spacecraft velocity, and the amount of tolerable smear due to spacecraft velocity.

b. DIRECT CONSTRAINTS

The TV Subsystem constraints evolved from the above indirect constraints. The maximum weight allowance for the TV Subsystem was 375 pounds. The Subsystem was to be contained in a structure that would be mounted on the top of the main spacecraft. The structure was to provide compatible mounting at its apex for the spacecraft omnidirectional antenna and routing for the spacecraft coaxial cable between the omnidirectional antenna and the spacecraft.

The power needed to operate the Subsystem was to be contained in the Subsystem and be completely independent of the Ranger Spacecraft power system. Circuitry had to be designed to allow the spacecraft to switch the

TV Subsystem power by either RF command or by on-board sequencing. In addition, the TV Subsystem transmitters were not to interfere with the normal receipt and execution of real-time commands by the spacecraft, and the RF output of the Subsystem was to be compatible with the directional-antenna RF-mixing system of the spacecraft.

While on the launch pad, for safety reasons, the TV Subsystem was not to be operated at a power level greater than 2 watts from any one source. For all Subsystem testing, the necessary connections were to be independent of the spacecraft cabling system and directly accessible on the Subsystem.

The Subsystem was to be divided into two channels, each channel having a set of cameras, a power supply, equipment to generate synchronizing signals for the cameras, equipment to combine the camera video with sync and tone-code signals, and equipment to apply the composite video signals to the RF transmitter.

A minimum amount of telemetry information was to be available during the cruise-mode portion of the mission to monitor Subsystem engineering parameters. However, during the terminal mode of the mission, telemetry was to be increased to provide detailed information on Subsystem operation.

Redundancy in the communications equipment was desired to ensure transmission of lunar information back to Earth. The use of existing Deep Space Instrumentation Facilities (DSIF) and the radio-frequency channel allocations placed a constraint on the design. Two 900-kc bandwidth communications channels, with center frequencies at 959.52 and 960.58 Mc, respectively, were made available by the FCC. A carrier between the two channels at 960.05 Mc was used for the transponder signal from the spacecraft Bus.

The transmission losses involved in spanning the approximate 240,000-mile Earth-lunar distance were studied to determine the constraint that would be placed on the required transmitter power output. This study indicated that a transmitter power of 15 db above one watt would be required for single-channel operation. If simultaneous transmission over both channels was desired, an additional 3 db of power would be required to overcome the losses in the combining network. The power selected and the operation into existing DSIF elements provided for a video signal-to-noise level in excess of 30 db even at threshold. The realizability of transmitters capable of a 900-kc bandwidth at a distance of 240,000 miles allowed the design of a camera system utilizing a 200-kc video bandwidth. The availability of two RF channels also allowed for two separate camera systems to meet the design objectives.

B. ANALYSIS OF IMAGING SYSTEM

1. Lunar Luminance for Typical Missions

The expected luminance of the lunar surface that may be seen by the Ranger cameras is determined by the correct application of the photometric data obtained by Earth-based observations. According to experimental photometry, the lunar luminance in the direction of the Earth as seen by an Earth-based observer is given as

$$R_e = R_n \, \Phi(g, \lambda) \qquad (1)$$

where

R_e is the luminance in the Earth direction (candle/ft^2);

R_n is the normal luminance, which is the value of the luminance when the surface is illuminated and observed along its normal, (candle/ft^2);

$\Phi(g, \lambda)$ is the photometric function (its value is normalized and equals unity when $(g = 0)$ (See Figure 1);

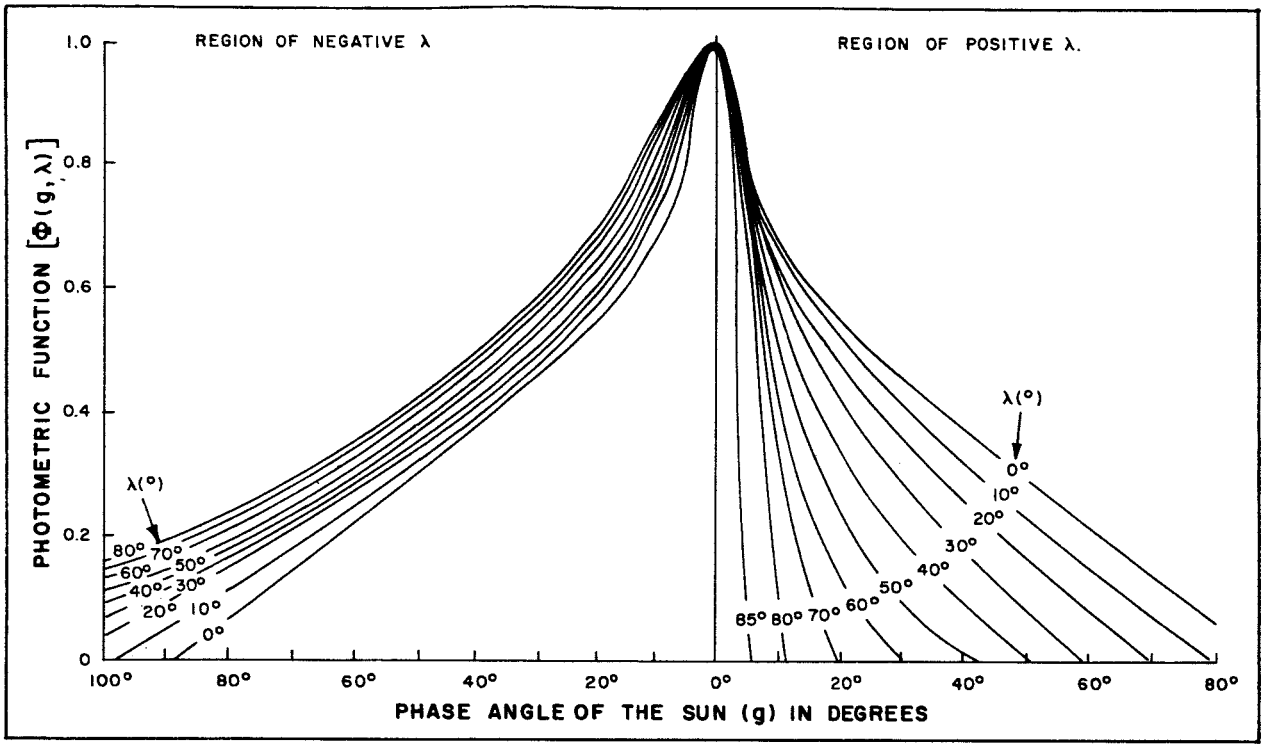

Figure 1. The Photometric Function Versus Phase Angle of the Sun

g is the phase angle of the Sun, also the angle between the observer and the Sun measured at the area being viewed; and

λ is the longitude of the point being observed. (λ is measured along the radiance equator. For an Earth-based observer, the radiance equator coincides with the lunar equator.)

The normal luminance can be expressed in terms of the solar constant by the following equation:

$$R_n = A_n \frac{S_c}{\pi} \qquad (2)$$

where

A_n is the normal albedo (dimensionless ratio);

S_c is the solar constant (foot-candles).

Therefore, by substitution, the lunar luminance in the direction of the Earth-based observer becomes

$$R_e = \frac{S_c}{\pi} A_n \Phi(g, \lambda) \qquad (3)$$

The experimental photometric properties of the lunar surface as expressed by $\Phi(g, \lambda)$ does not agree with those obtained for most terrestrial materials.

The properties of $\Phi(g,\lambda)$ are such that: at full Moon, the luminances of all areas reach maximum values; the luminances are independent of latitude at any lunar phase, but depend solely on longitude; and all formations have approximately the same photometric function.

In order to design cameras for an impacting picture-taking mission, it is necessary to predict the luminance of the surface being

observed. In order to determine the luminance of the area under observation from the spacecraft, an equivalent area which is viewed under identical conditions must be found for an Earth-based observer. Figure 2 shows the surface under observation; the important lighting parameters are as follows:

- Observation angle (e) is the angle between the surface normal and the optical axis;
- Sun angle (s) is the angle between the surface normal and the Sun direction; and
- Phase angle (g) is the angle between the Sun vector and the optical axis.

If e, s, and g are scaled off on Figure 3, which shows the Moon as seen from the Earth, a point P is found which has the same value of the photometric function as the area under observation from the spacecraft.

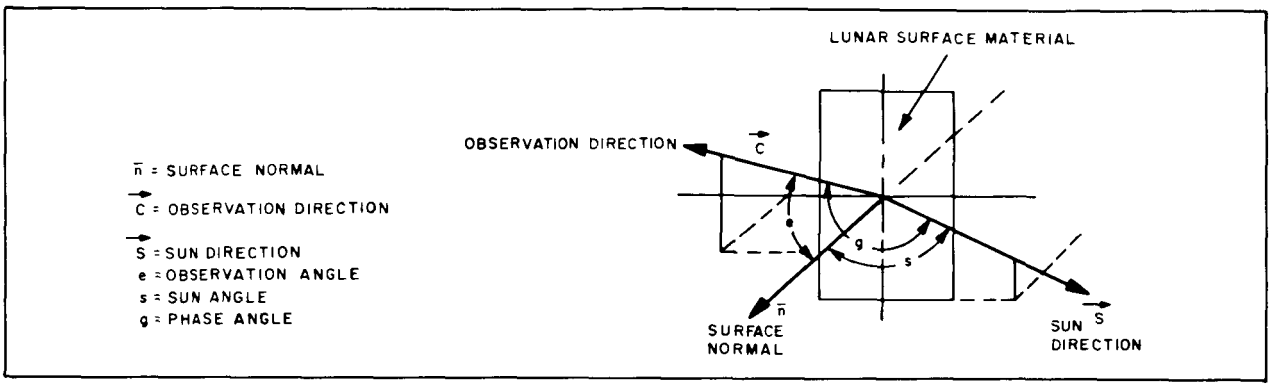

Figure 2. Area Under Observation

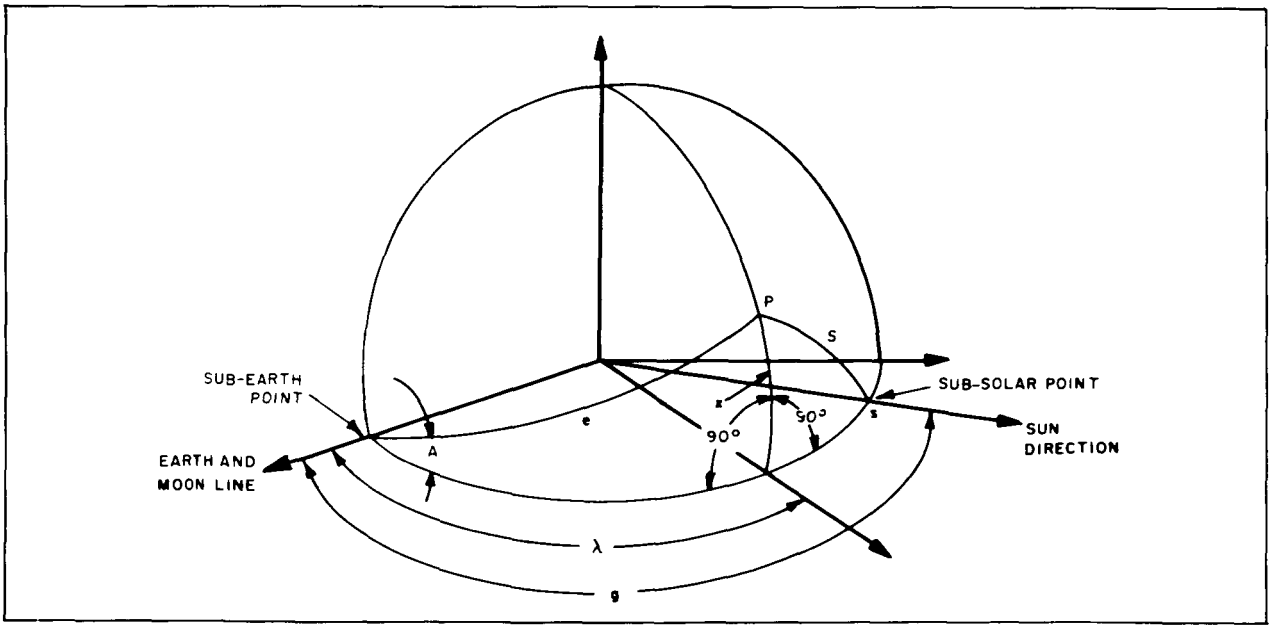

Figure 3. Determination of Equivalent Area for an Earth-Based Observer

From Figure 3, the value of the radiance longitude (λ) is found in the following manner:

In the spherical right triangle $(P, 90°, A)$

$$\cos \lambda = \frac{\cos e}{\cos x} \qquad (4)$$

$$\sin x = \sin e \sin A \qquad (5)$$

In triangle (P, A, s)

$$\cos A = \frac{\cos s - \cos g \cos e}{\sin g \sin e} \qquad (6)$$

Solving equations (4), (5), and (6) for $\cos \lambda$ yields:

$$\cos \lambda = \frac{\cos e \sin g}{(\cos^2 e + \cos^2 s - 2 \cos g \cos e)^{1/2}} \qquad (7)$$

The value of λ, as determined from equation (7) may be to the right or left of the Earth-Moon line. If angle A (Figure 3) is less than 90 degrees, λ is to the right and has a negative value; if greater than 90 degrees, λ is to the left and has a positive value. The values of λ are used in Figure 1 to find the value of the photometric function, Φ.

The values of e, s, and g required in equations (6) and (7) can be determined once the unit vectors along the observation direction, Sun direction, and surface normal are specified.

Neglecting the parallax of the Sun, a unit vector in the Sun direction is

$$\vec{s} = \vec{i} \cos \theta_s \cos \phi_s + \vec{j} \cos \theta_s \sin \phi_s + \vec{k} \sin \theta_s \qquad (8)$$

where

θ_s is the lunar altitude of the subsolar point;

ϕ_s is the lunar longitude of the subsolar point; and

$\vec{s}$, $\vec{i}$, $\vec{j}$, and $\vec{k}$ are unit vectors as shown in Figure 4.

The surface normal, $\vec{n}$, is depicted in Figure 5(b), which is an expanded view of area (A) in Figure 4, and is expressed as:

$$\vec{n} = \vec{R}_A \cos \gamma + \vec{k}' \sin \gamma \cos \sigma + \vec{j}' \sin \gamma \sin \sigma \qquad (9)$$

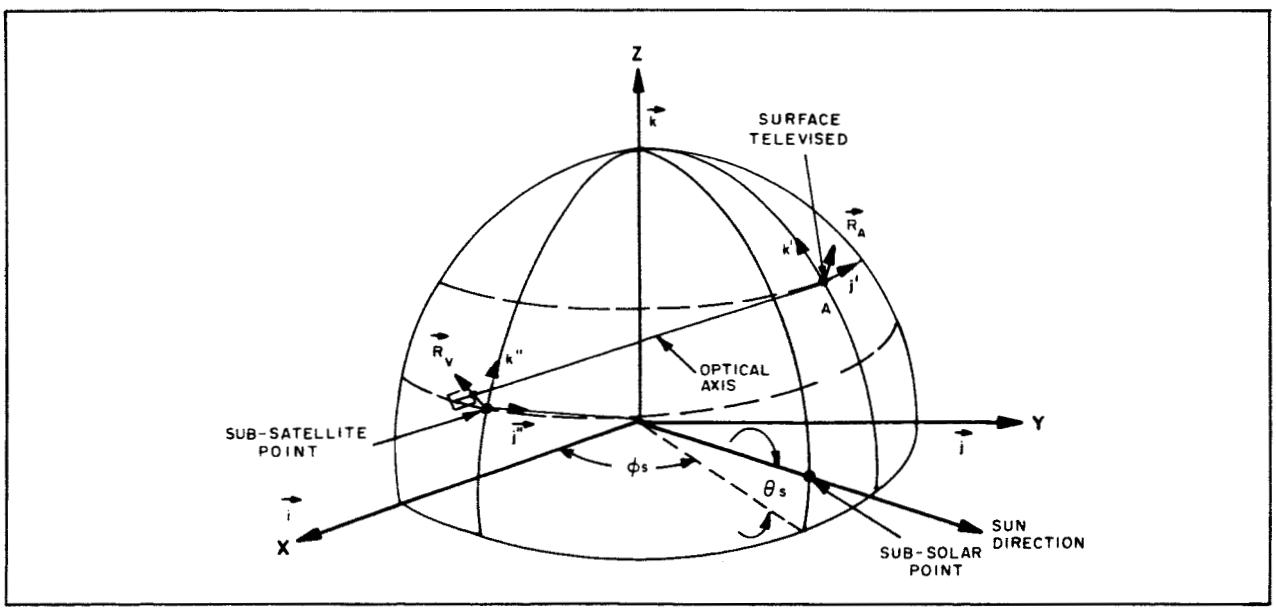

Figure 4. Geometry of the Required Vectors

where

$\vec{R}_A$ is the unit radius vector to the surface being observed;

$\vec{k}'$ is the unit vector along the lunar longitude at the point being observed;

$\vec{i}'$ is the unit vector along the lunar latitude circle at the point being observed;

γ is the angle between the normal and the radius vector; and

σ is the angle made with the $\vec{k}'$ vector by the projection of $\vec{n}'$ on the $\vec{k}', \vec{i}'$ plane.

The vector in the direction of the optical axis, is depicted in Figure 5(a), and is expressed as:

$$\vec{C}' = \vec{R}_v \cos\beta + \vec{k}'' \sin\beta \cos\alpha + \vec{i}'' \sin\beta \sin\alpha \quad (10)$$

where

$\vec{R}_v$ is the unit vector in the satellite direction;

$\vec{k}''$ is the unit vector along the meridian at the subvehicle point; and

$\vec{i}''$ is the unit vector along the latitude circle at the subvehicle point.

Earth-based studies indicate that the albedo is a slowly changing function of position, and changes in luminance of the scene are due only to variations in the photometric function caused by changes in either g or λ.

The value of g will vary over the photograph, because of the camera field-of-view; however, g can be assumed constant for any limited area of the photograph. It can be seen from Figure 1 that if the value of g is constant, only variations in λ will be responsible for changes in the scene luminance recorded in any area. The curves show that the degree of change in scene luminance with variations in λ depends on the value of g, being zero when g equals zero and increasing for progressively greater values of g.

In summary, the background luminance of the scene, against which surface features are detected, is set by the value of g. The dynamic range of the luminance depends on the value of λ, which varies due to changes in surface orientation.

Since the primary mission requirement was to determine the topological features of the lunar surface, the direction of observation and the lighting had to be selected to provide an appreciable shadow content. The required parameters are determined as a function of the distance between the impact area and the terminator (for missions with trajectories in the plane of the lunar equator and the camera axis aligned with the local vertical).

The parameters were calculated by means of the vector geometry shown in Figure 5. If it is assumed that the camera axis is aligned with the local vertical, then the area being observed is located at the nadir, and the coordinate systems shown in a and b of Figure 5 coincide.

Therefore,

$$\vec{k}' = \vec{k}'' = K \quad (11)$$

$$\vec{i}' = \vec{i}'' = -\vec{i} \sin\phi_p + \vec{j} \cos\phi_p \quad (12)$$

$$\vec{R}_v = \vec{R}_A = \vec{i} \cos\phi_p + \vec{j} \sin\phi_p \quad (13)$$

where

ϕ_p is the lunar longitude of the point being photographed.

If it is also assumed that the Sun direction is in the plane of the lunar equator, the vectors required to find g and λ are given by equations (8), (9) and (10). Since θ_s in equation (8) is equal to zero, equation (8) becomes:

$$\vec{s} = \vec{i} \cos\phi_s + \vec{j} \sin\phi_s \quad (14)$$

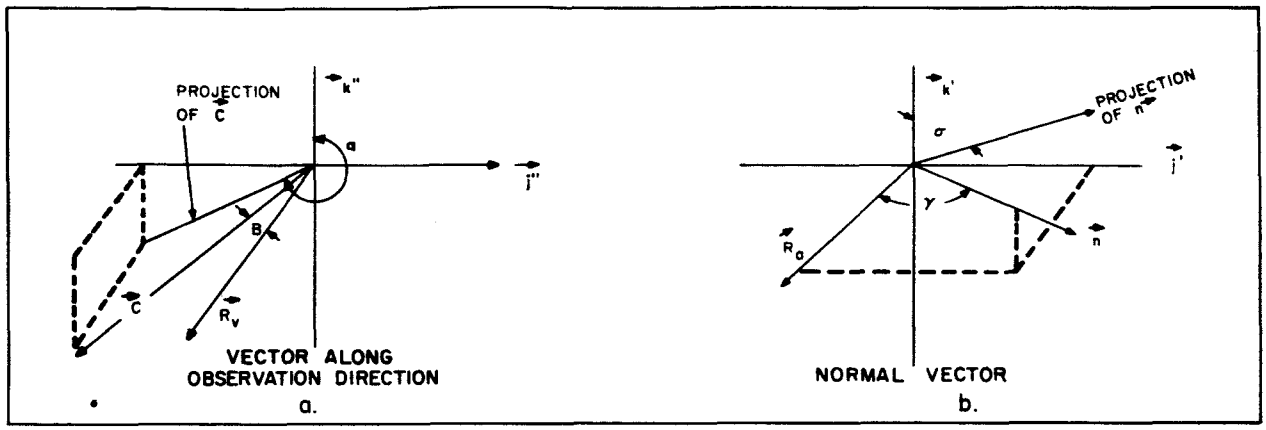

Figure 5. Vector Geometry

Substituting equation (12) for $\vec{j}'$ in equation (9) yields:

$$\vec{n} = \vec{R}_A \cos\gamma + \vec{k}' \sin\gamma\cos\sigma - \vec{i}\sin\gamma\sin\sigma\sin\phi_p + \vec{j}\sin\gamma\sin\sigma\cos\phi_p \quad (15)$$

Since

$$\vec{C} = \vec{R}_v = \vec{R}_A \quad (16)$$

substituting for $\vec{R}_A$ from equation (13) yields:

$$\vec{C} = \vec{i}\cos\phi_p + \vec{j}\sin\phi_p \quad (17)$$

Thus

$$\cos e = \vec{n}\cdot\vec{C} = \cos\gamma \quad (18)$$

$$\cos g = \vec{C}\cdot\vec{s} = \cos\phi_s\,\phi_p + \sin\phi_s\,\phi_p = \cos(\phi_s - \phi_p) \quad (19)$$

$$\cos s = n\cdot s = \cos(\phi_s - \phi_p)\cos\gamma + \sin\gamma\sin\sigma\sin(\phi_s - \phi_p) \quad (20)$$

Substituting equations (18), (19) and (20) into equation (7) reduces equation (7) to:

$$\cos\lambda = \frac{\cos\gamma}{(\cos^2\gamma + \sin^2\gamma\sin^2\sigma)^{1/2}} \quad (21)$$

As shown by equation (21), the range of values for λ is from zero, when the normal is in the meridian plane (σ equals zero or 180 degrees), to $\pm\gamma$, when the normal is in the equatorial plane. Consequently, for surface normals in the meridian plane, the photometric function is independent of γ.

The background luminance and the dynamic range of luminance can be determined as a function of distance from the terminator by using the curves in Figure 1 to obtain the value of the photometric function, $\Phi(g, \lambda)$, and then using this value in equation (3). Typical values of lunar luminance are plotted in Figure 6, assuming a normal albedo, A_n, of 0.1 and a solar constant, S_c, of 13,400 foot-candles.

2. Lunar Luminance for Nonperfect Missions

The curves in Figure 6 allow the lunar luminance to be determined for a trajectory in which the preestablished distance from the spacecraft impact point to the lunar terminator is not achieved, although the ability to make a terminal maneuver to align the camera with the local vertical is not impaired. The following analysis was used to determine the lunar luminance for the case in which the terminal maneuver cannot be made, causing the camera orientation to be maintained as during the flight.

For calculations in which the spacecraft is assumed near the lunar surface, the two

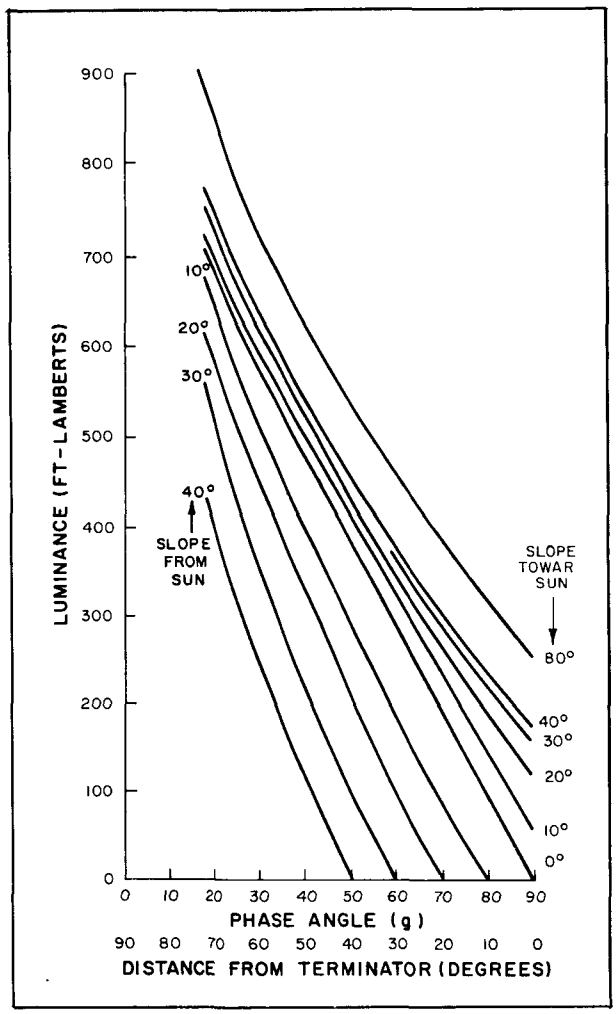

Figure 6. Typical Values of Lunar Luminance

coordinate systems shown in a and b of Figure 5 coincide. The camera orientation without a terminal maneuver is shown in Figure 7. The camera optical axis is maintained at 38 degrees with respect to the Sun vector. Assuming that the impact point is in the equatorial plane, the angles s, e, and g of Figure 3 are related as follows:

$$s = e + g \tag{22}$$

Substituting for s in equation (7) from equation (22) reduces equation (7) to

$$\cos \lambda = \cos e \tag{23}$$

As shown in Figure 7,

$$e = 90 - \phi_p - 38 \pm \gamma \tag{24}$$

The expected luminance under the aforementioned conditions is given in Figure 8 as a function of the distance between the impact point and the terminator. Figure 9 shows the expected luminances as a function of the distance between the impact point and the terminator when there is a terminal maneuver to align the optical axis along the velocity vector.

The curves shown in Figure 6 are based on a terminal maneuver that places the camera optical axis along the local vertical. Under actual conditions, however, the terminal maneuver places the camera optical axis along the velocity vector of the spacecraft. The trajectories in which the velocity vector and the camera axis coincide are limited to those with impact points that are approximately 45 degrees in longitude from the Earth-Moon line. (These trajectories are known as normal trajectories.) For impact areas not in normal trajectories, the angle (α) between the velocity vector and the surface normal can be approximated by:

$$\alpha = \frac{\beta - 45 - \phi_p}{1.39} \tag{25}$$

3. Vidicon Illuminance

The three fundamental characteristics to be considered in the design and evaluation of a camera system are (1) the transfer function, (2) signal-to-noise ratio, and (3) the aperture response. Basically, the transfer function relates light intensities in large areas of the scene to the output of the transducer, the signal-to-noise ratio specifies the ability of the system to detect variations in the light intensity of the scene, and the aperture response limits the ability of the system to reproduce the details in the existing scene. In order to establish values for these parameters, it is essential to determine the illuminance on the vidicon target.

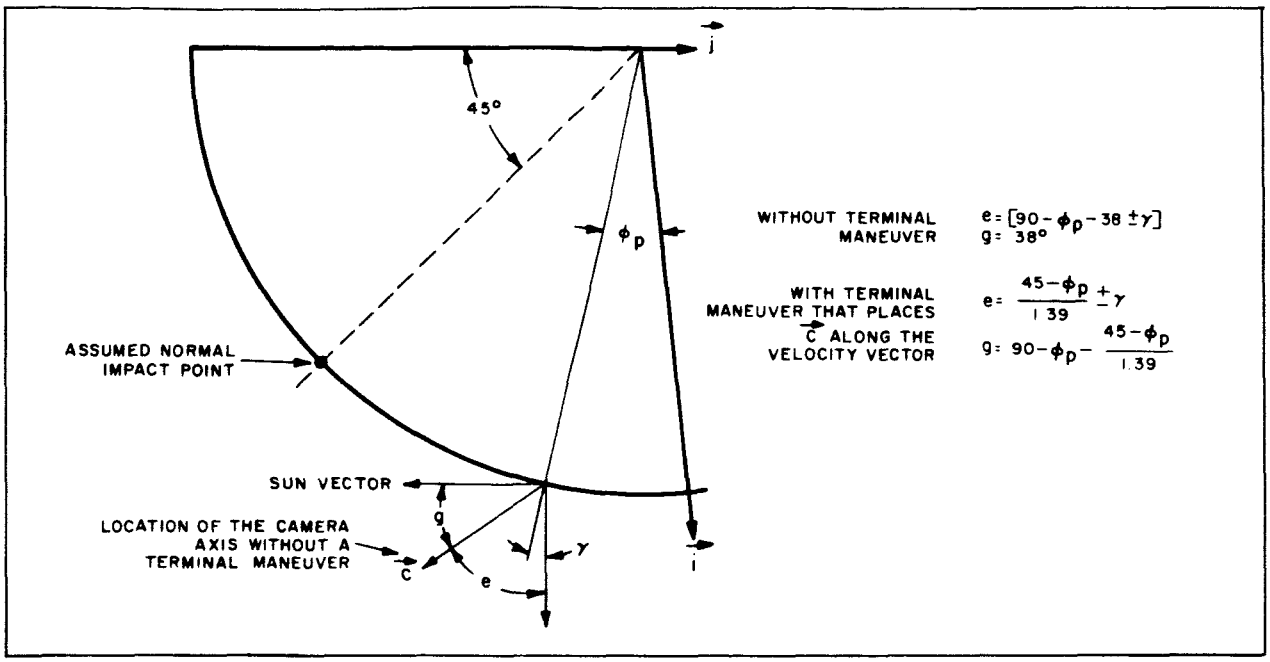

Figure 7. Camera Orientation Without a Terminal Maneuver

Generally, calculation of the illuminance in the image plane is based on the assumption that the scene luminance is constant. If it has a spatial distribution, the inability of the optical and electrical systems to reproduce a point source must be considered. The illuminance in the image plane is found in the following manner.

Consider Figure 10 which shows an elemental area $d\sigma$ in the object space. The luminance flux from this area falling on the aperture of the optical system is:

$$\Delta L = I_\theta \Omega \qquad (26)$$

where

ΔL is the flux falling on the aperture;

I_θ is the intensity in the direction of the collector;

Ω is the solid angle subtended by the collector as measured from x, y, in object space; and

θ is the angle the observation direction makes with the surface normal.

The intensity of the source in the direction of the collector can be expressed in terms of the luminance of the source as:

$$R_\theta = I_\theta / \cos\theta \, d\sigma \qquad (27)$$

where

R_θ is the luminance of the source in the direction of the aperture; and

$\cos\theta \, d\sigma$ is the projected area in the direction of the aperture.

At great distances from the optical system the solid angle subtended by the collector is:

$$\Omega = \frac{\pi D^2}{4r^2} \cos\beta \qquad (28)$$

where

$\frac{\pi D^2}{4} \cos\beta$ is the projected area of the collector in the direction of x, y;

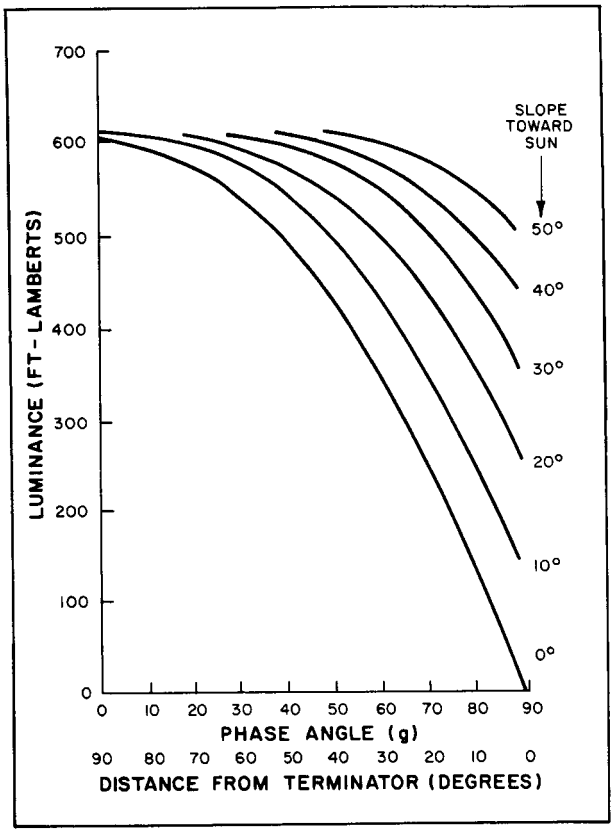

Figure 8. Range of Luminance Without a Terminal Maneuver

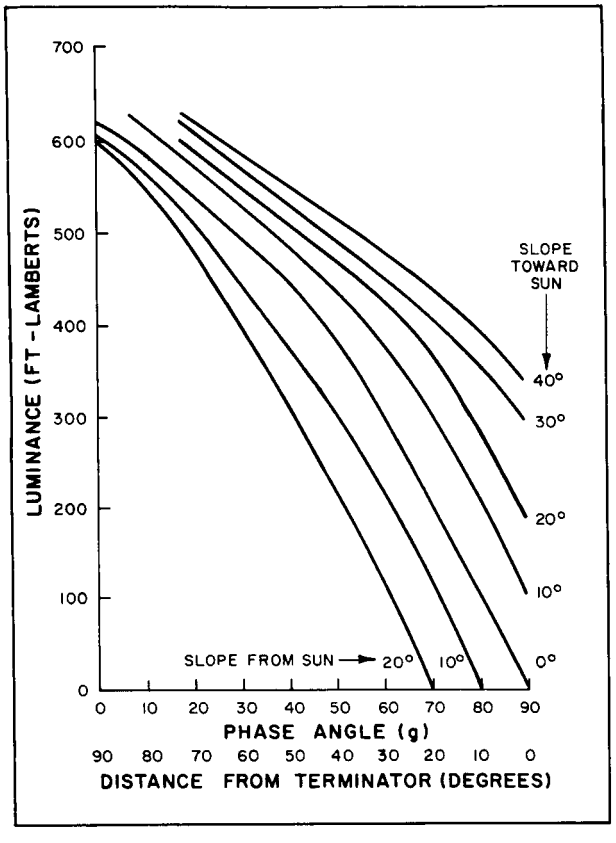

Figure 9. Range of Luminance With a Terminal Maneuver

β is the angle between the normal to the aperture and the observation direction;

r is the distance from the aperture to x, y; and

D is the aperture diameter.

Combining equations (26), (27) and (28) yields:

$$\Delta L = \left(\frac{R_\theta \cos \beta \pi D^2}{4}\right)\left(\frac{d\sigma \cos \theta}{r^2}\right) \qquad (29)$$

Letting

$$\frac{d\sigma' \cos \beta}{(r')^2} = \frac{d\sigma \cos \theta}{r^2} \qquad (30)$$

and

$$(r')^2 = \frac{F^2}{\cos^2 \beta} \qquad (31)$$

where

$d\sigma$ is the area in the image plane;

r' is the distance to the elemental image;

$d\sigma' \cos \beta$ is the projected image area along the observation direction; and

F is the focal length

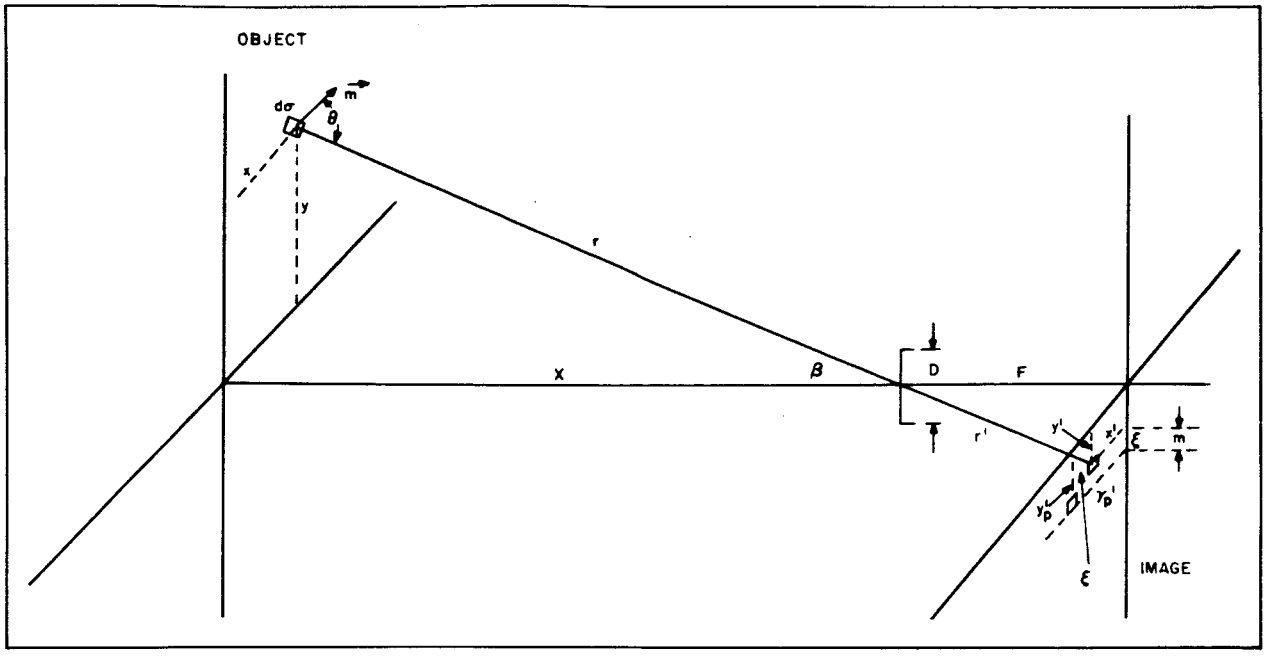

Figure 10. Geometrical Representation of the Object-Image Plane

Substituting for $(r')^2$ from equation (31) in equation (30) and then substituting the result for $\frac{d\sigma \cos\theta}{r^2}$ in equation (29) yields:

$$\Delta L = \frac{R_\theta \pi}{4\left(\frac{F}{D}\right)^2} \cos^4 \beta d\sigma' \qquad (32)$$

As $d\sigma$ approaches zero the flux ΔL is distributed in the image plane as though it originated from a point source. The flux, ΔL_p at x'_p, y'_p falling on an elemental area $\Delta x'_p \; \Delta y'_p$ is expressed by:

$$\Delta L_p = \frac{R_\phi \pi}{4\left(\frac{F}{D}\right)^2} \cos^4 \beta \, f(\xi, n) \, d\sigma' \qquad (33)$$

where

$f(\xi, n)$ is that fractional part of the total flux in the point image which enters $\Delta x'_p, \Delta y'_p$; and (ξ, n) are coordinates of the point (P) as measured in a system whose origin is placed at the geometrical image x', y' of x, y.

The illuminance at x'_p, y'_p due to a source at $d\sigma$ is expressed by:

$$\Delta E_p (x'_p, y'_p) = \left[\frac{\Delta L_p}{\Delta x'_p \, \Delta y'_p} = \frac{R_\theta (x,y) \pi}{4\left(\frac{F^2}{D^2}\right)}\right] \cdot \cos^4 \beta \, F(\xi, n) \, d\sigma' \qquad (34)$$

where $F(\xi, n)$ is the fractional part of the flux per unit area of the point image.

Integrating equation (34), the illuminance at P becomes:

$$E_p (x', y') = \frac{\pi \cos^4 \beta}{4\left(\frac{F^2}{D^2}\right)} \iint R_\theta (x,y) \, F(\xi, n) \, d\sigma' \qquad (35)$$

In order to evaluate this expression, the lunar luminance $R_\theta (x, y)$ and the point spread function $F(\xi, n)$ must be specified.

The illuminance of the vidicon target for a point on the optical axis can be simplified to:

$$E_p(x_o', y_o) = \frac{\pi R(\theta)}{4(f)^2} \tag{36}$$

where f is the aperture ratio and is equal to $\left(\frac{F}{D}\right)$.

The expression $\pi R(\theta)$ in equation (36) is expressed by:

$$\pi R(\theta) = S_c A_n \Phi(g, \lambda) \tag{37}$$

where

S_c is the solar constant in foot-candles;

A_n is the normal albedo;

$\Phi(g,\lambda)$ is the photometric function (its value is normalized and equals unity when g is equal to zero);

g is the angle between the observer and the Sun, with the viewed area as the vertex; and

λ is the longitude of the point being observed, measured along the radiance equator.

Substituting for $\pi R(\theta)$ in equation (36) from equation (37) yields:

$$E_p(x_o', y_o') = \frac{S_c A_n \Phi(g,\lambda)}{4(f)^2} \tag{38}$$

where E_p is in lumens per square foot (or foot-candles). The light energy E_i incident on the vidicon target is given by

$$E_i = Z(\Delta t)E_p \tag{39}$$

where Z is the lens transmission factor and Δt is the exposure time.

4. Vidicon Characteristics

The vidicon characteristics that have the greatest effect on image quality are spectral response, sensitivity and modulation transfer function.

In order to obtain acceptable television pictures of the lunar surface, the spectral components of the light reflected from that surface must be considered. Observations with Earth-based equipment indicate that the reflectance of the Moon's surface is almost constant for any wavelength of the incident solar illumination; with a slight rise toward the infrared end of the spectrum. Therefore, the spectral characteristic of the light reflected from the lunar surface is very close to that of solar light, as shown by the Johnson solar curve in Figure 11. This curve has a peak value at approximately 460 millimicrons.

The spectral response of two vidicon types that were supplied during the program is shown in Figure 12. Early in the program, vidicons were used in which the thin conducting layer of the vidicon target was a transparent gold deposit. Later vidicons were of the "Bis-Tic" type, whose curve is shown on the right of Figure 12. Both vidicon types have an antimony-sulphide oxy-sulphide (ASOS) photoconductive layer, and both have a spectral response that is adequate for obtaining acceptable pictures of the lunar surface.

Vidicon sensitivity is expressed as the vidicon target current resulting from a light source with a known spectral response. The sensitivity of a number of vidicons was determined using a collimator light source with the response shown in Figure 11. When the luminance of the collimator was set at 650 footlamberts, a vidicon in a camera with an f/0.95 lens and a 2-millisecond shutter period provided a target current output of 13 nanoamperes.

The vidicons that were used have a transfer function (γ) value ranging from 0.80 to 0.95, with an average value of 0.90. The target

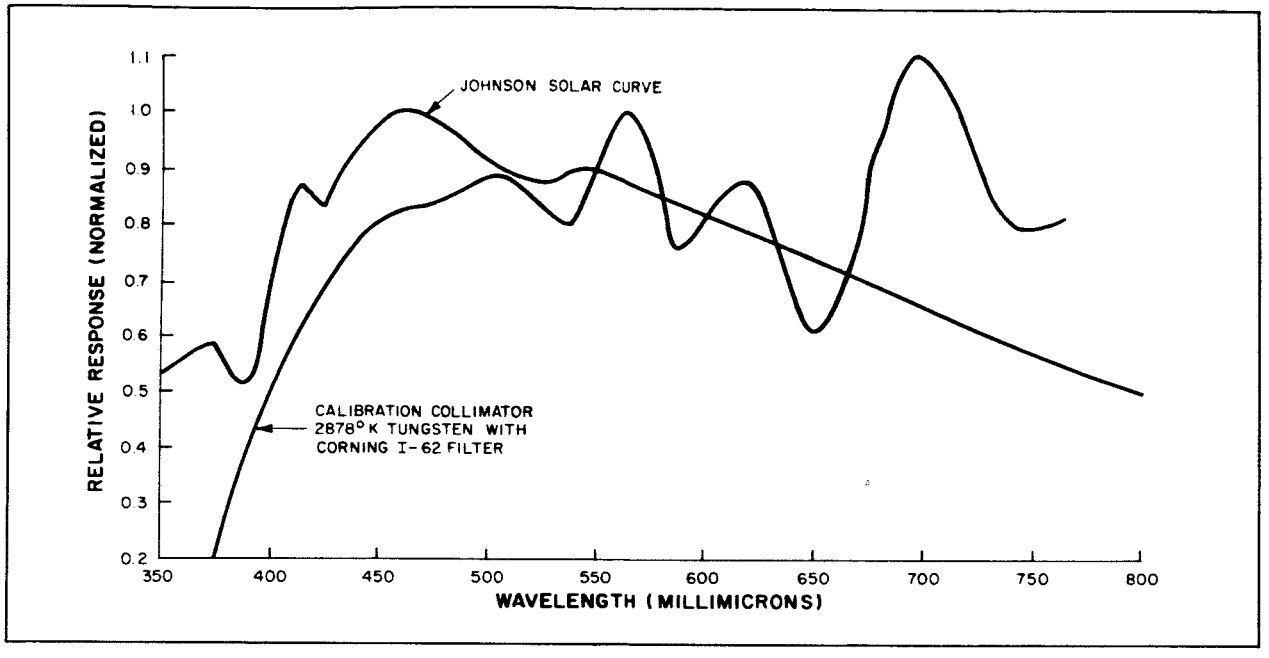

Figure 11. Spectral Response of Collimator Light Source Compared to Solar Spectrum

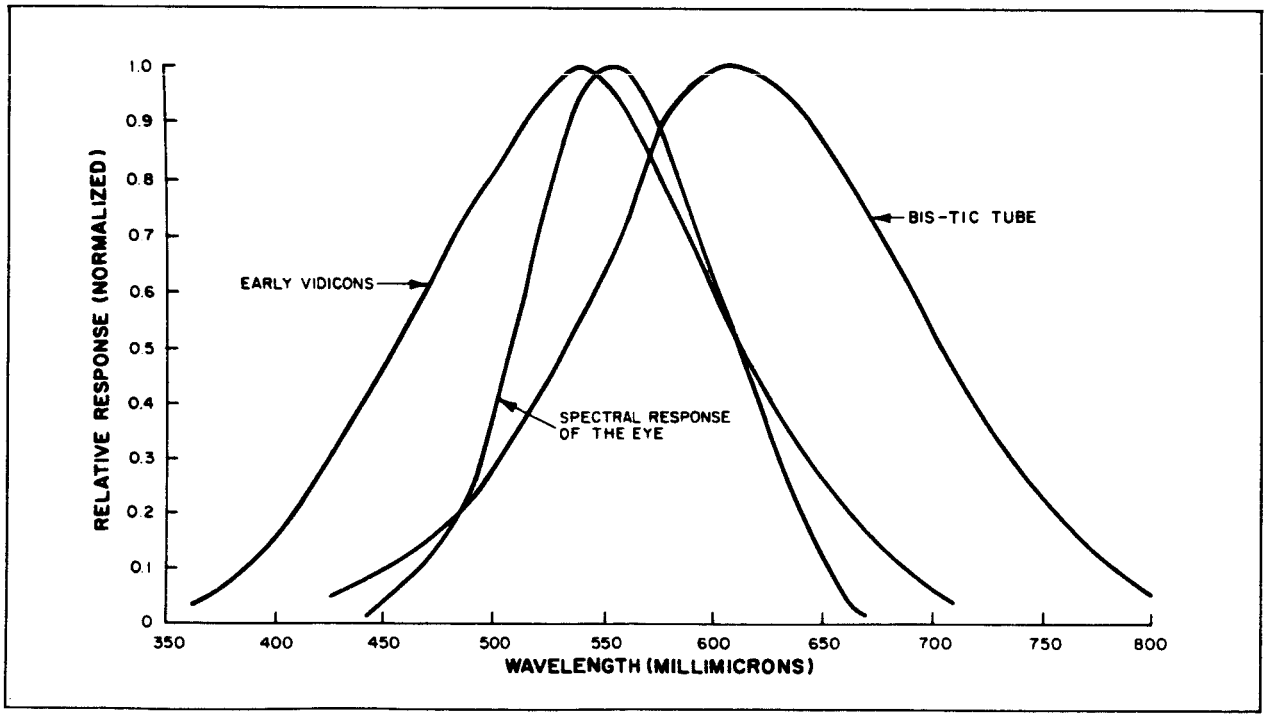

Figure 12. Spectral Response of Typical Vidicons Compared to that of the Eye

current for any scene luminance is found by using the relationship:

$$\left(\frac{E_1}{E_2}\right)^{\gamma} = \frac{I_1}{I_2} \qquad (40)$$

where

I_1 is the current produced by exposure E_1; and

I_2 is the current produced by exposure E_2.

The exposure (E) of the vidicon photoconductor is computed by using the following equation:

$$E = \frac{BZ(\Delta t)}{4(f)^2} \qquad (41)$$

where

E is the exposure in foot-candle-seconds;

B is the collimator source luminance in footlamberts;

Z is the transmission factor of the lens;

Δt is the exposure time; and

f is the F-number of the lens.

C. ANALYSIS OF COMMUNICATIONS SYSTEM

1. Communications System Constraints

Design of the communications system was governed by a number of constraints. First, the RF bandwidth was limited to less than 1 Mc with a carrier frequency of 960 Mc. Second, the parameters of the Deep Space Information Facility (DSIF) antenna and the spacecraft antenna were fixed. (These parameters are shown in Tables 1 and 2.) And third, the requirement was imposed to use existing equipment wherever possible. Furthermore, there were practical limits to the amount of power, weight, and volume that could be allocated to the communications equipment in the TV Subsystem. The power limitation was a major problem. For RF power outputs in the range of 20 to 100 watts, the efficiency of an RF power amplifier ranges from 10 to 20 percent. Thus the two 60-watt transmitters were the major power consumers in the TV Subsystem.

2. Desired Signal-to-Noise Ratio

The amount of RF power selected is based on recovering the video signal on Earth at an acceptable signal-to-noise ratio. For commercial television, a signal-to-noise ratio of 30 to 35 db is generally accepted as good quality reception. A 30-db *S/N* with FM (triangular) noise is considered to yield a picture equivalent to that obtained with an *S/N* of 35 db for a flat noise spectrum, as in AM. In commercial television, low-frequency noise (such as ignition noise) in the picture is considered more objectionable than the overall graininess caused by high-frequency noise. However, when the interest is mainly in fine picture detail, as in the Ranger mission, a lower *S/N* with flat noise is preferable to a higher *S/N* with triangular noise. A 30-db *S/N* was selected as the minimum acceptable *S/N* for the communications link. The *S/N* was defined as the ratio of peak-to-peak signal (full black-to-white video) to rms noise. This *S/N* corresponds to a 24-db *S/N* when rms values are used for both the signal and the noise. The conversion from rms to peak-to-peak signal is 9 db, less 3 db of loss due to the sync tip of the signal.

3. Selection of Modulation

a. GENERAL

The selection of a minimum acceptable *S/N* made possible a trade-off analysis to select the type of modulation for the communications link. The basic types of analog modulation are AM, single-sideband AM, FM, FM with feedback, and phase modulation. There are other types of analog modulation, which require the use of subcarriers, but these

TABLE 1
RCA DSIF PERFORMANCE ANALYSIS

Receiving System Parameter	Value	Tolerance
Antenna gain (85 foot)	45.7 db	±0.8 db
Axial ratio	0.5 db	±0.1 db
Diplexer loss	0.23 db	±0.03 db
Line loss	0.3 db	+0.2 db -0.0 db
Maser gain (2 Mc BW)	9.6 db	±0.5 db
Parametric amplifier gain (10 Mc BW)	20.0 db	
System noise temperatures:		
Diplexer and line loss	33.3° K	+13.2° K - 1.8° K
Antenna loss	29.2° K	+ 0.2° K - 4.3° K
Maser parametric amplifier	38.0° K	± 5.0° K
Moon	31.0° K	+ 2.6° K - 4.2° K
Total noise temperature	131.5° K	+21.0° K -15.3° K

types are not as efficient as direct modulation when only one information channel is needed. Phase modulation (PM) and FM with feedback (FMFB) were eliminated early for use in the TV Subsystem. PM was not satisfactory because it is difficult to implement true phase modulation over a wide frequency range that includes essential DC signal components. FMFB (and phase-lock detection) was dropped because it was still in the laboratory stage for wideband systems, and its development did not fit into the Ranger program schedule.

True single-sideband modulation cannot be used for slow-scan video because of the low-frequency response that is required. However, vestigial-sideband modulation can be used. In this type of modulation, the carrier is suppressed 6 db, and the required bandwidth is approximately 0.6 of double-sideband AM bandwidth.

A third form of AM, double-sideband suppressed carrier, was investigated. This type requires the same bandwidth as conventional AM, but it does not require the power normally used in transmitting a carrier.

The foregoing analog types of modulation were also compared with digital modulation. The various modulation techniques were compared and FM was selected as being best suited for transmission of the video data from

TABLE 2
SUMMARY OF PERFORMANCE ANALYSIS FOR RCA DSIF

Parameter	Value	Tolerance
Transmitter power (60 watts)	17.8 db	±1.0 db
Losses		
RCA circuit	3.5 db	±0.4 db
JPL circuit	1.7 db	+0.3 db -0.4 db
Spacecraft antenna	-19.9 db	±0.4 db
Antenna pointing	0.3 db	+0.1 db -0.3 db
Polarization	0.14 db	±0.1 db
Path loss	204.5 db	
DSIF antenna	-45.7 db	±0.8 db
Receiving circuit	0.53 db	+0.23 db -0.03 db
Total losses	145.1 db	+2.33 db -2.43 db
Total power received (input to maser)	-127.3 db	+3.43 db -3.33 db
System noise temperature	131.5° K	+21.0° K -15.3° K
Noise bandwidth	800 kc	±100 kc
Receiver noise power	-148.4 dbw	+1.2 dbw -1.1 dbw
Received Carrier-to-noise ratio	21.1	±4.53

the TV Subsystem. The analyses of the various types of modulation considered are reviewed in the following text.

b. AMPLITUDE MODULATION

The spectrum for amplitude modulation is expressed by:

$$A(1 + M \sin \omega_M t) \sin \omega_c t \qquad (42)$$

where

- A is the amplitude of the unmodulated carrier;
- M is the modulation index $(0 \leq M \leq 1)$;
- ω_c is the angular frequency of the carrier; and
- ω_M is the angular frequency of the modulation.

Expanding expression (42) yields:

$$A \sin \omega_c t + \frac{MA}{2} \sin (\omega_c - \omega_M)t + \frac{MA}{2} \sin(\omega_c + \omega_M)t \qquad (43)$$

This expansion shows the frequency components of the AM carrier. The first term indicates the amount of power in the carrier (which contains no information) and the second and third terms indicate the amount of power in the sidebands (either of which contains all the information).

In a limited power situation, it is desirable to conserve power by not transmitting the carrier. The power transmitted in double-sideband AM is expressed as:

$$P_T = K^2 + (MK)^2 \qquad (44)$$

$$P_M = (MK)^2 \qquad (45)$$

where

- P_T is the total power transmitted;
- P_M is the modulation power; and
- K is the rms value of the unmodulated carrier, which is equal to $\frac{A}{\sqrt{2}}$.

The modulation loss is defined as the ratio of P_T to P_M. Thus,

$$\frac{P_T}{P_M} = \frac{K^2(1+M^2)}{K^2 M^2} = 1 + \frac{1}{M^2} \qquad (46)$$

For double-sideband suppressed-carrier transmission, P_T is equal to P_M; therefore, there is no modulation loss. Vestigial sideband AM suppresses the carrier 6 db, but also reduces the modulation power by 6 db. Thus, the modulation loss is the same as that for double-sideband AM. The modulation loss for these two types is plotted in Figure 13 as a function of the modulation index (M). When M is equal to 0.8 (which is a reasonable index of AM in order to keep distortion at an acceptable level), the modulation loss is 4.1 db.

Although, the modulation loss is the same for vestigial AM and double-sideband AM, the noise bandwidth is less for vestigial AM.

Double-sideband suppressed carrier transmission is easily achieved by the use of a balanced modulator. However, in order to recover the transmitted data, a reference signal is required. This signal is normally obtained by reinserting a small amount of the carrier into the transmitted signal, and then recovering this carrier with a narrow-band carrier-tracking receiver. This system is not satisfactory for video signals because of the low-frequency components in the signal. The carrier tracking link acts as a high-pass filter and causes low-frequency distortion of the video signal. Of all the AM schemes available, only double-sideband AM or vestigial sideband AM was feasible for use in the TV Subsystem. For double-sideband AM with a

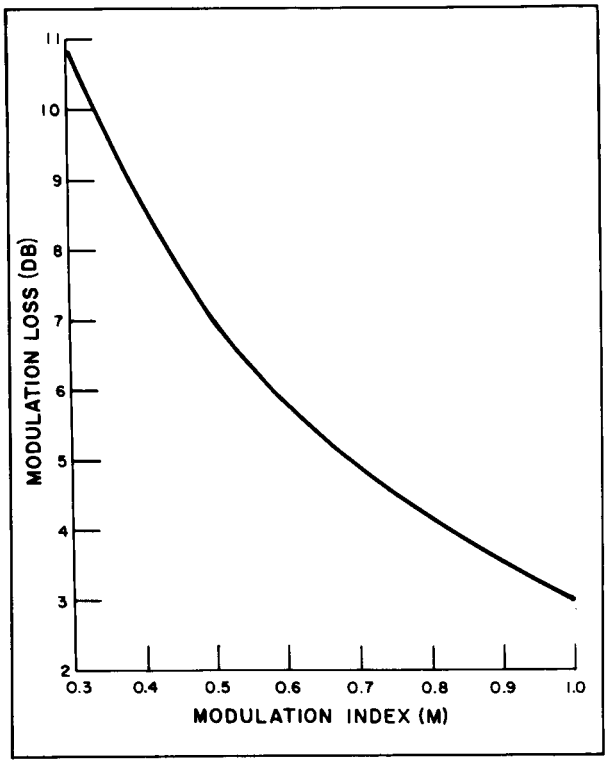

Figure 13. Modulation Loss for DSB-AM and VSB-AM as a Function of Modulation Index

modulation index of 0.8, the relative transmitter power required to obtain a picture with a 30-db S/N (24 db rms-to-rms) is given by:

$$P_{DSB-AM} = S/N + 2B + \text{Modulation loss (in db)} \quad (47)$$

$$= 24 + 3 + 4.1 + 10 \log B$$

$$= 31.1 \text{ db} + 10 \log B$$

where B is the required modulation bandwidth. For vestigial sideband AM with the same modulation index, the relative transmitter power required to obtain a picture with the same S/N is given by:

$$P_{VSB-AM} = S/N + 1.2B + \text{Modulation loss (in db)} \quad (48)$$

$$= 24 + 0.8 + 4.1 + 10 \log B$$

$$= 28.9 \text{ db} + 10 \log B$$

c. FREQUENCY MODULATION

Frequency modulation provides an improvement in the signal-to-noise ratio when the carrier is demodulated. This improvement factor is a constant as long as the system is above threshold. As a conservative estimate, threshold is assumed to occur at a carrier-to-noise ratio of 12 db. For minimum power consumption, the system should be designed to operate at threshold. Therefore an FM improvement of 12 db is required to raise the carrier-to-noise ratio of 12 db to the desired signal (rms)-to-noise (rms) ratio of 24 db.

The FM improvement (I_{FM}) is a function of IF bandwidth, and is given by:

$$I_{FM} = M \sqrt{\frac{3 B_{IF}}{2 B}} \quad (49)$$

where

M is the modulation index;

B_{IF} is the required IF bandwidth; and

B is the modulation bandwidth.

The IF bandwidth (B_{IF}) is given by:

$$B_{IF} = 2(M+1) B \quad (50)$$

Substituting for B_{IF} from equation (50) to equation (49) yields:

$$I_{FM} = M \sqrt{\frac{3[2(M+1) B]}{2B}} \quad (51)$$

Reducing equation (51) yields:

$$I_{FM} = M \sqrt{3(M+1)} \quad (52)$$

FM improvement versus modulation index is plotted in Figure 14. As shown in the figure, an FM improvement of 12 db requires a modulation index of 1.45. This modulation requires an IF bandwidth of 4.9B, as computed by means of equation (50).

In summary, the FM system requires a carrier-to-noise ratio of 12 db in an IF bandwidth of 4.9B, and has no modulation loss.

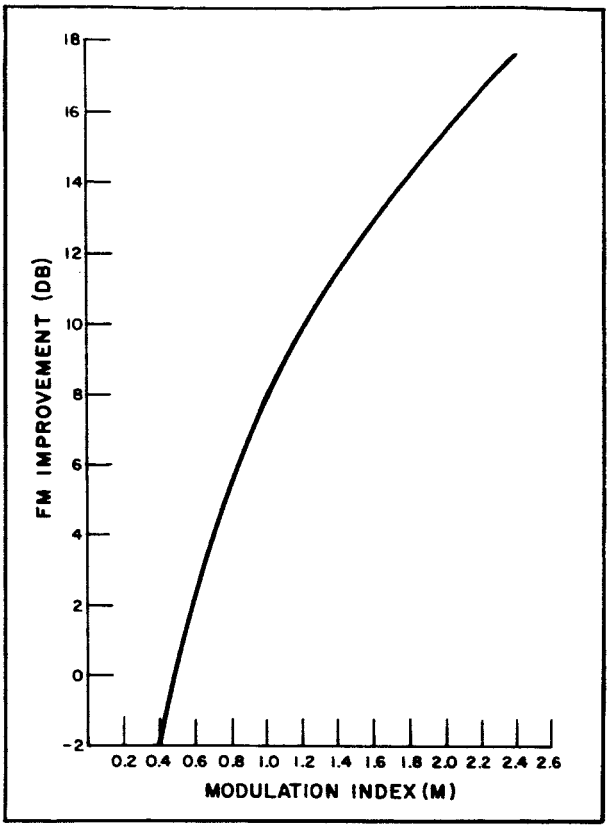

Figure 14. Signal-to-Noise Improvement in FM Transmission as a Function of Modulation Index

Thus, the relative transmitter power required for a picture with a 30-db S/N is:

$$P_{FM} = R_{CN} + 4.9B \text{ (in db)}$$
$$= 12 + 6.9 + 10 \log B \qquad (53)$$
$$= 18.9 \text{ db} + 10 \log B$$

where R_{CN} is the carrier-to-noise ratio.

A comparison of equations (47), (48) and (53) shows that FM requires 10 db less transmitter power than vestigial-sideband AM, and 12.2 db less power than double-sideband AM. An additional advantage of FM over AM is that higher efficiency power-amplifier stages may be used. An AM transmitter requires Class A power amplifiers to provide linear amplification after modulation while an FM transmitter can use Class C amplifiers. A Class A stage has a maximum plate efficiency of 85 percent. (At the frequency used, the overall efficiency of the power amplifiers in the TV Subsystem was 50 percent.)

d. DIGITAL MODULATION

Pulse-code modulated (PCM) transmission was investigated to obtain a comparison of digital and analog techniques. For good-quality digital television, it is generally accepted that 6-bit PCM is required to minimize quantization noise (contouring). If 6-bits per sample are used at the theoretical minimum sampling rate of twice the highest modulation rate, and 1-bit per cycle is assumed, a bandwidth of 12B is required. Assuming an acceptable word error rate of 1 in 10^4 (i.e., 0.01 percent of the picture elements are wrong), the required bit error rate is determined from the following expression:

$$(1 - P_{WE}) = (1 - P_{BE})^N \qquad (54)$$

where

P_{WE} is the probability that a word is in error;

$(1-P_{WE})$ is the probability that a word is correct;

P_{BE} is the probability that a bit is in error;

$(1-P_{BE})$ is the probability that a bit is correct; and

N is the number of bits per word.

For a low error rate ($P_{BE} \leq 10^{-2}$) the first two terms in the binomial expansion can be used to represent $(1-P_{BE})^N$. Thus,

$$1 - P_{WE} = 1 - NP_{BE} \qquad (55)$$

or

$$P_{BE} = \left(\frac{1}{N}\right) P_{WE} \qquad (56)$$

Substituting 10^{-4} for P_{WE} and 6 for N yields:

$$P_{BE} = \frac{1}{6} \times 10^{-4} \tag{57}$$

In order to achieve this error rate, an S/N of 9.3 db is required in a 6B bandwidth. Therefore, the relative transmitter power for 6-bit PCM is:

$$\begin{aligned} P_{PCM} &= S/N + 12B \text{ (in db)} \\ &= 9.3 + 10.8 + 10 \log B \\ &= 20.1 \text{ db} + 10 \log B \end{aligned} \tag{58}$$

This power can be reduced by using 2 bits per cycle instead of 1 bit per cycle. At 2 bits per cycle, the relative transmitter power is reduced 3 db to 17.1 db + 10 log B.

In summary, there is very little difference in the transmitter power required for PCM or FM. However, PCM had two disadvantages, which led to the choice of FM over PCM. First, there were serious problems to be solved in developing an analog-to-digital converter that operates at 400,000 to 800,000 samples per second. Second, the RF bandwidth required for the PCM system was prohibitive. For a baseband of 6B to 12B (depending on the number of bits per cycle of bandwidth), the RF bandwidth would be 12B to 24B, as opposed to an RF bandwidth of 4.9B for the FM system. A major system constraint was the RF bandwidth limitation of 1 Mc. At this bandwidth, the FM system could support a 200-kc baseband while the PCM system could only support a 42- to 82-kc baseband.

4. Preemphasis Considerations

Preemphasis is utilized in FM transmission to improve the signal-to-noise ratio (S/N). The higher modulating frequencies are boosted to provide more frequency deviation of the carrier than that provided by the lower frequencies. This high-frequency boost is reduced at the receiver, restoring a flat overall frequency characteristic. When the high frequencies are attenuated, the noise picked up by the receiver is also reduced. Since most of the noise occurs at the higher frequencies, the overall S/N is improved by the preemphasis technique. If the increase in S/N is not needed, the deviation, and consequently the RF bandwidth, can be reduced to reestablish the required S/N. A reduction in RF bandwidth is accompanied by a decrease in the transmitter power needed to obtain the desired S/N.

This technique was used in the TV Subsystem where the reduced bandwidth also served to establish adequate guard bands between the video channels and the JPL transponder channel.

A plot of the actual preemphasis and deemphasis used in the Ranger system is shown in Figure 15. If a frequency scale factor of $1{:}2\pi 35$ is used, the networks can be represented by the following Laplace transforms and the schematic diagrams of Figures 16 and 17.

The preemphasis is represented by:

$$\frac{e_o}{e_i} = \frac{S+1}{S+4} \tag{59}$$

The deemphasis is represented by:

$$\frac{e_o}{e_i} = \frac{1}{4}\left(\frac{S+4}{S+1}\right) \tag{60}$$

The FM noise voltage above threshold is directly proportional to frequency; noise power is directly proportional to frequency squared. The total power output of a linear system is given by:

$$\overline{e_n^2} = \frac{1}{2\pi} \int_{-\infty}^{\infty} |H(j\omega)|^2 \, \Phi(j\omega) \, d\omega \tag{61}$$

where $H(j\omega)$ is the impulse response of the network; and

$\Phi(j\omega)$ is the spectral density of the power into the network.

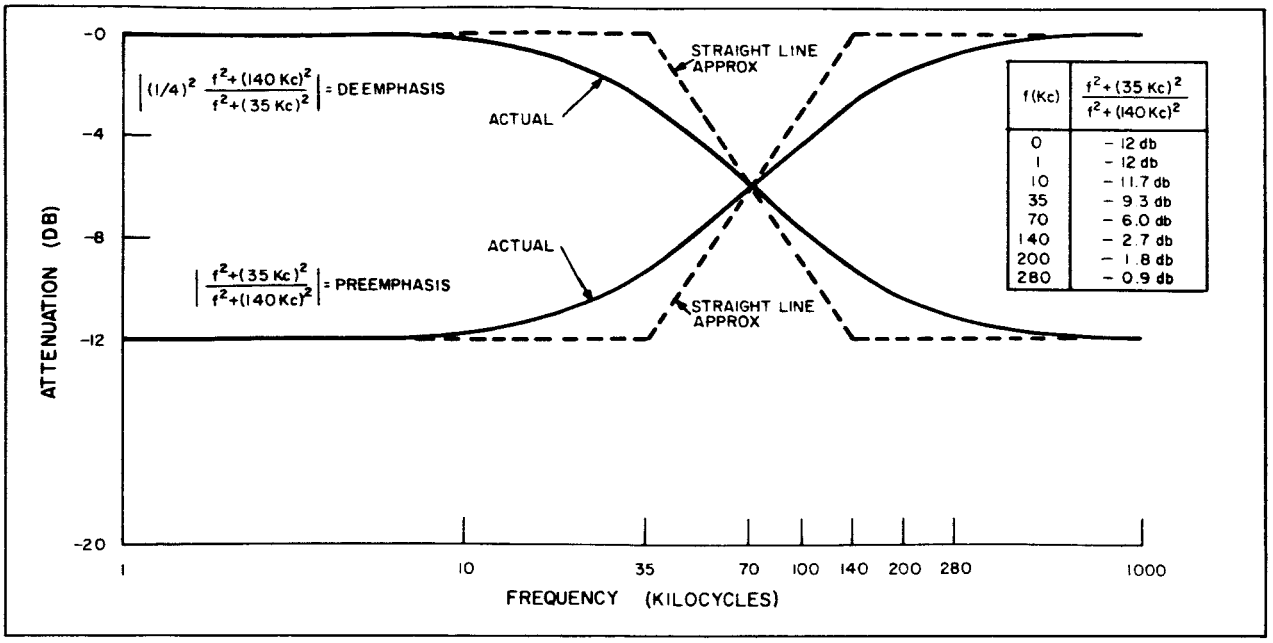

Figure 15. Preemphasis and Deemphasis Versus Frequency

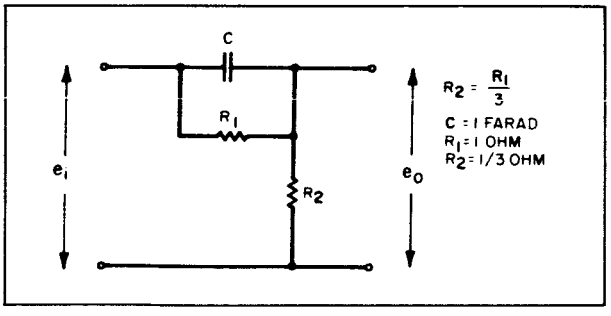

Figure 16. Preemphasis Network

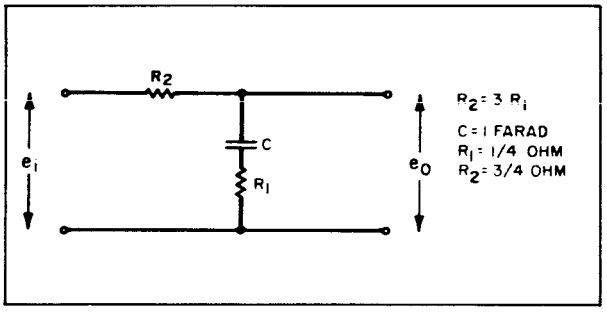

Figure 17. Deemphasis Network

For this analysis, the low-pass filter is assumed to be an ideal filter with a cutoff frequency at 200 kc (or S is equal to 200/35 for the frequency scale factor previously selected). The limits of integration are thus reduced to 200/35 or ±5.7. For a flat system (no deemphasis), $H(j\omega)$ is equal to 1; for a deemphasized system, $H(j\omega)$ is given by:

$$H(j\omega) = \frac{1}{4}\left(\frac{j\omega + 4}{j\omega + 1}\right) \qquad (62)$$

In both cases, $\Phi(j\omega)$ is equal to ω^2. The total noise power output of the flat system is given by:

$$\overline{e_n^2} = \frac{1}{2\pi}\int_{-5.7}^{5.7} \omega^2\, d\omega = \frac{1}{2\pi}\left[\frac{\omega^3}{3}\right]_{-5.7}^{5.7} = \frac{61.7}{\pi} \qquad (63)$$

The total noise power output of the deemphasized system is given by:

$$\overline{e_n^2} = \frac{1}{2\pi} \int_{-5.7}^{5.7} \frac{1}{16} \frac{(\omega^2 + 16)}{(\omega^2 + 1)} \omega^2 \, d\omega \qquad (64)$$

$$= \left(\frac{1}{2\pi}\right)\left(\frac{1}{16}\right) \int_{-5.7}^{5.7} \left[\omega^2 + 15 - \frac{15}{\omega^2 + 1}\right] d\omega$$

$$= \left(\frac{1}{\pi}\right)\left(\frac{1}{16}\right) \left[\frac{\omega^3}{3} + 15\omega - 15 \arctan \omega\right]_{\omega = 0}^{\omega = 5.7}$$

$$= \frac{7.9}{\pi}$$

Thus, the total noise power reduction achieved with deemphasis is equal to the factor $\frac{61.7}{7.9}$ or 8.93 db. With this amount of preemphasis improvement, the FM improvement required was only 4.0 db. The modulation index (at low frequencies) was therefore reduced from 1.45 to 0.65. With these parameters, the communication system was able to transmit and receive a 200-kc video modulation bandwidth with an optimum signal-to-noise ratio, and provide an 80-kc guard band on either side of the JPL beacon, and a 20-kc guard band at the outer edges of the band. The channel allocations and the RF spectrum are shown in Figure 18. The system also provided sufficient bandwidth to permit the use of a 225-kc subcarrier for the transmission of engineering telemetry.

5. Link Analysis

The RF channel assigned to the Ranger Spacecraft was a 2-Mc band centered at 960 Mc. The use of this channel posed no special problems for the type of communications required by the Ranger mission. In fact, 960 Mc is near the theoretical noise figure limit of the

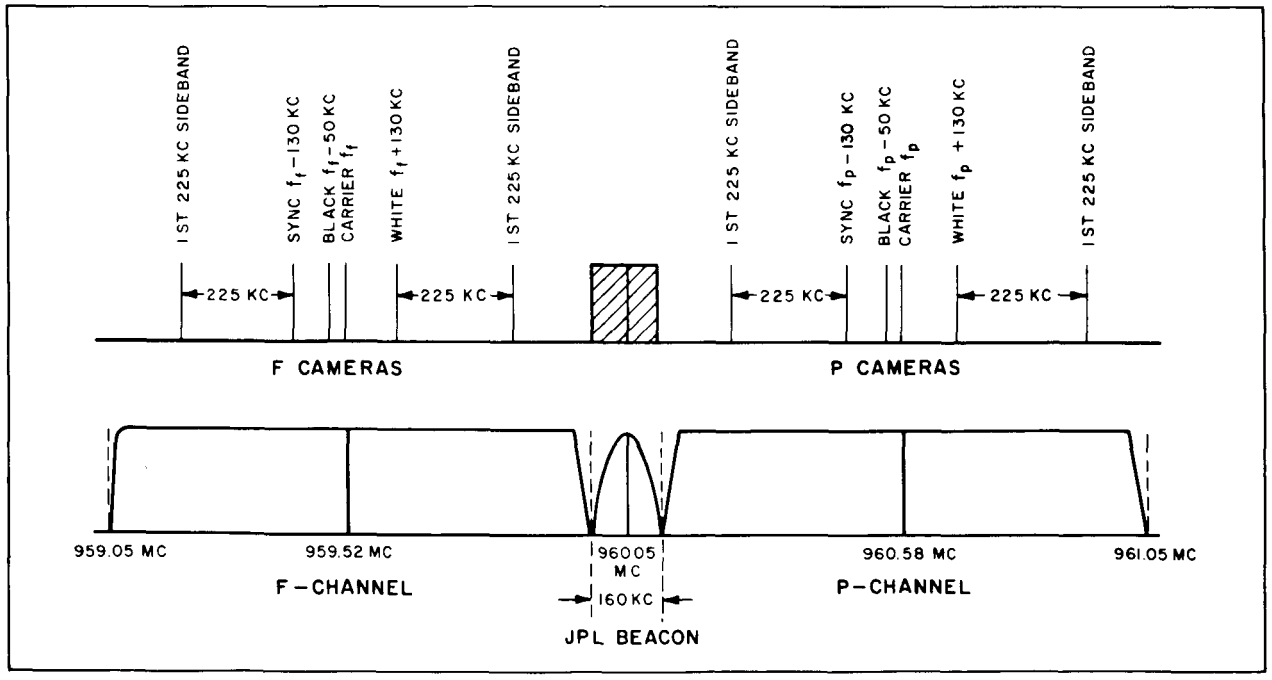

Figure 18. Channel Allocations and RF Spectrum

Maser preamplifier used in the ground station receiving system. (The noise sources occurring at various frequencies are shown in Figure 19.) This frequency was also an optimum choice in terms of the state of development and reliability of space vehicle transmitters.

A major term considered in the link analysis was the path between antennas. This loss is given by:

$$\frac{P_R}{P_T} = \left(\frac{\lambda^2}{4\pi d^2}\right) G_T G_R \qquad (65)$$

where

λ is the wavelength, which is equal to approximately 0.3 meter;

d is the Earth-to-Moon distance, which is equal to 4.02×18^8 meters;

G_T is the gain in db of the transmitting antenna over an isotropic antenna;

G_R is the gain in db of the receiving antenna over an isotropic antenna;

P_T is the transmitted power; and

G_R is the received power.

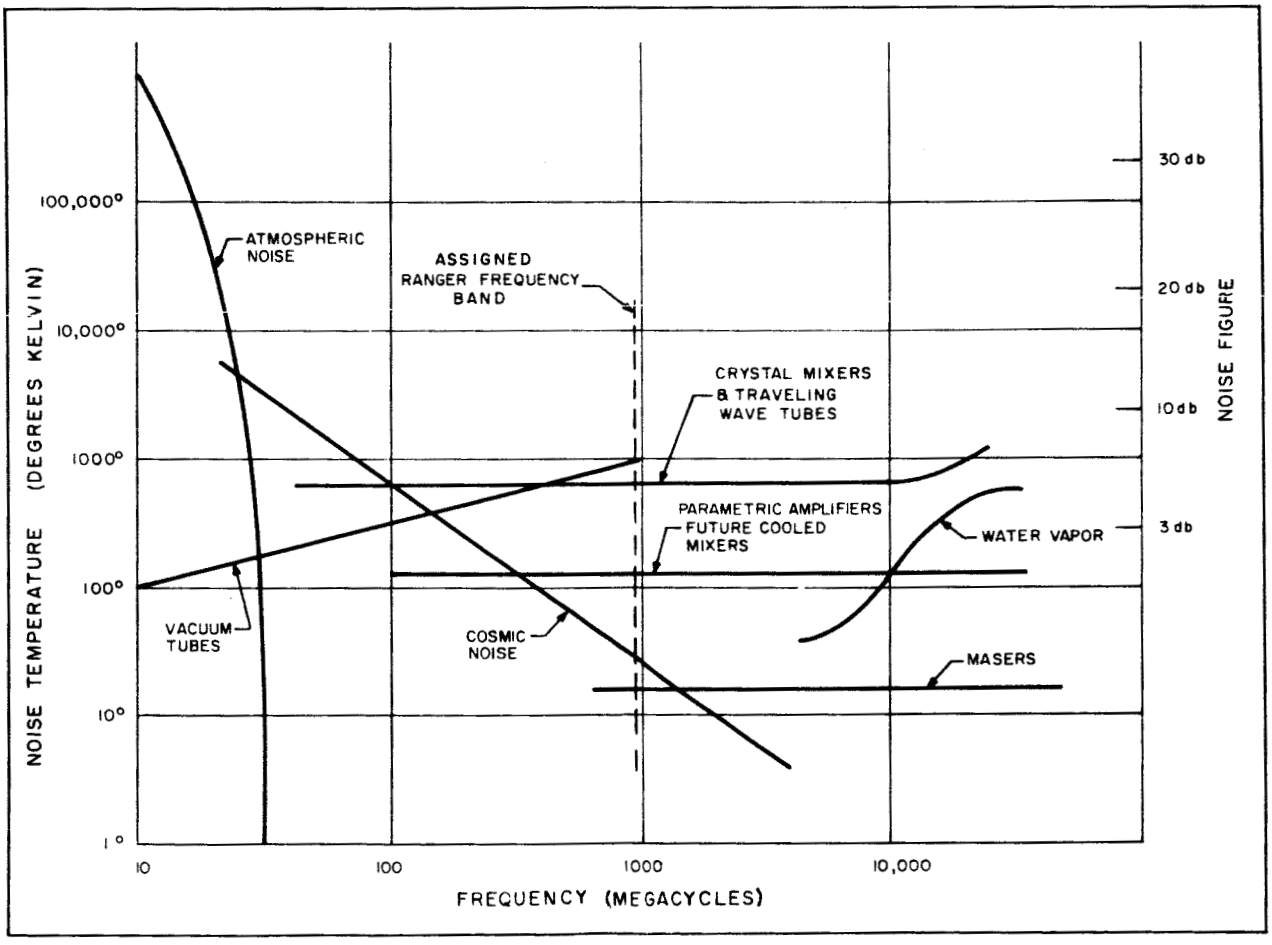

Figure 19. Noise Densities and Their Sources

Therefore,

$$\frac{P_R}{P_T} = -204.5\ db + G_T + G_R$$

Another term considered was receiver noise power, which is defined as

$$P_N = 10\ log\ \sigma + 10\ log\ T_E + 10\ log\ B \qquad (66)$$

where

P_N is the receiver noise power;

σ is Boltzmann's constant;

T_E is the effective noise temperature, which is equal to T_A plus T_R, or 131.5° K;

T_A is the effective temperature at the antenna terminals when connected to a perfectly noiseless receiver;

T_R is the effective noise temperature of the receiver, referred to T_A; and

B is the noise bandwidth, which is equal to 800 ± 100 kc.

Evaluating equation (66) yields:

$$P_N = -148.4\ dbw$$

All of the terms in the link analysis are listed in Table 2. This tabulation shows that the carrier-to-noise ratio exceeds threshold by approximately 4 db, even when the worst-case tolerances are used.

6. Configuration of the TV Subsystem Communications in the Spacecraft

Two 900-kc channels, one on either side of the JPL beacon, were available for the transmission of video information. In order to use these channels to obtain the maximum amount of data, it was decided to operate two camera and transmitter chains, each occupying a separate channel, and each completely independent of the other. This arrangement is shown in Figure 20, which shows the two channels being combined in a Four-Port Hybrid. The composite video signal from the Four-Port Hybrid is combined with the JPL

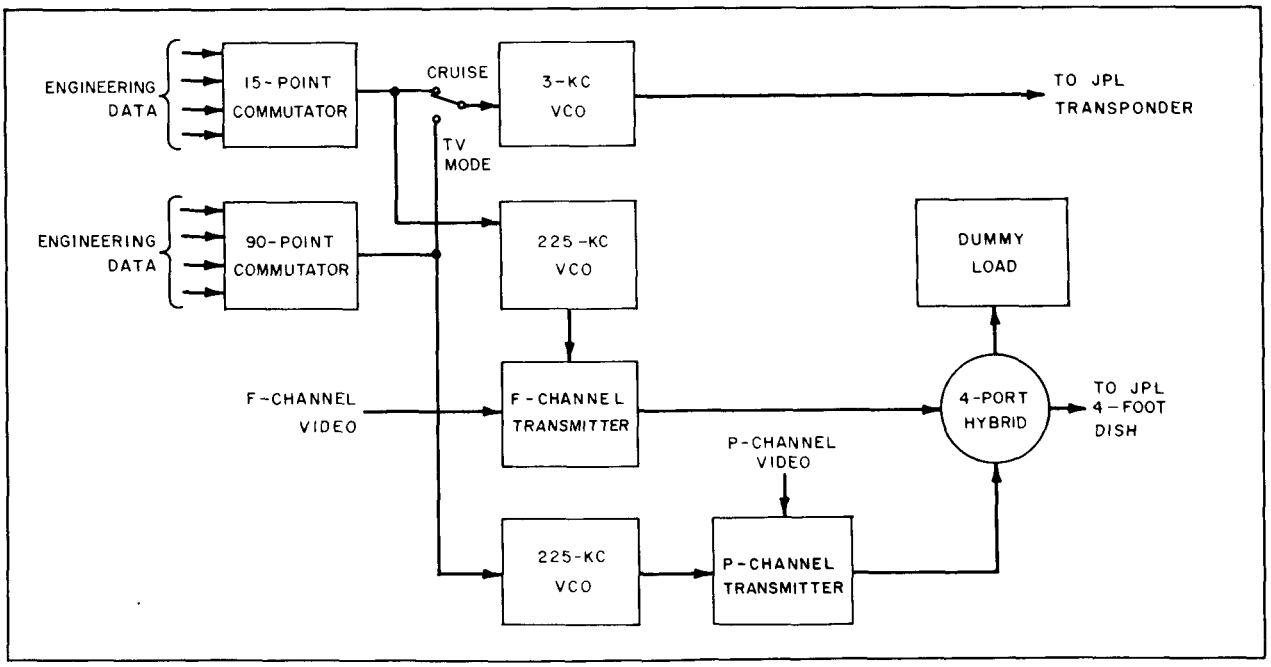

Figure 20. Functional Block Diagram of the TV Subsystem Communications in the Spacecraft

transponder signal in a directional coupler before being transmitted over the high-gain antenna of the spacecraft.

The foregoing method of combining the three channels (F-Channel, P-Channel, and JPL transponder) is passive; i.e., no RF switching is required. The use of the Four-Port Hybrid resulted in a 3-db loss in each video channel; however, the close proximity of the channels precluded the use of diplexers (filters) for combining the channels. Also, the full on-line redundancy achieved by the use of the Four-Port Hybrid provided the highest probability that the last group of pictures (closest to the lunar surface) would be transmitted.

With the basic configuration described, link analysis indicated the need for a power amplifier with an RF output capability of 60 watts. The complete transmitter chain consisted of an FM modulator, which was crystal-controlled at 20 Mc; two frequency multipliers (a X4 and a X12); an intermediate power amplifier; a 60-watt power amplifier; a DC-to-DC converter, which provided the required operating voltages from the TV Subsystem batteries; and a telemetry processor, which conditioned the telemetry data and regulated the power amplifier cathode current. The block diagram of a single transmitter chain (F-Channel or P-Channel) is shown in Figure 21.

D. ANALYSIS OF OVERALL TV SUBSYSTEM

1. Signal-to-Noise Ratio

The signal-to-noise ratio at the output of the camera depends on the lunar scene luminance and is given as

$$\frac{S_{p\text{-}p}}{N_{rms}} = \frac{I_s}{I_N} = \frac{I_k\left(\frac{B_l}{B_k}\right)^{\gamma}}{I_N} = K\left(\frac{B_l}{B_k}\right)^{\gamma} \qquad (67)$$

where

$S_{p\text{-}p}$ is the peak-to-peak video signal;

N_{rms} is the rms noise signal;

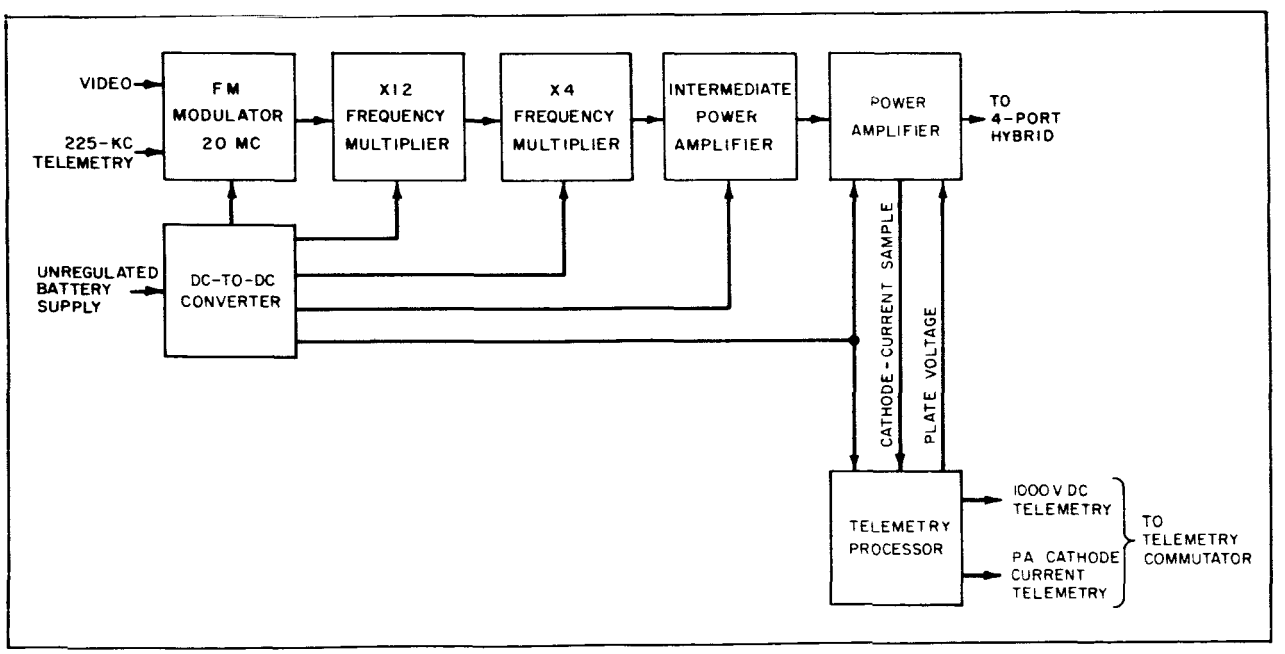

Figure 21. Block Diagram of a Single Transmitter Chain (F-Channel or P-Channel)

I_s is the vidicon target current due to the video signal;

I_N is the vidicon target current due to noise;

I_K is the vidicon target current due to maximum illumination;

B_K is the value of maximum illumination to which system gain is adjusted;

B_I is the actual illumination encountered;

γ is the vidicon transfer function; and

K is the ratio $\frac{I_K}{I_N}$.

The signal-to-noise ratio of the spacecraft communication chain, independent of the camera is given as

$$\frac{S_{p\text{-}p}}{N_{p\text{-}p}} = \left(\frac{C}{N}\right)\left(\frac{F_D}{F_M}\right)\sqrt{\frac{3B_{WIF}}{2F_M}} \qquad (68)$$

where

$N_{p\text{-}p}$ is the peak-to-peak noise signal;

$\frac{C}{N}$ is the carrier-to-noise ratio;

F_D is the deviation frequency;

F_M is the video frequency; and

B_{WIF} is the IF bandwidth.

In order to obtain proper operation of the TV Subsystem, the gain of the video amplifier in the camera is adjusted so that the maximum illumination expected will provide 1.5 volts at the output of the video combiner. At the same time, the deviation frequency F_D is set at ±130 kilocycles for a ±0.75-volt DC input to the modulator. The performance of the TV Subsystem is related to two items, which are, (1) the value of maximum illumination B_K to which system gain is adjusted, and (2) the actual scene illumination B_I encountered.

Therefore,

$$V_O = V_K\left(\frac{B_I}{B_K}\right)^{\gamma} \qquad (69)$$

where

V_O is the voltage at the output of the video combiner; and

V_K is the voltage at the output of the video combiner due to maximum illumination.

and

$$\frac{V_o}{V_K} = \frac{F_I}{F_{DK}} \qquad (70)$$

where F_I is the frequency deviation due to the actual illumination(B_I); and

F_{DK} is the frequency deviation due to maximum illumination.

Substituting for V_O from equation (69), equation (70) becomes:

$$\frac{V_K\left(\frac{B_I}{B_K}\right)^{\gamma}}{V_K} = \frac{F_I}{F_{DK}} \qquad (71)$$

Therefore,

$$F_I = F_{DK}\left(\frac{B_I}{B_K}\right)^{\gamma} \qquad (72)$$

The deviation frequency(F_I), due to the actual illumination, can be substituted for F_D in equation (68). Substituting for F_I from equation (72) to equation (68) yields:

$$\frac{S_{p\text{-}p}}{N_{p\text{-}p}} = \left(\frac{C}{N}\right)\frac{F_{DK}\left(\frac{B_I}{B_K}\right)^{\gamma}}{F_M}\sqrt{\frac{3B_{WIF}}{2F_M}} \qquad (73)$$

which gives the combined signal-to-noise ratio of the camera and the communication chain.

An evaluation of equation (73) reveals that the signal-to-noise ratio of the TV Subsystem can be maximized if the ratio $\frac{B_I}{B_K}$ is maximized. This function can be performed by an automatic aperture control that adjusts for the actual illumination B_I and maintains the ratio $\frac{B_I}{B_K}$ at a maximum value. For systems that have to record a wide range of scene illuminance, such a technique would be essential. In the case of Ranger, however, the range of anticipated illumination did not exceed the dynamic range of the vidicon. Moreover, an automatic aperture control could not be used because maximum lens aperture and maximum vidicon sensitivity were required for a mission close to the lunar terminator.

Another possibility is to maximize the signal-to-noise ratio by causing (F_{DK}) (equation 73) to vary inversely with the ratio $\frac{B_I}{B_K}$. This can be accomplished in either of two ways. First, the video amplifier gain can be controlled automatically to maintain the ratio $\frac{V_O}{V_K}$ at its maximum value. Second, the maximum deviation frequency (F_{DK}) can be altered automatically as a function of the illumination. Either of these control problems could be solved by the use of an auxiliary set of optics and a sensor with the same field-of-view as the vidicon. This type of auxiliary equipment is necessary to permit the fast response required with changing scene illumination in the terminal phase of the picture-taking mission. The foregoing arrangement also requires the use of electromechanical devices to synthesize the control problem. The additional equipment and the prospect of moving parts weighed heavily against this technique.

The control problem could also be synthesized by modifying the video gain or the maximum deviation frequency in a few discrete steps as a function of vidicon illumination. As an alternative to electromechanical devices, the control elements could be limited to diodes and lumped circuit parameters. If an effective means could be conceived to integrate sample output data from the vidicon target image, the video itself could be the control signal. The major drawbacks to any control technique that utilizes an auxiliary photometric sensor are the additional equipment complexity and the problems of setting and maintaining the precise calibration required.

In the interest of simplicity and reliability, a third control method was adopted for the TV Subsystem. In this method, the maximum deviation frequency and the gain of the video amplifier are fixed. This technique is most effective when the spacecraft trajectory can be controlled to limit viewing to those areas of the lunar surface that provide illumination within the dynamic range of the camera. However, there was the possibility of a nonstandard mission in which the point of impact would be closer to the subsolar point than originally planned. There was also the possibility that the values of lunar brightness predicted for close viewing of the lunar surface would be in error. Complete allowances could be made for these two nonstandard conditions, within the dynamic range capability of the camera, by setting the video amplifier gains and the maximum frequency deviation to correspond to the highest illumination possible at the subsolar point.

If complete allowances were made for the worst-case nonstandard conditions, the reduction in signal-to-noise ratio during a standard mission would jeopardize the quality of the photographs. Therefore, allowances were only made for moderately nonstandard conditions. The video gain of the 75-mm f/2 cameras on Ranger VI and Ranger VII was set for a B_K value of 2700 footlamberts; the gain of the 25-mm f/0.95 cameras was set for 650 footlamberts. After the successful flight of Ranger VII, there was increased confidence in accomplishing the desired spacecraft trajectory. As a result,

less emphasis was placed on nonstandard missions, and the gain of the 75-mm f/2 cameras was set for a B_K of 1500 footlamberts, which provided a corresponding improvement in the signal-to-noise ratio.

2. Sine-Wave Response of the TV Subsystem

The TV Subsystem contains several electro-optical transducing systems in cascade. These systems transform the real scene into a two-dimensional image, which is ultimately preserved in the primary film recording at the ground station. The elements of the electro-optical system are shown in Figure 22. The ability of these elements to reproduce an image can be defined by the two-dimensional point spread function of the image at the output of the element. The image at the output of the total system is the result of a convolution (i.e., the mathematical process of scanning one function with another) of the cascaded point spread functions. The point spread function is defined as the resolving aperture of the image-forming device, referred to the image plane.

The accuracy of reproduction of real scene detail is determined by the geometry and intensity distribution of the point image. Each of the elements of the imaging system, such as the lenses; the vidicon; the kinescope; and the photographic film, form point images of a finite size. If the point image of each of these elements is described by a two-dimensional point-spread function, the point-spread function of the final image is the result of the convolution of the point-spread functions of the cascaded elements. The light flux distribution in the final image is readily computed by scanning the flux distribution function that describes the real scene with the function that described the point-spread function of the imaging system.

Since it is quite difficult to develop the two-dimensional function that represents the scene, optical systems are usually analyzed by testing with test objects that have an intensity distribution of one dimension only. In the test, the point image of the optical system scans the one-dimensional test object to produce a line image that is described by its line transmittance function. The output produced by two optical systems with line transmittance functions in series is the convolution of the line transmittance functions.

The intensity distribution of a one-dimensional line-pattern object can be expressed by a one-dimensional periodic function, which is a Fourier series with a fixed term and a series of harmonic sine-wave terms (or line spectrum). The intensity function of the image has the same line spectrum, but differs in amplitude and phase. The differences in amplitude and phase are characteristic of the particular aperture. If test objects are used that have a constant amplitude in one dimension and

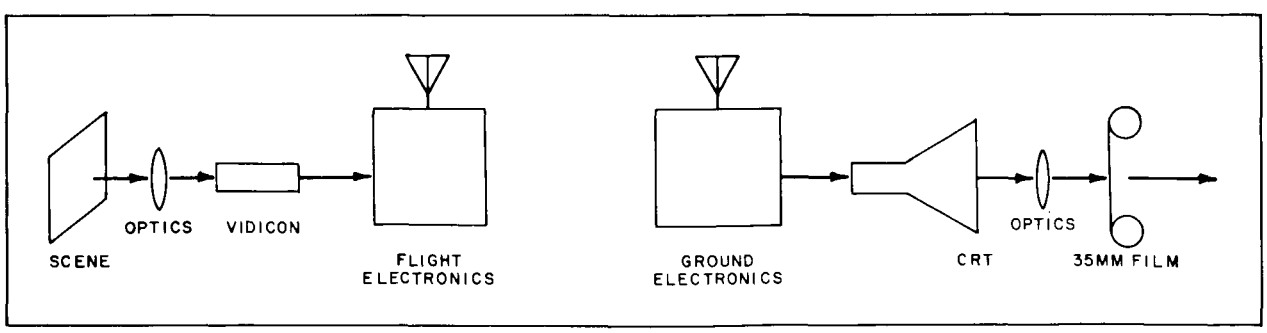

Figure 22. Elements of the Electro-Optical System

an intensity distribution of only one sine-wave term, the resulting image is the same periodic sine wave, and differs from the test object in amplitude and phase only.

A normalized Fourier spectrum of the transform of the aperture is described by the continuous function.

$$r_{\tilde{\psi}}, \theta = g(N) \qquad (74)$$

where

$r_{\tilde{\psi}}$ is the sine-wave response factor of the aperture;

θ is the phase angle of the aperture; and

N is the line number equal to twice the spatial frequency that is obtained by convolution with sine-wave objects of constant amplitude and spatial frequencies from zero to infinity.

The Fourier spectrum is a description of the aperture properties in the frequency domain and is the transform of the transmittance function in the space domain. The cascading of apertures in the frequency domain can be described by convoluting the Fourier transforms of the individual apertures. The impulse function (or time function), $I = f(t)$, for electrical circuit elements is analogous to the aperture functions of the optical elements. The frequency-domain transforms of the electrical and the optical elements can be combined by convolution.

In order to determine the value of the sine-wave response characteristic ($r_{\tilde{\psi}}$) of a television system, a one-dimensional sine-wave test pattern of period N_i is aligned so that the scanning direction is parallel to the sine function. The output ($\tilde{\psi}_{N_i}$) of the system at the test object period (N_i) is then compared with the output ($\tilde{\psi}_{N_o}$) of a reference period (N_o) to yield the sine-wave response characteristic ($r_{\tilde{\psi}}$). Thus

$$r_{\tilde{\psi}} = \frac{\tilde{\psi}_{N_i}}{\tilde{\psi}_{N_o}} \qquad (75)$$

The sine-wave response of the various elements of the TV Subsystem was calculated using the foregoing methods. In comparing the sine-wave response of the photo-optical elements, it became clear that the vidicon was the limiting factor in reproducing scene detail. However, the analysis highlighted the need for exercising great care in selecting the other system elements and in specifying the bandpass of the electrical channel, in order to prevent further reduction in the response of the system. With this design goal in mind, each of the major elements of the system was evaluated and specified. The electrical channel of the TV Subsystem was specified to have a uniform response that would decrease no further than 3 db at the edge of the passband of the scanning aperture. The edge of the passband was defined as the point where the sine-wave response ($r_{\tilde{\psi}}$) decreases from unity to zero. In practice, this point corresponds to a relative resolution response* of 2 percent. The bandpass of the electrical channel is the resultant of the combined bandpasses of the individual channel elements in series, as shown in Figure 23.

3. Evaluation of Translational Smear

Translational smear of pictures is caused by the displacement of the image plane relative to the object during the exposure time of the camera. This motion results in a reduction of image sharpness. A quantitative evaluation of smear was derived with the aid of the model shown in Figure 24.

The figure represents a three-dimensional model of the spacecraft-Moon geometry in the final seconds before impact. The model is a tetrahedron, which is formed by the intersection of four triangular planes. Three of these planes are of interest in this analysis. The lunar surface is represented by the plane

*The response to a given number of TV lines normalized with respect to a black bar on a white field.

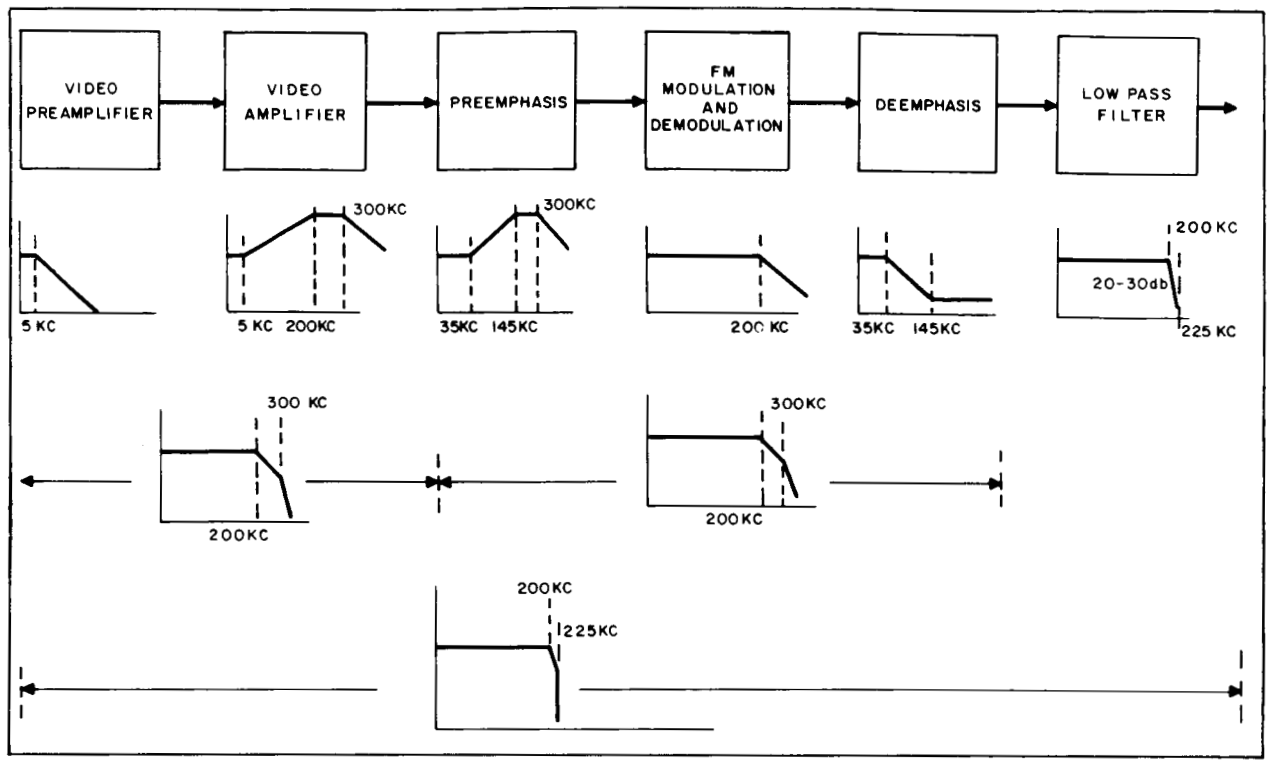

Figure 23. Bandpass of the Electrical Channel

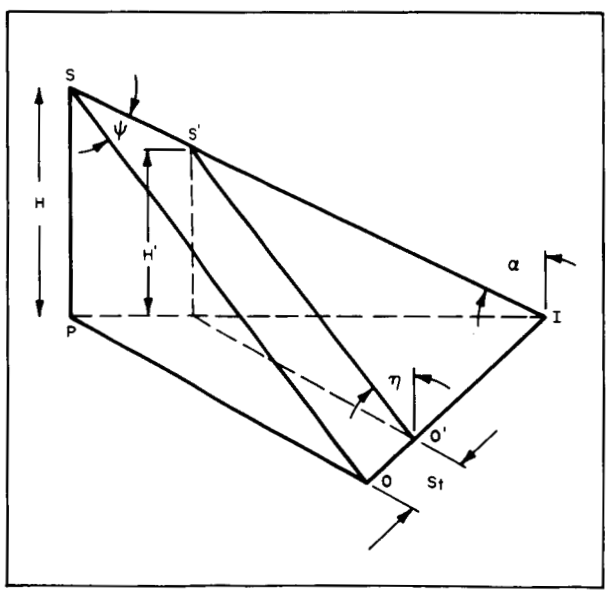

Figure 24. Spacecraft-Moon Geometry during Final Picture-Taking Phase

PIO. The spacecraft trajectory relative to the lunar surface is described by plane *SPI*. The third plane of interest is *SOI*. This plane is bounded by the spacecraft-to-impact distance, the camera-to-surface distance along the camera optical axis (range), and the path formed by the sweep of the optical axis along the lunar surface.

The spacecraft is at position *S* at the beginning of shutter actuation, and at position *S'* when the exposure is completed. The altitude of the spacecraft at point *S* is represented by *H*, and at point *S'* by *H'*. Point *I* is the spacecraft's impact point on the lunar surface.

In order to analyze image smear, only one point in the image plane can be considered at a time. Thus, a single optical ray to a point on the image plane is shown intersecting the lunar surface at point *O* when the spacecraft is at position *S*, and a ray to the same point

on the image plane is shown intersecting the lunar surface at point O' when the spacecraft is at position S'. The smear (S_t) of the point on the image plane is the distance between points O and O'. The distance SO is the camera range and is equal to $\frac{H}{\cos \eta}$.

All values in this analysis are normalized with respect to the distance (SI) that the spacecraft travels before impact. These normalized values make it possible to calculate a relative velocity for: (1) the rate of approach of the spacecraft to the lunar surface; (2) the rate of approach of the spacecraft ground track (PI) to the impact point; and (3) the rate of the intersection formed by the camera optical axis and the lunar surface as it approaches the impact point. The velocity of this intersection can be used directly to determine the smear at the corresponding point in the image plane.

If a normalized value of 1 is assigned to the distance SI, the altitude of the spacecraft is equal to $\cos \alpha$, and the distance traveled by the ground track of the spacecraft is equal to $\sin \alpha$. The camera range (SO) is equal to $\frac{\cos \alpha}{\cos \eta}$, and the ground distance (PO) to the camera axis intersection is equal to $\cos \alpha \tan \eta$. The magnitude of the line of smear (OI), by the law of cosines is

$$(OI) = \sqrt{1 + \left(\frac{\cos \alpha}{\cos \eta}\right)^2 - 2\left(\frac{\cos \alpha}{\cos \eta}\right) \cos \psi} \qquad (76)$$

For trajectories where the angle ψ between the camera optical axis and the velocity vector of the spacecraft is small (less than 10 degrees), the distance along the spacecraft velocity vector and the camera range are of nearly equal magnitude. The normalized length of OI, in this case, is closely approximated by $\sin \psi$. Thus,

$$S_t = V(\Delta t) \sin \psi \qquad (77)$$

where

S_t is the smear distance covered by the camera axis along line OI during one picture exposure;

V is the velocity of the spacecraft along the velocity vector SI; and

Δt is the exposure time.

A plot of S_t versus ψ for different values of Δt is shown in Figure 25.

The smear expressed as optical line pairs is given by:

$$\gamma_t = \frac{S_t}{R_i} \qquad (78)$$

where

γ_t is the smear in optical line pairs; and

R_i is the intrinsic resolution in meters per optical line pair,

and

$$R_i = \frac{Vt \cos \alpha}{FN_m \cos^2 \eta} \qquad (79)$$

where

F is the focal length of the camera in mm;

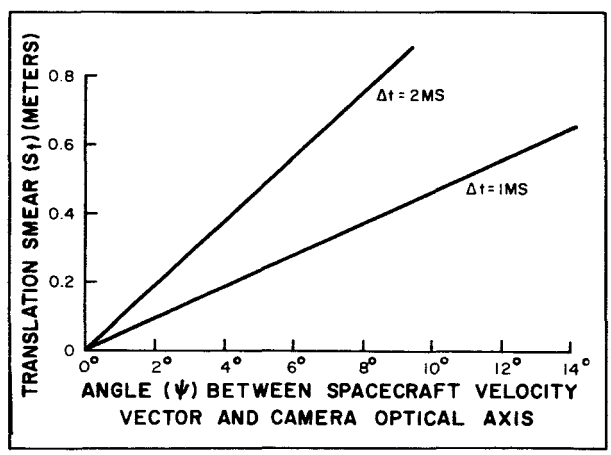

Figure 25. Translational Smear as Function of the ψ Angle and Exposure Time

t is the time to impact in seconds;

N_m is the line density of the scanned image in optical line pairs per mm, and is a constant for the system.

Substituting from equations (77) and (79) to equation (78) yields

$$\gamma_t = V(\Delta t) \sin \psi \left(\frac{FN_m \cos^2 \eta}{Vt \cos \alpha} \right) \tag{80}$$

The term V cancels out of equation (80) yielding

$$\gamma_t = (\Delta t) \sin \psi \left(\frac{FN_m \cos^2 \eta}{t \cos \alpha} \right) \tag{81}$$

Since η is almost equal to γ for a ψ of less than 10 degrees, equation (81) is simplified to

$$\gamma_t = \frac{FN_m \cos \eta \cdot \sin \psi (\Delta t)}{t} \tag{82}$$

For typical values of $\cos \eta = 1$; $\psi = 1°$; $\Delta t = 2$ milliseconds:

$N_m = 35.7$ optical line pairs per mm;

$F = 75$ mm; and

$\gamma_t = \frac{0.0932}{t}$ optical line pairs.

For a focal length (F) of 25 mm

$$\gamma_t = \frac{0.031}{t} \text{ optical line pairs}$$

A plot of smear (γ_t) and intrinsic resolution R_i versus time-to-impact (t) is shown in Figure 26.

4. Resolution

The degree of resolution that can be obtained of lunar surface features is a function of the parameters shown in Figure 27. The resolution (R_n) on a surface normal to the camera optical axis is given by:

$$R_n = \frac{H}{FN_m \cos \eta} \tag{83}$$

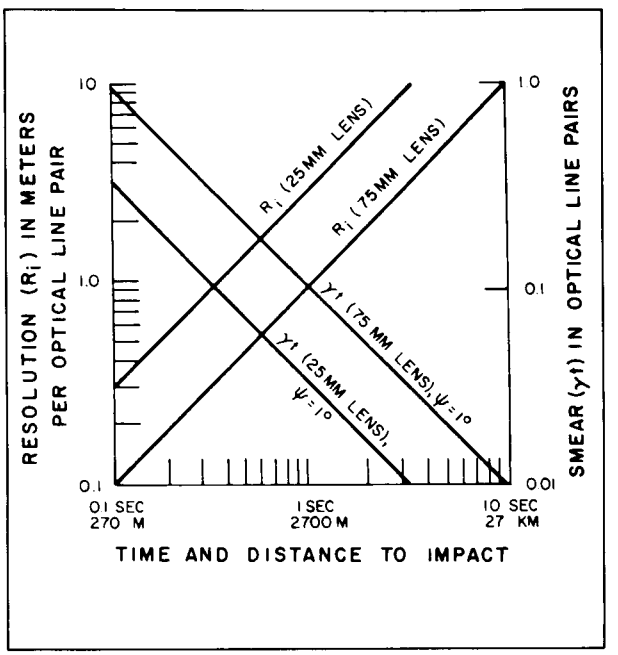

Figure 26. Smear and Intrinsic Resolution versus Time-to-Impact

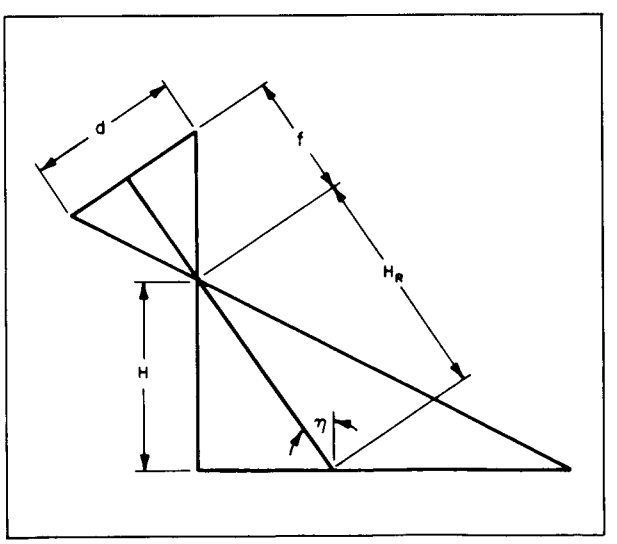

Figure 27. Surface Resolution Model

where

H is the spacecraft altitude above the lunar surface;

N_m^* is the line density of the scanned image in optical line pairs per mm; and

η is the angle between the normal to the lunar surface and the camera optical axis.

The resolution of the lunar surface, however, varies from equation (83) by a factor of $\frac{1}{\cos \eta}$, because of the larger area observed. This surface resolution is known as the intrinsic resolution(R_i) of the system and is expressed as

$$R_i = \frac{H}{FN_m \cos^2 \eta} \tag{84}$$

The altitude (H) of the spacecraft can be expressed as

$$H = Vt \cos \alpha \tag{85}$$

*N_m is also defined in TV lines per mm as

$$N_m = \frac{\text{No. of TV lines}}{nd}$$

where d is the raster height in mm and n is the number of TV lines per optical line pair.

where

V is the velocity of the spacecraft;

t is the time-to-go before impact; and

α is the angle between the velocity vector and the normal to the lunar surface at the impact point.

Substituting for H from equation (85), equation (84) becomes

$$R_i = \frac{Vt \cos \alpha}{FN_m \cos^2 \eta} \tag{86}$$

The curve in Figure 28 shows the velocity profile of the spacecraft for the terminal phase of a typical trajectory. Resolutions(R_i) obtained for various values of focal length (F) during the terminal phase are listed in Table 3.

5. Lens Selection

The selection of a lens for the mission was greatly influenced by the requirement that the lens must either be already qualified for space applications, or be of such design that qualification would be a short-time process. This

TABLE 3
INTRINSIC RESOLUTION (METERS PER OPTICAL LINE PAIR)

Time to Impact (seconds)	Altitude in Meters	Focal Length		
		25-mm	75-mm	150-mm
1.0	2700	3.00	1.00	0.50
0.5	1300	1.50	0.50	0.25
0.4	1080	1.20	0.40	0.20
0.3	710	0.90	0.30	0.15
0.2	541	0.60	0.20	0.10
0.1	270	0.30	0.10	0.05

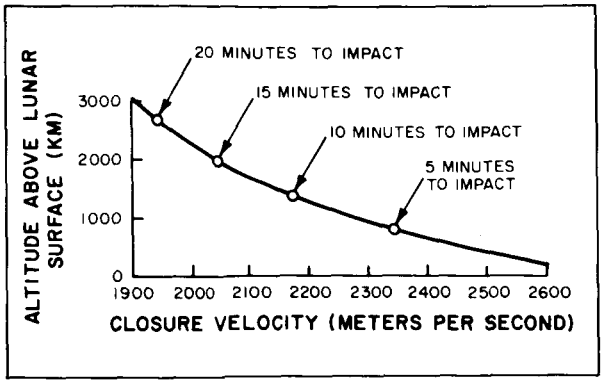

Figure 28. Spacecraft Lunar Closure Velocity as a Function of Altitude

requirement was imposed because the schedule for the fabrication of hardware did not allow sufficient time for a lens development program.

Preliminary studies indicated the need for a large aperture lens to provide an adequate signal-to-noise ratio. However, lens weight increases approximately as the cube of the lens diameter, and a heavier lens requires a heavier structure and camera housing. Thus, the weight limitations imposed on the TV Subsystem eliminated the use of lenses with long focal length.

Optical performance factors such as the modulation transfer function, the sine-wave response, and the off-axis illumination weighed heavily in the choice of a lens. Two lenses in the 75-mm f/2 class were considered: the Bausch and Lomb Super Baltar and the Elgeet Cine-Raptar. These lenses had equal prospects of being adapted mechanically to the rigors of the space environment. The axial and edge-of-format response was measured for each lens. These responses, as compared to the sine-wave response of the vidicon, are shown in Figures 29 and 30. The Elgeet lens had superior on-axis response, but the off-axis response fell off rapidly. The off-axis data are shown in the graph inserts of Figures 29 and 30. The Bausch and Lomb lens exhibited the best overall performance and was therefore selected for use in the F- and P-Cameras.

Attention was then directed to the selection of a second lens of larger aperture for some of the TV Subsystem cameras. The use of two different lens types in the system expanded the capability of the TV Subsystem to accommodate a wide range of scene luminance, and ensured that adequate pictures of the lunar surface would be obtained even if the range of possible impact areas extended from the subsolar point to within 10 degrees of the terminator. The lens selected for this purpose was an Angenieux 25-mm f/0.9 lens. The modulation transfer function and the off-axis illumination characteristics for this lens are shown in Figure 31. The Angenieux lens provided a wide field-of-view and increased camera sensitivity to the extent that shadow detail with an average luminance of only 50 foot-candles could be recorded.

6. Selection of Vidicon Scanning Rate and Frame Time

The values of horizontal sweep rate and vertical frame time are selected on the basis of the video-bandwidth, the number of TV lines in the picture, the required retrace time for the horizontal sweep, the aspect ratio and the Kell factor. The aspect ratio selected for the Ranger cameras was unity, since a square format allows the maximum photoconductor area to be scanned in a given time. The Kell factor (k_v) is given as

$$k_v = \frac{N}{N_s} \qquad (87)$$

where N_s is the number of scan lines required to produce the desired resolution; and

N is the desired resolution in TV lines.

This constant has been determined experimentally to have a value of 0.707.

The time duration of the smallest TV element on a horizontal line is determined by the bandwidth (B) and is equal to $\frac{1}{2B}$. The time to scan

one horizontal line (t_h) is, therefore,

$$t_h = N\left(\frac{H}{V}\right)\left(\frac{1}{2B}\right) = \frac{k_h}{f_h} \qquad (88)$$

where N is the number of TV lines in the picture. (N has a value of 800 for the F-Cameras and 200 for the P-Cameras);

$\frac{H}{V}$ is the aspect ratio, which has a value of 1;

f_h is the horizontal sweep frequency; and

k_h is given by

$$k_h = \frac{t_h}{t_h + t_{hr}}$$

where t_{hr} is the horizontal retrace time.

The vertical frame time, or the time to read-out the picture (T_R), is given by

$$T_R = \frac{t_h}{k_h} \bullet N_S \qquad (89)$$

Substituting for t_h from equation (88) and for N_S from equation (87) yields:

$$T_R = \frac{N}{2B} \bullet \frac{H}{V} \bullet \frac{1}{k_h} \bullet \frac{N}{k_v}$$

Therefore,

$$T_R = \frac{N^2}{2Bk_hk_v} \bullet \frac{H}{V} \qquad (90)$$

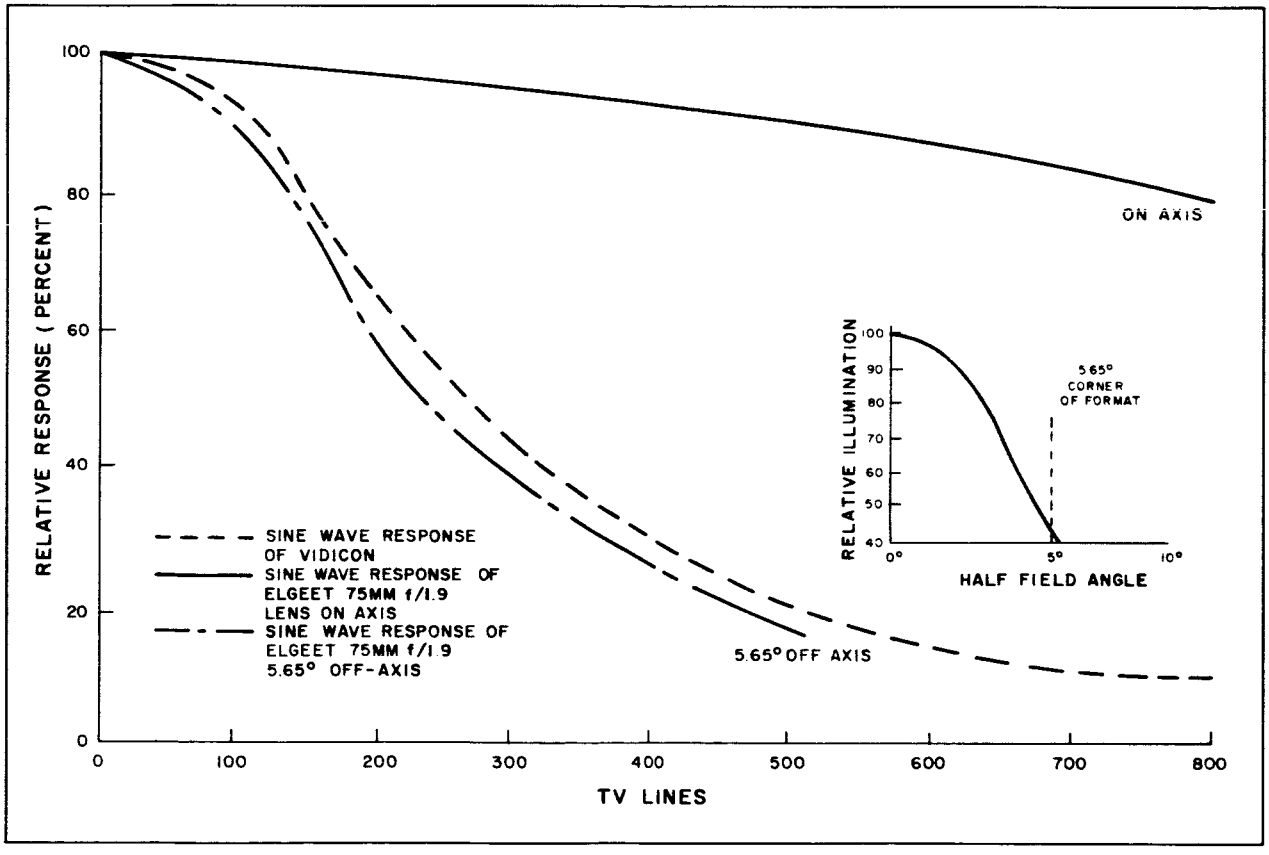

Figure 29. Sine-Wave Response of Elgeet 75-mm f/1.9 Lens

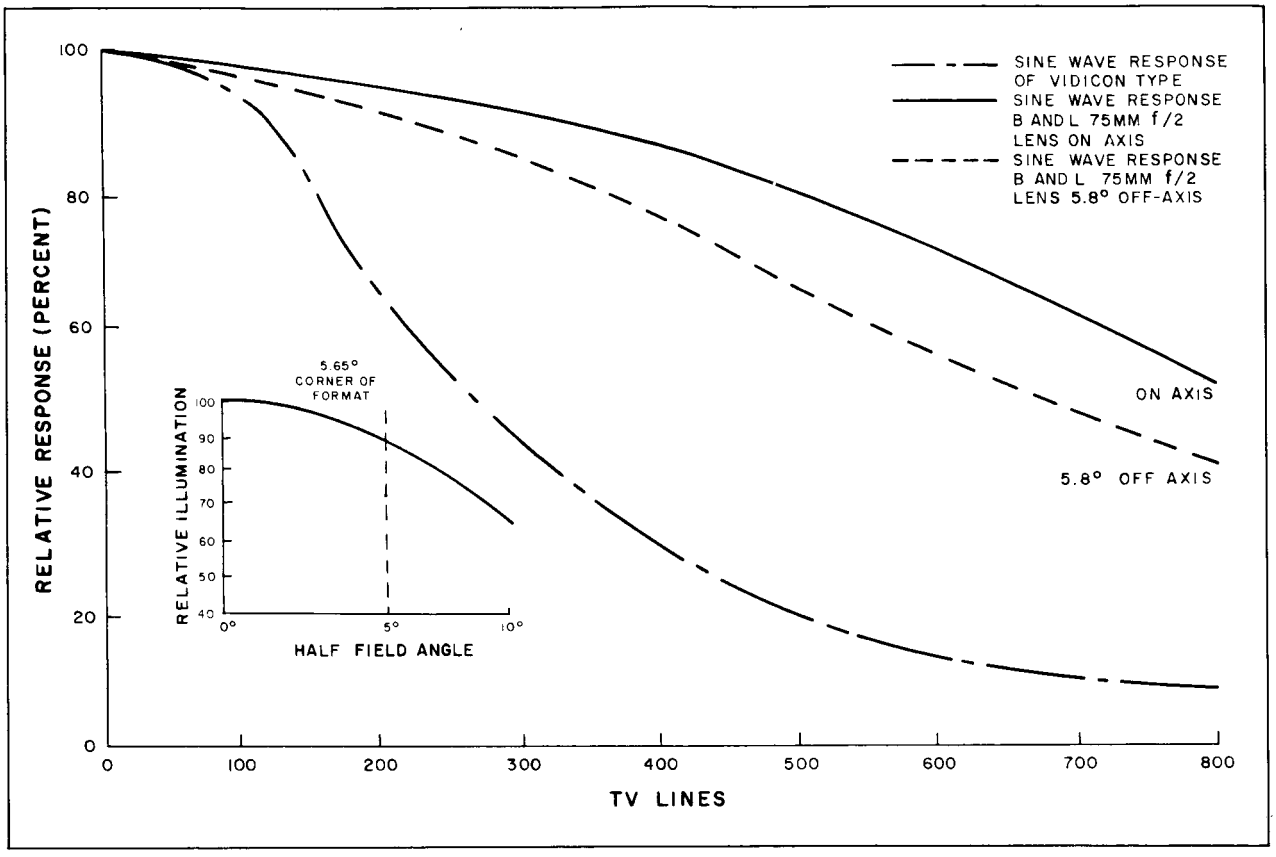

Figure 30. Sine-Wave Response of Bausch and Lomb 75-mm f/2.0 Lens

The preceding equations were used to determine the values of the F-Camera parameters. These values are shown in Table 4.

The P-Camera parameters were selected to give greater resolution than that obtained with the F-Cameras. This increase in resolution was accomplished by decreasing the scanned area and maintaining the same sweep velocity. The values of the P-Camera parameters are shown in Table 5. These values were determined by using equations (87) through (90). The reduced vertical frame time of the P-Cameras ensured that a picture of the lunar surface could be scanned and transmitted from a distance very close to the lunar surface, just before impact.

7. Erase Cycle Considerations

The bandwidth limitations and resolution requirements dictated the use of a storage-type, slow-scan vidicon. Because of the high image-retention characteristics of this type of vidicon, a residual image remains on the vidicon photoconductor for a relatively long period of time after readout. In order to maximize the available time for picture taking, an erase cycle was added to the operation of the vidicon. The erase cycle consists of two operations. The vidicon photoconductor is first flooded with light, which bleaches the previous image and discharges the photoconductor. The photoconductor is then uniformly recharged with a

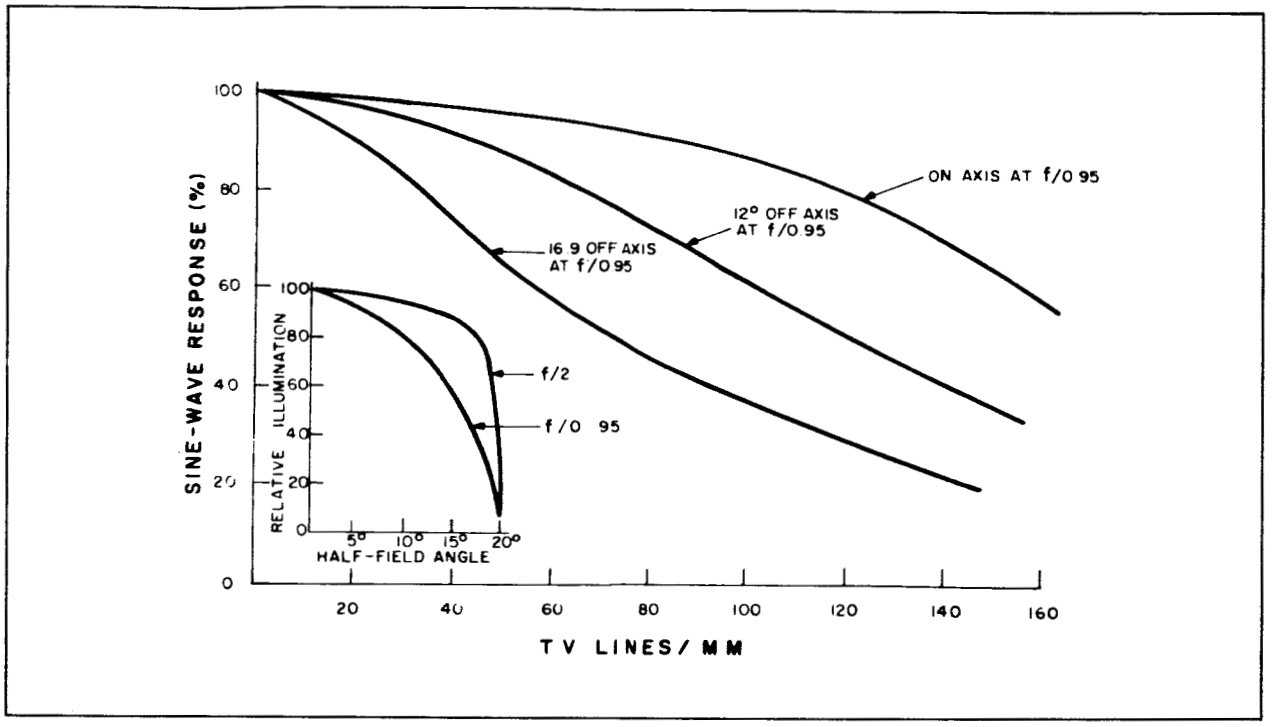

Figure 31. Modulation Transfer Function and Off-Axis Illumination Characteristics for the Angenieux Lens

TABLE 4
F-CAMERA PARAMETERS

Parameter	Value
Horizontal read time (t_h)	2 milliseconds
Horizontal retrace time (t_{hr})	0.22 millisecond
Horizontal sweep frequency (f_h)	450 cps
Number of scan lines (N_S)	1150
Number of TV lines per picture height (N)	800 TV lines
Vertical frame time (T_R)	2.56 seconds
Scanned area	0.442-inch square

TABLE 5
P-CAMERA PARAMETERS

Parameter	Value
Horizontal read time (t_h)	555 microseconds
Horizontal retrace time (t_{hr})	111 microseconds
Horizontal sweep frequency (f_h)	1500 cps
Number of scan lines (N_S)	305
Number of TV lines per picture height (N)	216 TV lines
Vertical frame time (T_R)	0.2 seconds
Scanned area	0.11-inch square

rapidly scanning beam. The vidicon is exposed for the next picture after the erase cycle is completed. The total cycle of camera operation from one exposure to the next requires 4.72 seconds for the F-Cameras and 0.66 second for the P-Cameras.

8. Number of Cameras Selected

The number of cameras to be included in the TV Subsystem was selected on the basis of optimum utilization of the available time. A single F-Camera requires a minimum of 4.72 seconds between consecutive exposures. The read period is only 2.56 seconds, or 54 percent of this time. Therefore, a second F-Camera was added to provide continuous transmission of video information on the F-Channel. The second camera was read out while the first was being erased.

The P-Camera utilized an even smaller percentage of the picture-taking cycle for readout. This camera requires a minimum of 0.66 second between consecutive exposures. The read period is 0.2 second, or 30 percent of this time. Four cameras of this type, operating sequentially, are needed to provide continuous transmission of video data over the P-Channel. While one camera is being read out, each of the other three is in a different phase of its erase cycle. Continuous sequential operation of the P-Cameras ensured that one of these cameras would return a closeup picture of the lunar surface, just prior to impact.

The operating cycles for the F- and P-Cameras are shown in Table 6.

9. Camera Pointing Array

The manner in which the cameras were pointed from the spacecraft was the result of tradeoffs

TABLE 6
CAMERA OPERATING CYCLES

Operation	Time (Seconds)	
	F-Camera	P-Camera
Shutter operation	0.08	0.08
Read scan	2.56	0.20
Lamp flash	0.08	0.08
Erase scan	2.00	0.30

among several objectives. It was desired to obtain wide area coverage of the lunar scene, but at the same time obtain picture-nesting and minimize smear. Picture nesting was essential to identify the area of the lunar surface being photographed. In this technique, the P-Cameras view a portion of the scene photographed by the F-Cameras, thus facilitating identification of the scene in the higher-resolution P-Camera pictures. Wider area coverage was obtained by diverging the optical axes of the cameras by an amount that was within the constraint of permissible smear, and that furnished sufficient overlap of the viewed scene to provide nesting.

The camera pointing arrangement was also constrained by the structural features of the spacecraft. Thus, the position of the omni-directional antenna precluded the use of an arrangement where the cameras are pointed along the longitudinal axis of the spacecraft.

The pointing array used in the initial configuration of the TV Subsystem is shown in Figure 32. At that time, the 75-mm f/2.0 lens was used on all cameras. The P-Cameras were arranged in a cluster about an axis designated the common optical axis (COA). The COA was to be aligned with the spacecraft velocity vector by a terminal maneuver of the spacecraft. In this arrangement, the pictures from all four P-Cameras give overlapping coverage of the viewed scene, and the COA is contained in the overlapped area. The area that was to be covered by each of the F- and P-Cameras is shown in Figure 33. The F-Camera pictures do not contain the COA, but overlap the area viewed by the P-Cameras.

A decision was made during development of the TV Subsystem to change the lenses on Cameras F_a, P3, and P4 to a 25-mm f/0.9 lens. This lens increased the sensitivity of the cameras and allowed acceptable pictures to be taken even if a substandard trajectory brought the spacecraft closer to the lunar terminator than was planned.

The shorter focal length of the 25-mm lens increased the field of view of the cameras, and resulted in a modification to the camera-pointing arrangement, as shown in Figure 34. No change was made in the P-Camera array, but the F-Cameras were both changed. The F_a Camera, with its wider field-of-view, was changed to include the COA in its pictures. The areas covered by the cameras after the modification are shown in Figure 35.

10. Photographic Platform

Experimental observations have shown that the maximum value of image smear (γ) that

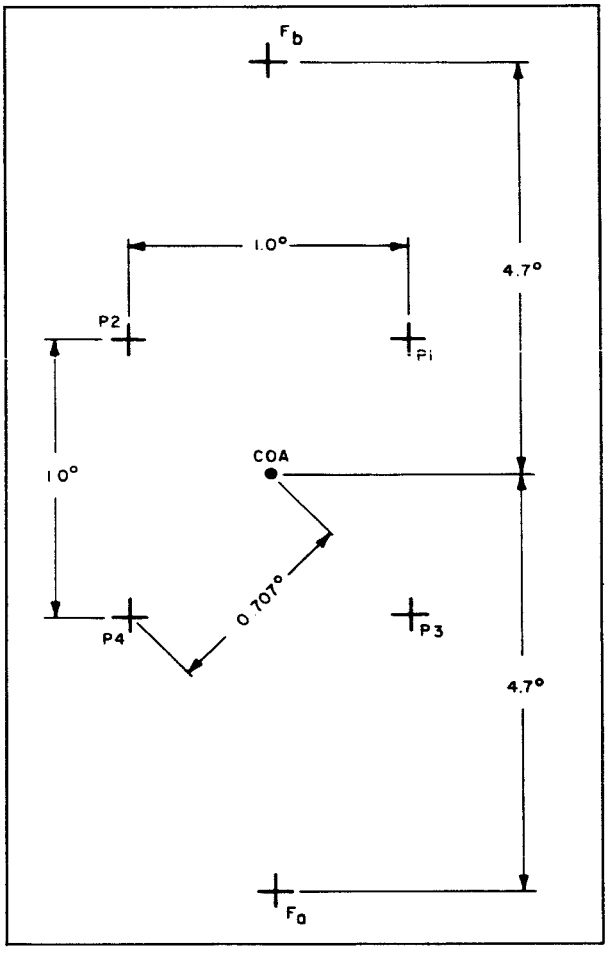

Figure 32. Camera Pointing Array, Earlier Configuration of TV Subsystem

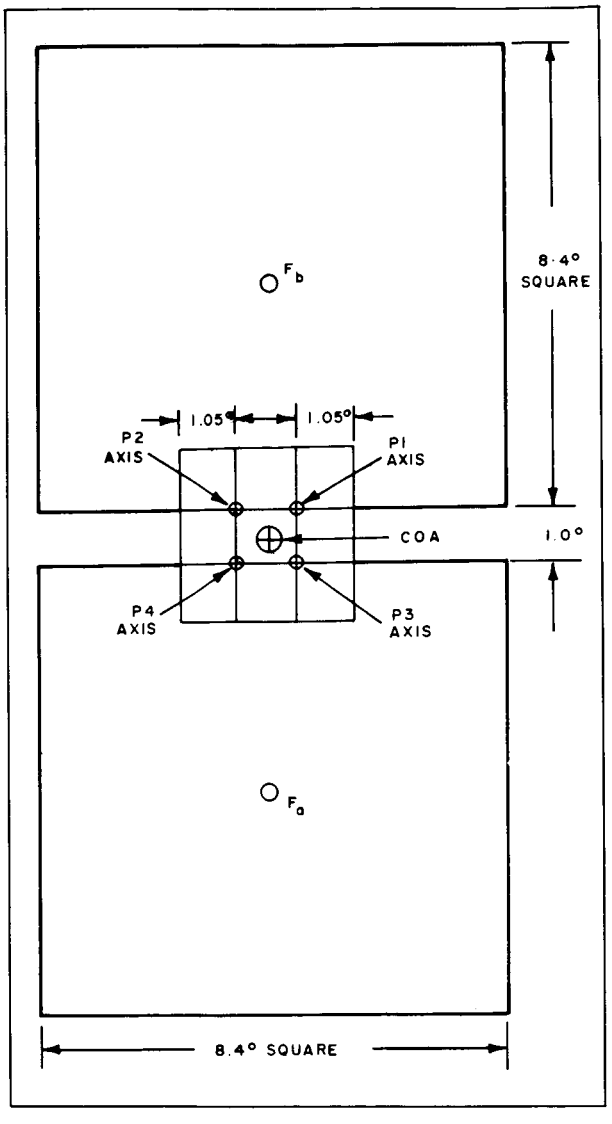

Figure 33. Area Coverage of Earlier Pointing Array

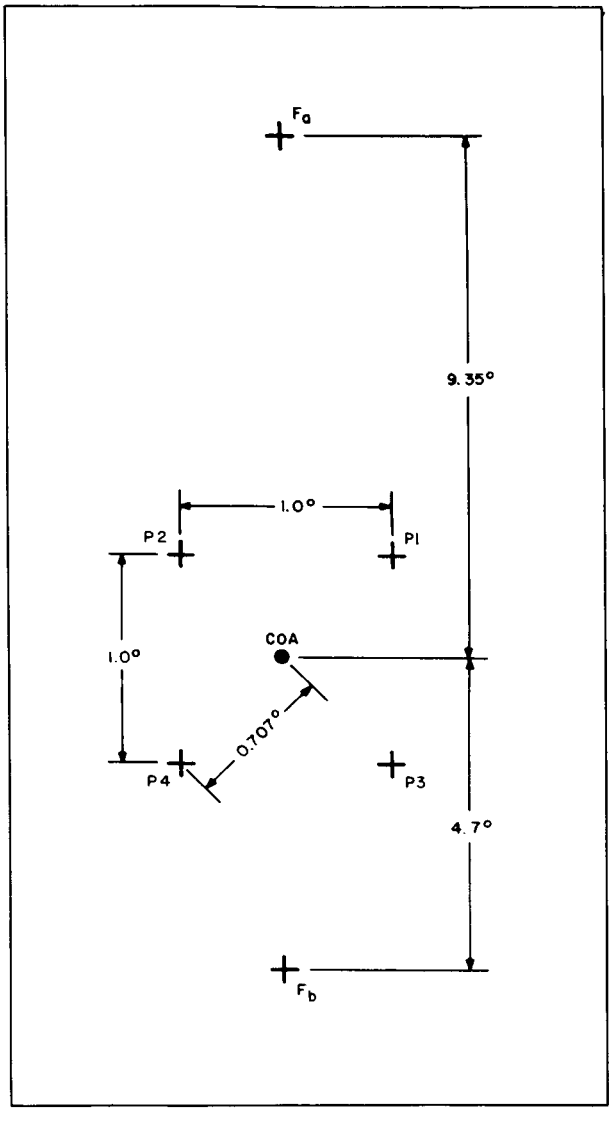

Figure 34. Camera Pointing Array, Final Configuration of TV Subsystem

is acceptable is 0.7 optical line pair. Image smear is zero when the optical axis of the camera is perfectly aligned with the velocity vector of the spacecraft. In the Ranger mission, smear was a function of the divergent pointing arrangement of the camera array, and also a function of any misalignment that might occur between the common optical axis (COA) of the camera array and the velocity vector.

The spacecraft attitude control system can maintain the common optical axis (COA) of the camera array to within 0.5 degree of the velocity vector. As shown in Figure 34, the P-Camera axes are displaced 0.7 degree from the COA. The edge-to-center field-of-view is 1.5 degrees for the P-Cameras with the 75-mm lens, and 4.6 degrees for the P-Cameras with the 25-mm lens. Therefore, the worst-case conditions of displacement (ψ) from the velocity

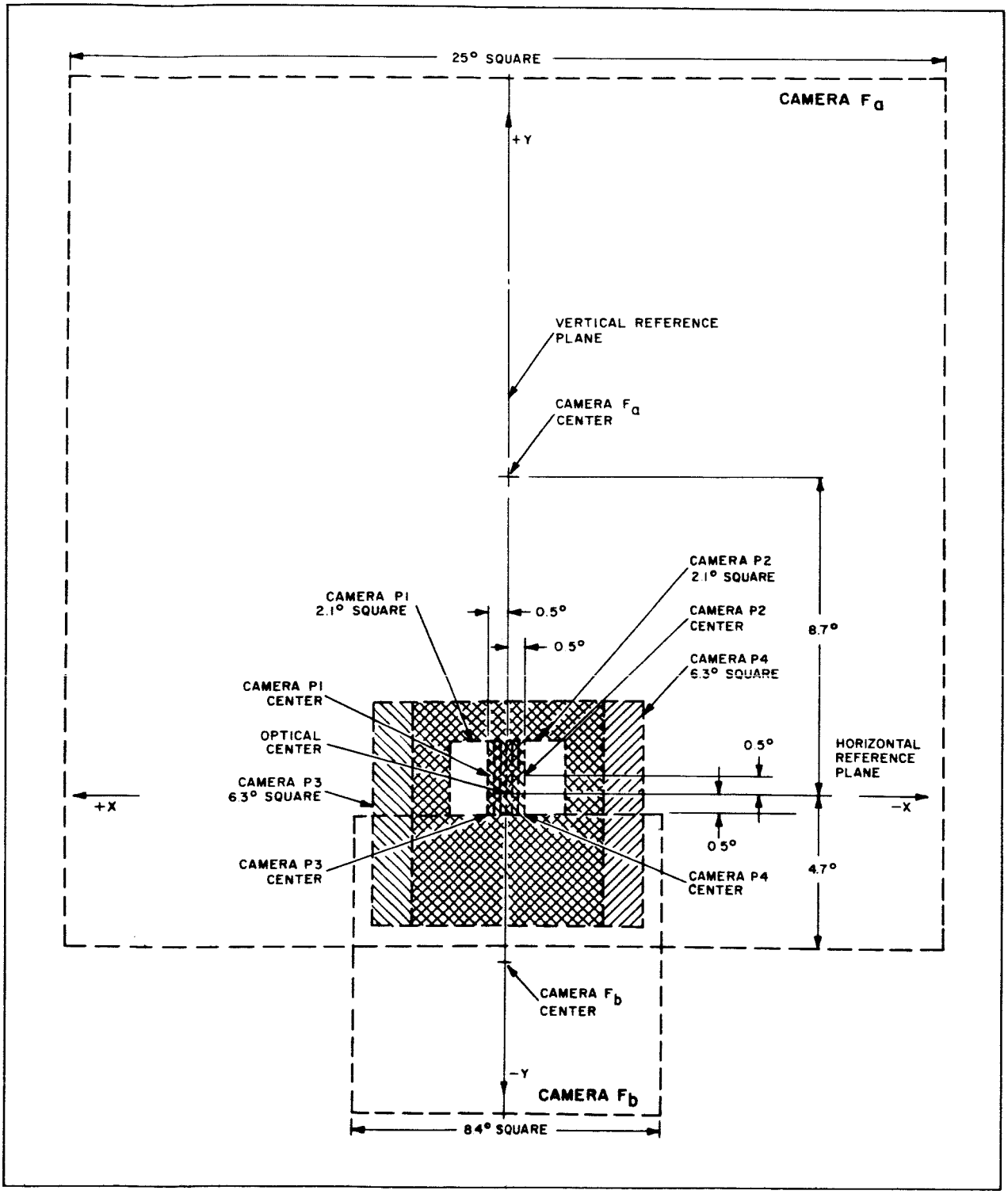

Figure 35. Area Coverage of Final Pointing Array

vector are 1.2 degrees for the axes of the four P-Cameras, 2.7 degrees for the edge of the lens of the 75-mm P-Camera, and 5.8 degrees for the edge of the lens of the 25-mm P-Camera. The Fb Camera is displaced 4.7 degrees from the COA. The worst-case conditions for this camera are 5.2 degrees for the camera axis and 9 degrees for the edge of the lens.

The image smear is given by

$$\gamma_t = \frac{FN_m \cos\eta \, Sin\,\psi\,(\Delta t)}{t} \qquad (91)$$

where

γ_t is the image smear in optical line pairs;

F is the focal length of the camera lens in mm;

N_m is the line density of the scanned image in optical line pairs per mm;

η is the angle between the normal to the lunar surface and the camera optical axis;

ψ is the angle between the velocity vector and the camera axis;

Δt is the exposure time in seconds; and

t is the time-to-go (in seconds) before impact.

Equation (91) is simplified by substituting the following numerical values:

F = 25 mm or 75 mm;

N_m = 35.7 optical line pairs per mm;

$\cos\eta$ = 1; and

Δt = 2×10^{-3} second.

The simplified forms of equation (91) are

$$\gamma_t \text{ (75-mm lens)} = \frac{5.35 \sin\psi}{t} \qquad (92)$$

$$\gamma_t \text{ (25-mm lens)} = \frac{1.785 \sin\psi}{t} \qquad (93)$$

The values of smear obtained with these equations are plotted in Figure 36. For worst-case angles of ψ, the maximum smear value of 0.7 optical line pair occurs in the center of the 75-mm P-Camera picture at 0.160 second prior to impact. The value of smear in the center of the 25-mm P-Camera picture is negligible all the way to impact. One corner of the 75-mm P-Camera picture reaches the smear value of 0.7 optical line pair at 0.35 second before impact, and a corner of the 25-mm P-Camera picture reaches this value of smear at 0.25 second before impact.

A shorter exposure time would move the point at which smear becomes visible closer to the impact time; however, a loss in signal-to-noise ratio would result. Since only a small portion of the picture shows smear, the 2-millisecond shutter is a satisfactory compromise.

11. Power-Supply Design Considerations

The purpose of the TV Subsystem Power Supply was to provide and regulate the electrical power needed to operate the Subsystem

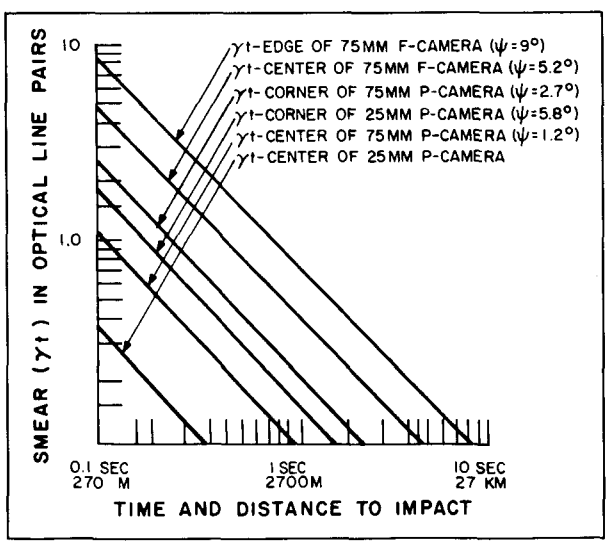

Figure 36. Smear versus Time-to-Go Before Impact

during the various prelaunch, launch and flight phases of the lunar mission. The principal design constraint was that the power supply be completely independent of the spacecraft power supply. Other limitations were weight, volume, reliability, shelf life, and ease of handling.

The approach to the design of the power supply was based on the anticipated electrical load profile for the mission. The profile indicated low power requirements during the 66-hour cruise mode, and sizeable demands during the 15- to 30-minute terminal mode. For this application, a combined solar array and battery supply was compared with a supply composed of batteries only. The study revealed that the cruise-mode demand was insufficient to warrant the additional complexity of a solar array. Moreover, an array of practical size would be of little value in offsetting the peak power demand of the terminal mode because the period of operation was too short to allow time for battery recharge.

As a result of the study, it was decided to concentrate on the use of batteries alone for the power source. Since the batteries were not going to be recharged during the mission, the ability to withstand numerous charge-discharge cycles was not a factor in selecting the batteries. Prime consideration was given instead to energy storage per unit weight and per unit volume. In both categories, the silver-zinc cell proved superior to nickel-cadmium, lead acid, nickel-iron, and silver-cadmium.

Battery design parameters were also dependent on the peak-current requirement of the mission. The capacity of the batteries was selected to provide a safe margin over and above the worst-case mission requirements.

Sealed rather than vented construction was necessary to avoid electrolyte leakage and outgassing. Sealed construction eliminates the possibility of dry-charging the batteries and activating them in the field by the addition of electrolyte; however, the shelf life of the sealed battery is long enough to prevent storage problems.

Two batteries were used to supply power for the TV Subsystem. Each battery functioned independently of the other; one supplied power to the F-Channel, the other to the P-Channel.

Both the series type and the buck-boost type of regulator were considered for use in the power supply. The series-type regulator had been used successfully in several previous projects. It is lightweight and reliable, but has the disadvantage of being inefficient, dissipating a relatively large amount of heat. This lost power places an additional demand on the batteries. Buck-boost regulators are more efficient but involve a more critical feedback loop and more complex circuitry; therefore, they are generally less reliable and heavier.

The total weight of the power supply depends principally on the energy density of the batteries, the power profile, and the efficiency and weight of the regulator. These factors were taken into account to calculate the total power-supply weight that would result from the use of each type of regulator. A comparison of the calculated weights indicated that a power supply with a buck-boost regulator is 12.5 pounds lighter than a supply with a series regulator, if the buck-boost regulator weighs 5 pounds and is 88 percent efficient and the series regulator weighs 20 ounces and is 70 percent efficient. The heavier buck-boost regulator results in a lighter power-supply, because the higher efficiency of this regulator permits the use of a lighter battery.

The selection of the type of regulator was basically a choice between the somewhat lighter power-supply obtained with the buck-boost regulator and the more reliable series-regulator. The choice for the Ranger TV Subsystem was the more reliable series-regulator.

12. Thermal Design Considerations

a. REQUIREMENTS

The thermal design of the TV Subsystem was required to utilize passive means of temperature control to maintain the temperature of

Subsystem components within the required limits during all phases of the mission. The two principal phases of the mission are the 66-hour, Sun-oriented cruise mode and the 1-1/4-hour terminal mode initiated by the terminal maneuver. The terminal mode consists of three phases. These are as follows:

- Terminal mode prior to TV Subsystem turn-on;
- Terminal mode during TV Subsystem warm-up; and
- Terminal mode during full-power operation of the TV Subsystem.

The Sun-oriented cruise mode required a steady-state thermal design, since temperatures would reach equilibrium during the cruise period of approximately 66 hours.

For purposes of thermal analysis, the shape of the Subsystem was assumed to be a frustum of a right circular cone with base diameters of 14.5 and 26 inches and with a height of 57.7 inches. Figure 37 illustrates the assumed thermal model. The antenna/Subsystem interface was thermally insulated and assumed to be adiabatic, thus eliminating the effect of the antenna in the thermal design problem. The

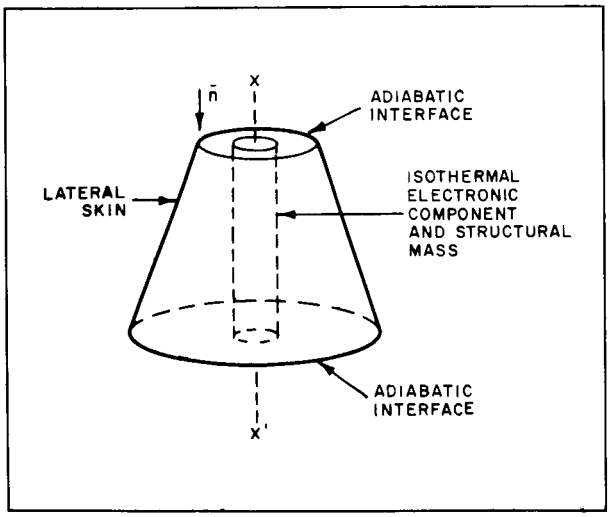

Figure 37. Assumed Thermal Model

thermal design was based on the following considerations:

- A high value of solar absorptivity and a low value of emissivity would be required to compensate for the low ratio of projected surface area to lateral surface area.
- During the terminal maneuver, low emissivity would tend to trap the thermal dissipation resulting from operation of the electronic equipment.
- The Subsystem/Bus interface was thermally insulated and assumed to be adiabatic.

b. THERMAL ANALYSIS FOR THE CRUISE MODE

A thermal analysis was performed for the Sun-oriented cruise mode. The following assumptions were made:

- The Sun vector was parallel to the axis of the spacecraft in the $\bar{n}$ direction.
- All electronic packages were thermally connected to the center structure so that the packages and structure could be characterized by one temperature.
- The lateral surface was isothermal (a valid assumption when the Sun vector was as assumed).
- The energy exchange between the isothermal components and the lateral surfaces was solely radiant.

Based on these assumptions, thermal energy equations for the electronic components and lateral surfaces are as follows:

Surface equation:

$$m_s C_s \frac{dT_s}{dt} = S a_s \bar{A}_s + K_{cs}\sigma \left[T_c^4 - T_s^4\right] - \sigma \epsilon_s A_s T_s^4 \qquad (94)$$

Component equation:

$$m_c C_c \frac{dT_c}{dt} = \rho_c - K_{cs}\sigma \left[T_c^4 - T_s^4\right] \qquad (95)$$

where the subscript c refers to the components and the subscript s to the lateral surface, and

m is the weight;

C is the specific heat;

T is the temperature;

t is time;

A is the surface area;

S is a solar constant;

α is the solar absorptivity;

σ is the Stefan-Boltzmann constant;

ϵ is the emissivity;

$\bar{A}$ is the surface area projected toward the Sun;

ρ is the internal heat generation; and

K_{cs} is an unknown radiation coupling factor between the components and the lateral surface.

Since steady-state conditions are assumed for the cruise mode, the change of temperature with respect to time for the components and the lateral surface is zero. Thus the equations were solved with the following results:

$$\sigma T_s^4 = \frac{S\alpha_s \bar{A}_s - \rho_c}{\epsilon_s A_s} \qquad (96)$$

$$\sigma T_c^4 = \frac{\rho_c}{K_{cs}} + \frac{S\alpha_s \bar{A}_s + \rho_c}{\epsilon_s A_s} \qquad (97)$$

Since the ratio of projected to total area was quite small for the lateral surface, a value of 0.9 was assigned to α_s. A conservative value of 10 watts was used for internal dissipation in the components (ρ_c) during cruise mode. $\bar{A}_s$ was calculated to be 2.5 square feet, and A_s to be 25.6 square feet. A desirable average component temperature (T_c) of 10° C was assumed. The preceding values were used to obtain a graphical solution of K_{cs} for the cruise mode in terms of the emissivity (ϵ_s) of the external surface, as shown in Figure 38.

The radiation coupling factor K_{cs} is a function of the internal geometry, the emissivity of the components, and the emissivity of the inside of the lateral surface. From multiple reflection theory,

$$K_{cs} = \frac{\epsilon_c \epsilon_s' A_c}{\epsilon_s' + \frac{A_c}{A_s}\epsilon_c (1 - \epsilon_s')} \qquad (98)$$

which reduces to

$$K_{cs} = \frac{A_c}{\frac{1}{\epsilon_c} + \frac{A_c}{A_s}\left(\frac{1}{\epsilon_s'} - 1\right)} \qquad (99)$$

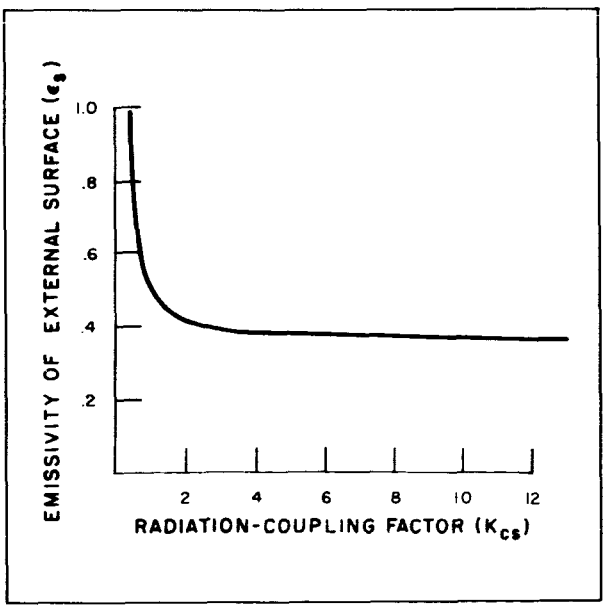

Figure 38. Combinations of K_{cs} and ϵ_s to Maintain an Average Component Temperature of 10° C during Cruise Mode

where the prime denotes the internal surface. Equation (99) and the curve in Figure 38 can be used to obtain a combination of internal and external emissivities of the lateral surface to keep the average component temperature at 10° C. For a coupling factor (K_{cs}) of 2.5 square feet, the required external surface emissivity (ϵ_s) from Figure 38 is 0.4. If it is assumed that the components are essentially black, a value of 0.9 can be used for ϵ_c. Using the preceding values, equation (99) was solved for the internal surface emissivity (ϵ'_s), yielding a value of 0.115. This value of emissivity is easily obtained with the use of readily available coatings.

c. THERMAL ANALYSIS FOR THE TERMINAL MODE

The thermal analysis for the terminal mode was based upon the assumption that the spacecraft/Sun vector angle would result in the projection of maximum spacecraft area (8.3 square feet) to the Sun. Due to the three different phases of Subsystem operation occurring during this mode, equations (94) and (95) were used to derive a time-dependent equation, which defined the final temperature T_f in terms of the initial temperature T_i and other spacecraft parameters. A plot of the temperature solution for the time-dependent equation of the terminal mode is given in Figure 39. The final temperatures for the three phases of terminal operation, in order of occurrence, were found to be 19.5, 36, and 47° C, respectively.

d. RESULTS OF ANALYSIS

The analysis proved that the Ranger TV Subsystem could be designed on a purely passive basis and that the average component temperature could be limited to a range of 5 to 50° C. Since many of the assumptions made in the analysis were conservative, it was anticipated that an even-more-favorable temperature range could be achieved in the actual design.

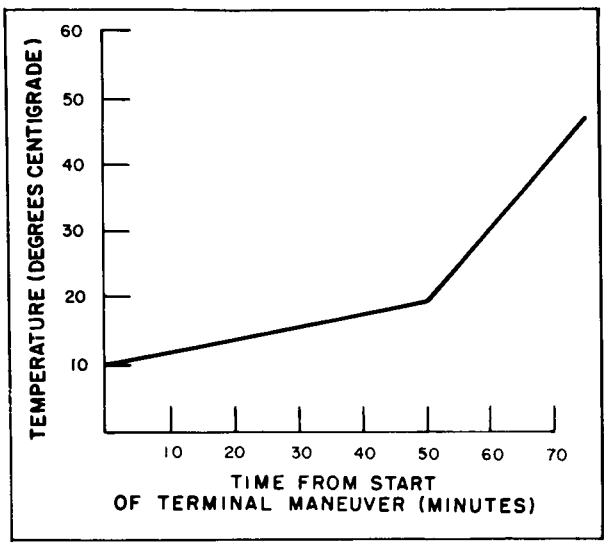

Figure 39. Plot of Average Component Temperature as a Function of Time from the Start of the Terminal Maneuver

13. Structural Design Considerations

The structural design was required to meet the mechanical and electrical interface requirements at the mating surfaces to the JPL bus and the omnidirectional antenna. It was also required to provide adequate strength, rigidity and thermal performance under the various environments encountered during the mission.

The principal contraints on the design of the TV Subsystem structure were the physical limitations imposed by the launch-vehicle nose-fairing geometry and the JPL bus interface. The allowable weight for the TV Subsystem was specified initially to be a maximum of 315 pounds. This was later changed to 383 pounds of which approximately 76 pounds was allotted to the structure. The nominal location and tolerance of the center-of-gravity were specified as well as the mass moments-of-inertia about axes passing through the center-of-gravity and parallel to the pitch, roll and yaw axes of the spacecraft. In order to provide the TV cameras with an unobstructed view during lunar approach and to achieve the specified center of gravity, it was necessary

to mount the cameras near the top of the TV Subsystem.

The first phase of the TV Subsystem structural design was to determine a payload shape within the aforementioned dimensional constraints. The resulting shape was a frustum of a right circular cone with a height of 46.5 inches and base diameters of 15.5 and 26 inches surmounted by a cylinder 15.5 inches in diameter and 13 inches high.

In order to provide the required structural strength and rigidity and to mount the main electronic components, a central longitudinal box beam was incorporated to act as a column for thrust axis loads and a cantilever beam for lateral loads. In addition to the baseplate, transverse bulkheads were included at various stations to connect the central box beam with the skin or thermal shroud and to serve as mounting surfaces for additional components. The TV cameras and the associated mounting bracket were secured to the top of the central box beam and enclosed in the cylindrical hat section.

High-strength aluminum alloys were selected for the structure because of their compatibility with the space environment, their high strength-to-weight ratio, fatigue properties, availability and ease of fabrication. The simple, proven, airframe-type, riveted and bolted construction method was consistent with the number of units to be produced in the specified time period. This type of construction required minimal tooling and permitted rework to accommodate component design changes and modifications.

The location of component assemblies other than the camera was influenced by the specified center-of-gravity location and mass moments-of-inertia as well as accessibility, signal path and thermal requirements. In positioning the batteries, which were the heaviest components, the prime considerations were the center of gravity and accessibility for replacement. By mounting the batteries at the base within the box beam, these considerations were satisfied.

The transmitter power amplifiers were located near the base on the box beam to utilize the battery thermal mass as a heat sink. The positions of other components were dictated primarily by physical constraints and signal paths.

Section III

Subsystem Description

A. SUBSYSTEM CONFIGURATION

The arrangement of the first prototype of the TV Subsystem is shown in Figure 40. As the final flight systems evolved, the basic subassemblies, as used on the first prototype, remained essentially the same; however, the overall arrangement of the TV Subsystem was modified extensively due to changes in the philosophy of operation and control.

As the result of a series of system concept and design reviews, JPL directed RCA to study alternate configurations of the TV Subsystem with the aim of evolving a configuration that would have an improved capability for obtaining lunar pictures during a nonstandard mission or under conditions of partial failure of the TV Subsystem. The results of the study indicated that this objective could be achieved best by a configuration in which the maximum degree of independence existed between the two camera and communication chains contained in the TV Subsystem. This philosophy was implemented by eliminating the common signal and power interfaces that existed between the F- and P-Camera chains, with the exception of the common communications elements required for simultaneous transmission of video from both channels. This "split-system" arrangement greatly increased the probability of obtaining lunar photographs in the event of failure of some portion of the equipment.

The Ranger VI failure in January of 1964 was the basis for additional changes, which resulted in the final TV Subsystem arrangement shown in Plate 1 at the rear of this book. This final configuration consists of two channels. Basically, each channel comprises television cameras, a video combiner, a transmitter, a power supply, and a camera sequencer. The operation of each channel is monitored by a telemetry system.

Each channel operates in a similar manner. The cameras, under the control of the camera sequencer, take pictures sequentially and are read out in the same way. The video and sync signals from all the cameras in the channel are combined in the video combiner and the composite signal is fed to the transmitter modulator. A subcarrier that contains telemetry data is also fed to the modulator. The transmitters in each channel continuously transmit data to Earth via a high-gain antenna. The transmitters are matched to the antenna by means of a four-port hybrid. The final sizes and weights of this configuration are listed in Table 7.

B. INTERSYSTEM CONTROL

Terminal-mode operation of the TV Subsystem is controlled by the camera sequencer in each channel. These units program the turn-on of plate power to the transmitter power amplifiers and control the sequence of camera operation so that a video signal is applied to the modulator at all times. While video data is being read out of one camera, the remaining cameras are prepared for the next exposure. This method of sequencing fully utilizes the time available for picture-taking and also ensures that video data will be transmitted from the spacecraft right up to the time of impact.

A block diagram of the camera sequencer is shown in Figure 41; its operation is as follows.

Upon receipt of the warm-up command, power to the camera sequencer is turned on and the 18-kc clock starts generating clock pulses. The clock pulses are fed to the division chain (counter), which has three outputs. One output is to the logic decoder that times and sequences

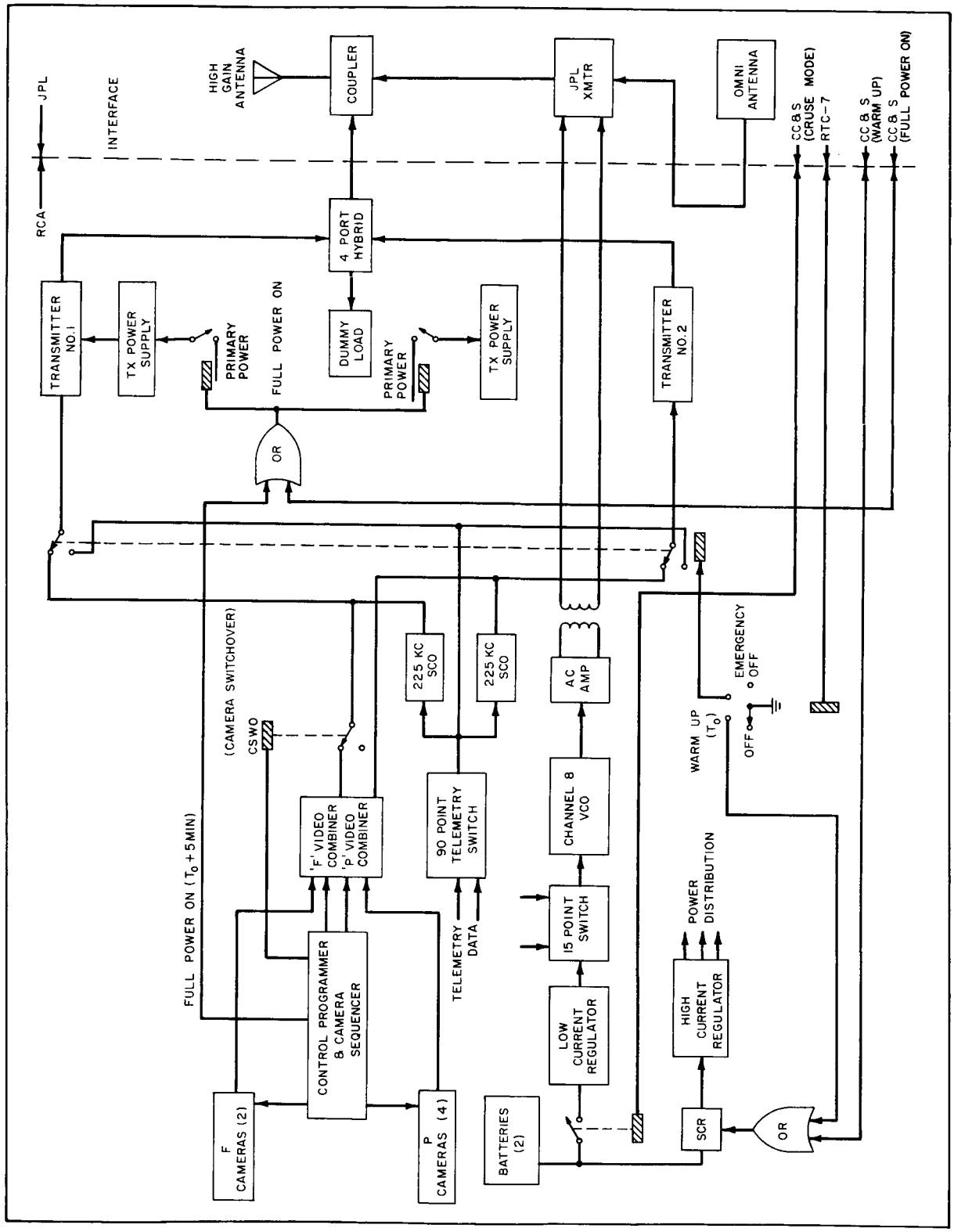

Figure 40. Block Diagram of First TV Subsystem Prototype

TABLE 7
FINAL CONFIGURATION OF THE RANGER TV SUBSYSTEM

Reference Designation	Assembly	Weight (lbs)	Size Length x Width x Height (in Inches)
A1A1	P1 Camera	6.188	10 x 4-1/2 dia. with shutter 4 x 1-1/4 dia.
A1A2	P2 Camera	6.221	10 x 4-1/2 dia. with shutter 4 x 1-1/4 dia.
A1A3	P3 Camera	5.895	10 x 4-1/2 dia. with shutter 4 x 1-1/4 dia.
A1A4	P4 Camera	5.882	10 x 4-1/2 dia. with shutter 4 x 1-1/4 dia.
A1A5	F_a Camera	6.755	10 x 5-1/2 dia. with shutter 4 x 1-3/4 dia.
A1A6	F_b Camera	7.346	10 x 5-1/2 dia. with shutter 4 x 1-3/4 dia.
A2	P1 Camera Electronics	8.726	13 x 3-1/2 x 5-1/2
A3	P2 Camera Electronics	8.391	13 x 3-1/2 x 5-1/2
A4	P3 Camera Electronics	8.410	13 x 3-1/2 x 5-1/2
A5	P4 Camera Electronics	8.146	13 x 3-1/2 x 5-1/2
A6	F_a Camera Electronics	8.025	13 x 3-1/2 x 5-1/2
A7	F_b Camera Electronics	8.347	13 x 3-1/2 x 5-1/2
A8	Video Combiner	3.095	6 x 12 x 2
A9	Control Programmer and Camera Sequencer	14.131	12-1/2 x 6 x 4-1/2
A10	Battery (F-Channel)	43.156	15 x 7-1/4 x 5-3/4
A11	Battery (P-Channel)	43.656	15 x 7-1/4 x 5-3/4
A12	HCVR (F-Channel)	2.687	3-1/4 x 4-1/2 x 4
A14	Transmitter (F-Channel)	4.786	10 x 5-3/4 x 2
A15	Power Amplifier (F-Channel)	3.574	8-3/4 x 3-1/2 x 3-3/4
A16	Transmitter Power Supply (F-Channel)	10.461	7-3/4 x 5-1/2 x 4-1/2
A17	LCVR	0.467	3-1/4 x 1-1/2 x 2-1/2

TABLE 7
FINAL CONFIGURATION OF THE RANGER TV SUBSYSTEM (Continued)

Reference Designation	Assembly	Weight (lbs)	Size Length x Width x Height (in Inches)
A19	Transmitter (P-Channel)	4.894	10 x 5-3/4 x 2
A20	Power Amplifier (P-Channel)	3.519	8-3/4 x 3-1/2 x 3-3/4
A21	Transmitter Power Supply (P-Channel)	10.498	7-3/4 x 5-1/2 x 4-1/2
A24	Four-Port Hybrid Ring	1.248	6 dia. x 1-5/8
A25	Dummy Load	2.877	14-1/4 x 1-3/4 x 1-1/2
A26	Telemetry Assembly	8.071	10-1/2 x 5-1/2 x 5
A27	Temperature Sensors	0.377	2-3/8 x 1-1/2 x 3
A28	Sequencer Power Supply	3.631	6 x 12 x 1-1/4
A29	Telemetry Processor (F-Channel)	0.456	4 x 2-7/8 x 2
A30	Telemetry Processor (P-Channel)	0.456	4 x 2-7/8 x 2
A34	DCU	2.132	3-1/2 x 4 x 4-3/4
A35	Electronic Clock	2.001	8 x 4 x 2
A37	HCVR (P-Channel)	2.659	3-3/4 x 4-1/2 x 4
A38	Filter	0.655	2-3/4 x 2-1/4 x 1-1/2
A39	CCU	2.024	4 x 3-3/4 x 3-1/2
A40	CSU	0.584	2 x 3-1/4 x 2-5/8
A41	CTU	0.230	2-1/2 x 1-3/4 x 1-1/2
A42	CTU	0.230	2-1/2 x 1-3/4 x 1-1/2
	Structure	73.710	
	Shrouds	10.656	
	Top Hat	2.813	
	Thermal Shield	0.400	
	Harnesses and Cables	23.806	
	Hardware	7.165	
	Total Weight	379.537	

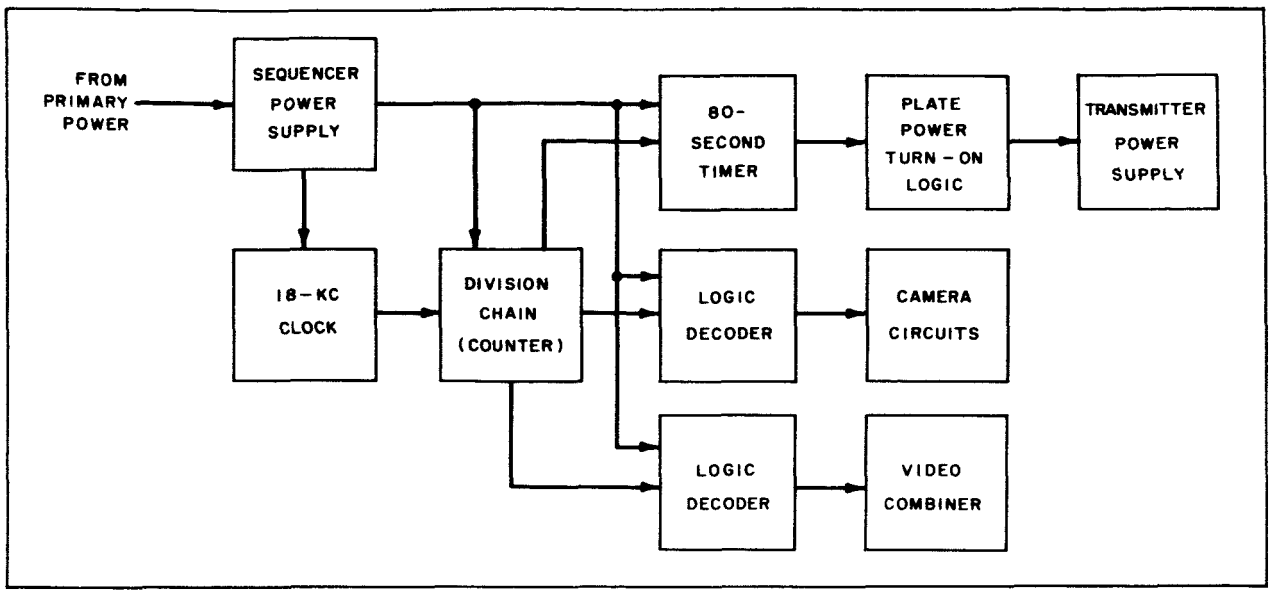

Figure 41. Block Diagram of Camera Sequencer

the cameras; another is to the logic decoder that controls the gates in the video combiner; and the third is a timed output, which starts the 80-second timer in the full-power command circuit. All timing and sequencing signals are referenced to the time of TV Subsystem turn-on. Eighty seconds after turn-on, the 80-second timer initiates the closing of the relay that applies plate power to the transmitter power amplifier, and transmission of the composite video signal commences. The logic decoders generate the sync and gating signals for the camera chain. The picture-taking sequence is repeated continuously until the spacecraft impacts the lunar surface.

C. COMMAND AND CONTROL

The purpose of the command and control system was to provide a means of real-time control by commands from the ground station, and to provide a means of operating the TV Subsystem in accordance with a prearranged program in the TV Subsystem.

The command and control system for the first prototype of the TV Subsystem was based on the following mission profile:

- No units of the TV Subsystem to operate during launch;
- Telemetry data (cruise-mode telemetry) to be furnished to monitor TV Subsystem temperatures and voltages during the voyage to the Moon; and
- Fifteen minutes of terminal-mode operations (5 minutes of warm-up time and 10 minutes of camera operation and transmission of video data).

An emergency mode of operation was also required to provide diagnostic telemetry data in the event that the spacecraft's high-gain antenna was not properly oriented and a signal strength loss resulted that was too great to obtain useful video data at the ground station. The telemetry data would indicate whether or not the TV Subsystem was functioning properly, and would be the basis for any necessary

modifications to future flight models of the TV Subsystem.

On the basis of the mission profile, the command and control system was designed to perform the following functions:

- Turn on the cruise-mode telemetry after launch;
- Turn on the TV Subsystem for 5 minutes of warm-up at 15 minutes before impact;
- Furnish a full-power command to turn on plate power to the transmitter power amplifiers after the 5-minute warm-up period;
- Place the TV Subsystem into an emergency mode for the transmission of diagnostic telemetry if the situation warrants; and
- Return the TV Subsystem to normal operation after the emergency situation is ended.

A limited number of interface commands were available from the spacecraft to the TV Subsystem for implementing these functions. There was one real-time command (RTC-7), two timed contact closures during the terminal mode, and one contact closure at the separation of the spacecraft and the Agena vehicle. Real-time switching in the TV Subsystem was accomplished by means of a four-position rotary switch (command switch). The positions were "zero", "warm-up", "emergency-on", and "emergency-off". The switch would advance one position each time an RTC-7 command was received.

The command system in the first prototype had several deficiencies. These were:

- There was no way to turn off the TV Subsystem in the event of an inadvertent turn-on.
- The two methods of turning on the TV Subsystem each required a real-time command from the ground station. In the first method, an RTC-6 command activated the spacecraft's Central Computer and Sequencer (CC&S), which then provided a turn-on command to the TV Subsystem. In the second method, an RTC-7 command turned on the TV Subsystem directly.
- Both turn-on signals (RTC-7 and CC&S) used the same circuits in the command switch.
- The full-power command circuitry was common to both transmitters.

The redesign to the split system incorporated changes to correct these shortcomings. A Power Control Unit (PCU) was added to allow the TV Subsystem to be turned off during flight. The transmission of four consecutive RTC-7 commands from the ground station would step the command switch through its complete cycle. When the command switch stepped from the "emergency-off" position to the "zero" position, the PCU would turn off the TV Subsystem.

An Electronic Clock was added to the F-Channel to give an alternate method of turn-on in the event that the communications link for real-time commands was lost. The Clock was to be turned on by a switch closure at spacecraft-Agena separation. The Clock could be set before launch to turn on the system at a particular time after spacecraft-Agena separation. A Clock turn-off command could be provided by an RTC-5 command if Clock turn-on was too early. The Clock was limited to the F-Channel because loss of the communication link for real-time commands would result in a lunar flyby mission instead of lunar impact. For a fly-by mission, the F-Camera pictures would furnish more useful information than the P-Camera pictures.

A separate circuit was incorporated for each turn-on command (CC&S and RTC-7). The full-power command circuits were separated for each transmitter by the use of isolation diodes.

Another major redesign to the command system occurred after the failure of the Ranger VI mission. The investigation of the failure indicated the probable cause of failure to be the result of an inadvertent turn-on of the TV Subsystem during the launch phase, when the vehicle was in the partial-pressure region. Thus, all the high-voltage circuits were probably destroyed by arcing. As a result of the failure analysis, the command circuits were redesigned to minimize the possibility of an inadvertent turn-on.

The major changes were as follows:

- Cruise-mode telemetry was to be turned on before launch and would remain on throughout the mission.
- The four-position rotary switch and the emergency telemetry mode were eliminated.
- The RTC-5 command was assigned to turn off the TV Subsystem.
- R-C differentiator circuits were installed in the command lines to prevent a failure in one line from inhibiting the other command inputs.
- Additional command lines and contact closures were made available from the spacecraft to provide more complete isolation of the command systems in the F- and P-Channels.

A simplified logic diagram of the command system used in Rangers VII, VIII and IX is shown in Figure 42. The first mission command (C_{RE}) is sent prior to launch, when the "cruise on" test button on the blockhouse control panel is pushed. This command passes through OR gate 8 and AND gate 8, which is conditioned by the presence of the P-Channel battery voltage. The output of AND gate 8 turns on the cruise-mode telemetry. The C_{RE} command also passes through OR gate 1 to ensure that the Clock is off.

The logic equation for turn-on of cruise-mode telemetry is as follows:

$$\text{Cruise mode on} = (S_{spd} + S_{30} + C_{RE})\, P_B \qquad (100)$$

where

- S_{spd} is the solar-panel microswitch closure that occurs when the solar panels are deployed;
- S_{30} is the switch closure that occurs at separation plus 30 minutes;
- C_{RE} is the closure of the "cruise on" test button on the blockhouse control panel; and
- P_B is the P-Channel battery voltage.

The next command to occur is the result of the switch closure (S_{OM}) at spacecraft-Agena separation. This command passes through AND gate 1, which is conditioned by the presence of the F-battery voltage (F_B). The output of AND gate 1 turns on the F-Channel Clock. The logic equation for Clock turn-on is

$$\text{Clock on} = S_{OM} F_B \qquad (101)$$

The F and P gate enable commands, which are, respectively, the outputs of OR gates 3 and 6, occur at separation plus 30 minutes or at separation plus 46 minutes when the solar panels are deployed. The logic equation is the same for both channels.

$$\text{Gate enable command} = S_{spd} + S_{30} + C_{RE} \qquad (102)$$

The C_{RE} function in this equation indicates that the gates can also be enabled by the "cruise on" test button on the blockhouse control panel. The C_{RE} function is used to permit testing of the TV Subsystem prior to launch; however, this command is removed when the umbilical connector is separated at launch. The reduced power jumpers from the blockhouse control panel are also disconnected when the umbilical connector separates.

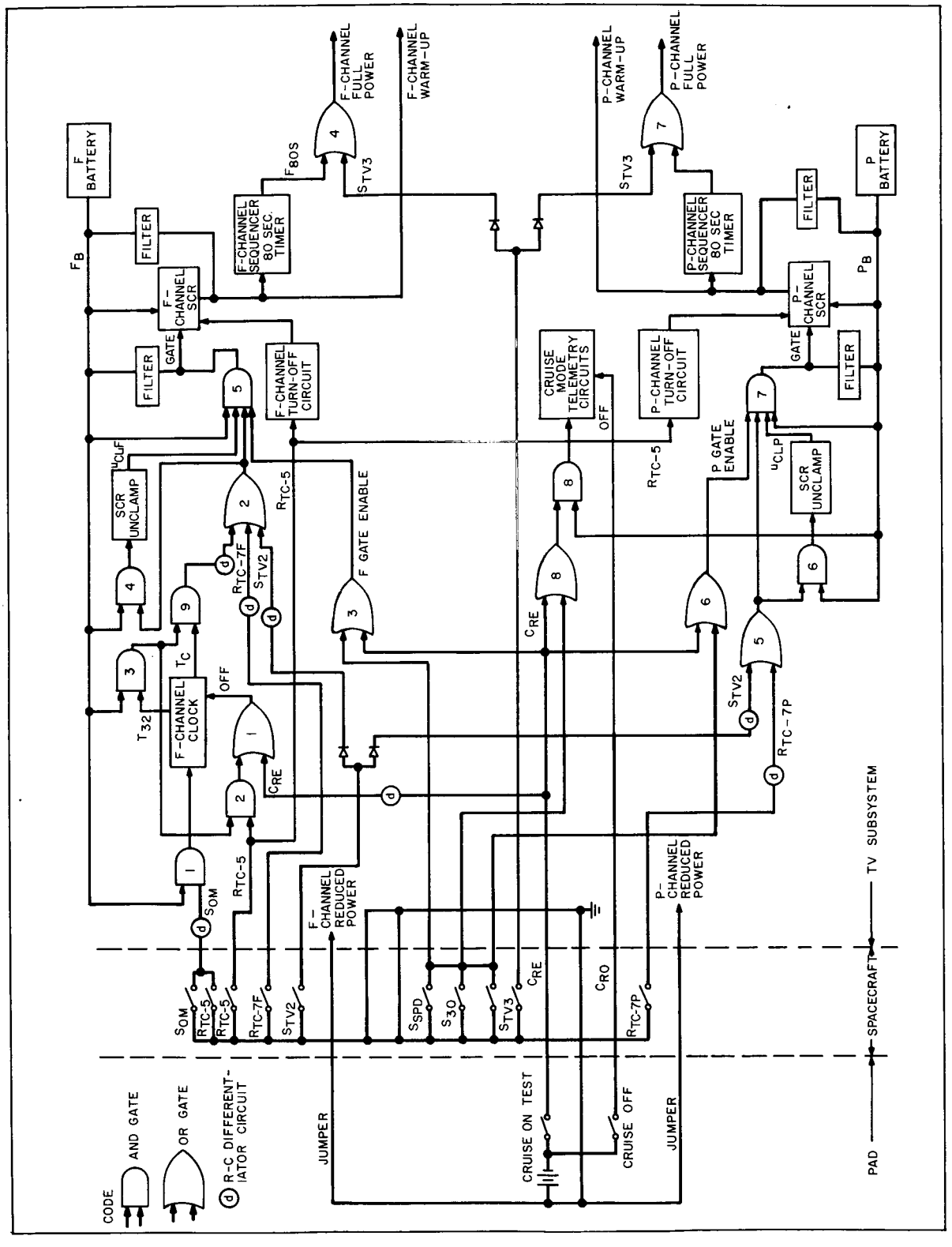

Figure 42. Logic Diagram of Command and Control Circuitry

At separation plus 32 hours the clock provides an output (T_{32}), which passes through AND gate 3 to condition AND gate 2 for an RTC-5 command. When the RTC-5 command is received, the output of AND gate 2 passes through OR gate 1 to turn off the clock. The T_{32} level at the output of AND gate 3 also conditions AND gate 9 to permit the clock command (T_C) to turn on the F-Channel at the proper time.

At approximately 60 minutes before impact, an RTC-6 command is sent to start the CC&S unit on the spacecraft. This unit provides the warm-up command (S_{TV2}) to the TV Subsystem 45 minutes later, and the full-power command (S_{TV3}) 50 minutes later. If both channels of the TV Subsystem are not turned on by 12 minutes before impact, the RTC-7 command is sent to the spacecraft. The logic equation for F-Channel warm-up (the output at AND gate 5) is as follows:

$$\text{F-Channel warm-up} = F_B (T_{32} T_C + S_{TV2} + R_{TC\text{-}7F})(S_{SPD} + S_{30} + C_{RE}) U_{CLF} \quad (103)$$

where U_{CLF} is the unclamp function that turns on the silicon-controlled rectifier that applies power to the F-Channel. The logic equation for P-Channel warm-up (the output at AND gate 7) is as follows:

$$\text{P-Channel warm-up} = P_B (S_{TV2} + R_{TC\text{-}7P})(S_{SPD} + S_{30} + C_{RE}) \quad (104)$$

The final command is the full-power command, which causes the plate power to be applied to the transmitter power amplifier. This command, which is the output of OR gate 4 in the F-Channel and OR gate 7 in the P-Channel, is generated by a timer in the camera sequencer 80 seconds after the warm-up command. In order to ensure full-power turn-on in the event of failure of the 80-second timer, the full-power command is repeated by the spacecraft CC&S at 5 minutes after the warm-up command. This second full-power command is designated S_{TV3}. The logic equations for the full-power commands are as follows:

$$\text{F-Channel full power} = F_{BOS} + S_{TV3} \quad (105)$$

$$\text{P-Channel full power} = P_{BOS} + S_{TV3} \quad (106)$$

D. TELEMETRY

A logic diagram of the telemetry circuits used in the final configuration of the TV Subsystem is shown in Figure 43. In operation, the cruise-mode telemetry is turned on at 30 minutes before launch by means of the "cruise on" test switch (C_{RE}) on the blockhouse test panel. Backup turn-on commands occur at separation plus 30 minutes (S_{30}) and when the solar panels are deployed (S_{SPD}). One of these three commands passes through AND gate 1, which is conditioned by the presence of the P-battery voltage P_B. The output of AND gate 1 operates the launching relay to turn on the Low-Current Voltage Regulator (LCVR) that supplies power to the cruise-mode telemetry circuits. The cruise-mode telemetry is applied to a 15-point commutator and transmitted to Earth via the Channel-8 transmitter in the spacecraft.

When either the F- or P-Channel is turned on, unregulated battery voltage is applied to the telemetry voltage regulator through OR gate 2. The output of this regulator is applied to:

- OR gate 3 to back up the LCVR;
- The 90-point commutator; and
- AND gates 3 and 4.

The output of the regulator turns off AND gate 3, removing the cruise-mode telemetry from the voltage-controlled oscillator (VCO) that modulates the Channel-8 transmitter. The same regulator output turns on AND gate 4 to place the output of the 90-point commutator

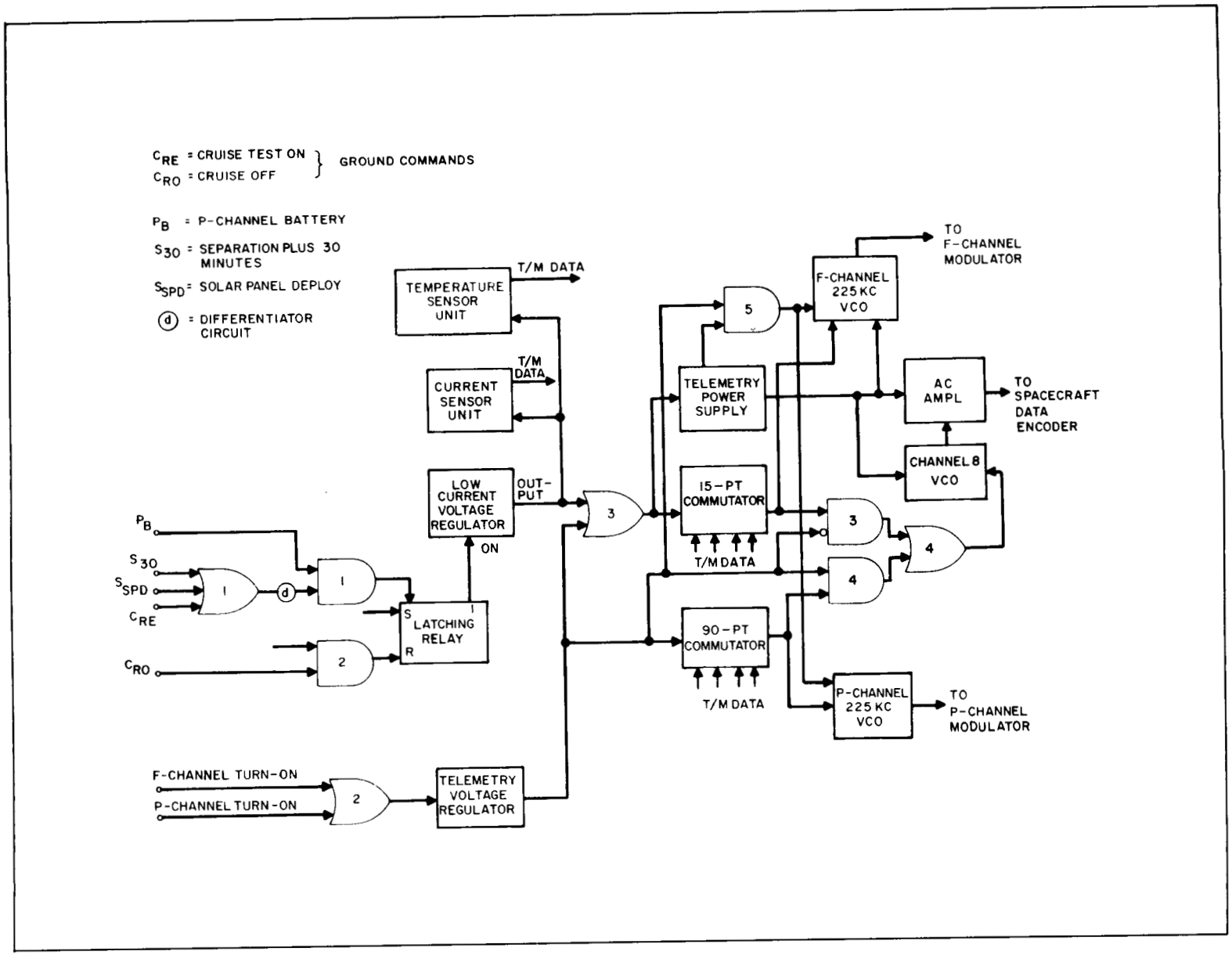

Figure 43. Logic Diagram of TV Subsystem Telemetry Circuits

on the Channel-8 VCO, and conditions AND gate 5 to pass power from the telemetry power supply to the F- and P-Channel VCO's. Thus, during the terminal mode, the 15-point telemetry is transmitted over the F-Channel transmitter, and the 90-point telemetry is transmitted over the P-Channel transmitter and over the Channel-8 transmitter.

Telemetry was used throughout the mission to verify the performance of the TV Subsystem and to determine the optimum procedures for terminal-mode operations. The sequence of the major telemetry events that occur throughout the mission is shown in Figure 44. Each event is described in the following paragraphs. The number of each item corresponds to the number in Figure 44.

1. Launch Minus Approximately 3 Hours

The TV Subsystem is turned on in reduced power approximately 3 hours before launch. At this time all telemetry data and video signals are checked to ensure proper operation. Special attention is given to the battery voltage telemetry to make certain that the batteries perform properly under load. The computer processed data is compared with the analog data presented on the strip chart, and the data received at the Space Flight Operations Facility at JPL is compared with the same data obtained at the Eastern Test Range (ETR) by the TV Subsystem launch team. These comparisons are made to ensure that all processing and display equipment is properly calibrated and functioning normally.

2. Launch Minus 30 Minutes

At approximately launch minus 30 minutes, the cruise-mode telemetry is turned on and remains on throughout the flight. The batteries are checked to see that they have recovered

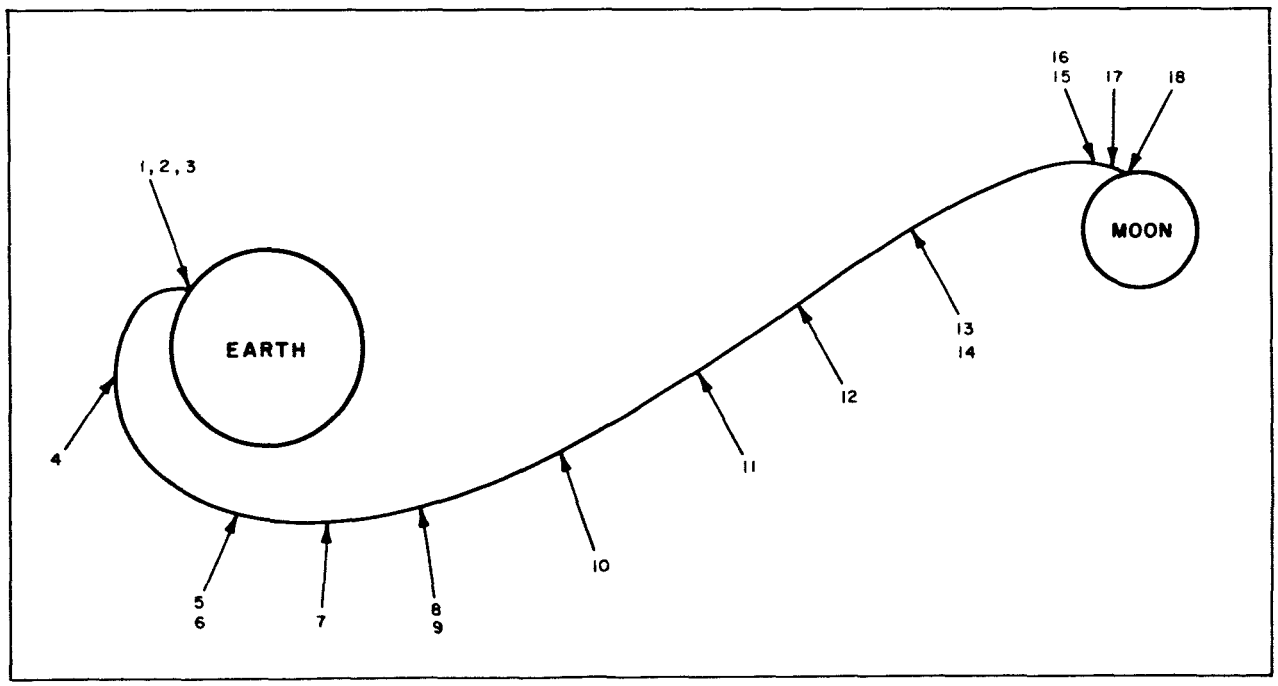

Figure 44. Sequence of Major Telemetry Events during Mission

properly after the reduced-power test. All other cruise telemetry data is checked for normal indications. Again, data received at both locations are compared to see that they agree.

3. Launch

During the critical boost phase, the telemetry data are checked to ensure normal Subsystem performance. The major items checked are:

(a) Inadvertent TV Subsystem Turn-on

(1) An increase in the data repetition rate from 1 point per second to 3 points per second indicating turn-on of terminal-mode 90-point telemetry.

(2) An increase in battery current and corresponding decrease in battery voltage.

(b) Changes in Temperature

Depending on time of launch, the spacecraft may or may not enter into the Earth's shadow. Also, because the spacecraft is not Earth-Sun oriented at this time, the external shroud temperatures change very quickly, indicating whether the TV Subsystem is experiencing a heat input or output.

4. Separation (approximately launch plus 30 minutes)

At this time the F-Channel clock is started. The clock-time telemetry point steps from zero to 0.8 volt and the F-Channel battery current increases indicating that the clock is on. At this time, the spacecraft is normally not in view of any DSIF station. Only the ETR downrange stations are tracking the spacecraft. Thus, when Johannesburg (DSIF-51) acquires the spacecraft, the telemetry data are reviewed to determine that Clock turn-on has occurred. Separation time is reported by the downrange tracking station.

5. Sun Acquisition (approximately L + 60 minutes)

The spacecraft acquires the Sun and the shroud temperature points on the cruise-mode telemetry reflect the new spacecraft orientation.

6. Earth Acquisition (approximately L + 3-1/2 hours)

At this time the spacecraft is going through a maneuver to acquire the Earth and again the external shroud temperatures reflect the changes in the spacecraft orientation.

7. Separation Plus 8 Hours

The Clock telemetry-point steps to 1.6 volts indicating the Clock-counting rate. These Clock-timing steps are used to update the predicted clock turn-on time.

8. Separation Plus 16 Hours

The Clock telemetry-point steps to 2.4 volts.

9. Midcourse Maneuver

The midcourse maneuver is performed between 16 and 17 hours after separation. The external shroud and lens temperatures are monitored to see that the changes in temperature are as expected for the changed spacecraft orientation. During the time of the midcourse motor-burn (6 to 20 minutes), the cruise-mode telemetry data is disconnected from the spacecraft Channel-8 transmitter input in order to obtain midcourse accelerometer data on Channel 8. After the midcourse maneuver is completed and the spacecraft reoriented to its normal cruise position, the external temperatures are monitored to check that they have returned to their premidcourse values. During the midcourse maneuver, the DSIF personnel are alerted to keep close watch on a spectrum analyzer, which will indicate the presence of an RF carrier, for a possible accidental TV Subsystem turn-on. The midcourse motor burn

changes the time of flight and corrects the spacecraft trajectory. Based on the telemetry indications at 8 and 16 hours after separation, the time of flight is adjusted so that F-Channel clock turn-on will be between impact minus 12 minutes and impact minus 45 minutes. (Note: the adjustment of the time of flight for the clock is a secondary consideration. The prime considerations for the maneuver are to establish the spacecraft impact point and to orient the omni-antenna field strength pattern.)

10. Separation Plus 24 Hours

The Clock telemetry point steps to 3.2 volts.

11. Separation Plus 32 Hours

The Clock telemetry point steps from 3.2 to 4.0 volts. Also, at this time two clock inhibits are released. The first inhibit prevents the clock from commanding the TV Subsystem to turn on; the second prevents the RTC-5 command from disabling the clock. These inhibit functions are not monitored on the telemetry.

12. Launch Plus 40 Hours

By this time, all the TV Subsystem temperatures are stabilized. The temperatures are compared with the predicted values and their effect on the terminal mode operation is considered.

13. Separation Plus 48 Hours

The Clock telemetry point steps from 4.0 to 4.8 volts.

14. Launch Plus 52 Hours

Starting at L+52 hours and at 4-hour intervals, the telemetry data is reviewed and the time-limiting parameters for terminal-mode operation of each channel are entered into a table from which the maximum operating time for each channel is determined. At these times, a terminal procedure matrix is also completed to determine the best terminal-mode procedure to use. The procedure matrix considers the following items:

- Will the Clock turn on the F-Channel?
- Is the P-Channel operating time greater than 15 minutes?
- Will the real-time commands be available?
- Will the CC&S commands be available?

15. Impact Minus 60 Minutes

The terminal maneuver is initiated at this time if it is required. The cruise-mode telemetry is monitored for the corresponding changes in temperatures due to the spacecraft maneuvers.

16. Separation Plus 60 Hours

The Clock telemetry point drops from 4.8 to 0.8 volts. (Note: The time of flight for a particular mission may be such that this event will not occur.)

17. Terminal Mode

A sequence of the terminal-mode parameters monitored is given in Table 8. This sequence assumes that both channels turn on at the same time; however, it is possible for F-Channel only to turn on via the backup Clock. The sequence would be much the same except on a per-channel basis.

18. Impact

All transmission ceases.

TABLE 8
TERMINAL-MODE TELEMETRY PARAMETERS

Telemetry Indications	Event or Result
1. Channel-8 telemetry data rate increases from 1 point per second to 3 points per second.	One or both channels of the TV Subsystem has turned on.
2. (a) There is meaningful data on P-Channel camera points 1 through 28 and P-Channel full-power command point 60 reads -2.4 volts.	Both channels are on in the warm-up mode.
(b) There is also meaningful data on F-Channel camera points 29 through 42 and F-Channel full-power command point 55 reads -2.4 volts.	
3. Battery current data points indicate an approximate 8- and 10-ampere load on the F and P batteries respectively, and the battery voltage for each channel drops to approximately -32 volts.	Confirms both channels on and in warm-up.
4. Video-combiner output signal is normal for both channels.	Normal video signal being applied to both transmitter inputs.
5. Full-power command telemetry points (55 and 60) for each channel drop to -0.6 volt.	Both channels have been commanded into full power by the camera sequencer.
6. The battery current increases by approximately 5 amperes on each channel.	Confirms both channels are operating in full power.
*7. F-Channel transmitter telemetry normal.	F-Channel transmitter operating normally.
*8. F-Channel camera telemetry normal.	F-Channel cameras operating normally.
*9. P-Channel transmitter telemetry normal.	P-Channel transmitter operating normally.

TABLE 8
TERMINAL-MODE TELEMETRY PARAMETERS (Continued)

Telemetry Indications	Event or Result
*10. P-Channel camera telemetry normal.	P-Channel cameras operating normally.
11. All telemetry reviewed and normal.	TV Subsystem operating normally.
12. Transmitter heat-sink temperatures for each channel are normal and increasing at the predicted rate.	Indicates proper tuning and operation of the power amplifiers for each channel.
13. Continued review of the following telemetry is normal. (a) Transmitter heat-sink temperatures (b) Battery voltages and currents (c) Transmitter IPA and PA cathode currents (d) Video-combiner output signal levels.	Confirms continued normal operations.

*Final confirmation of proper operation depends on the receipt of video data at the Goldstone Tracking Station.

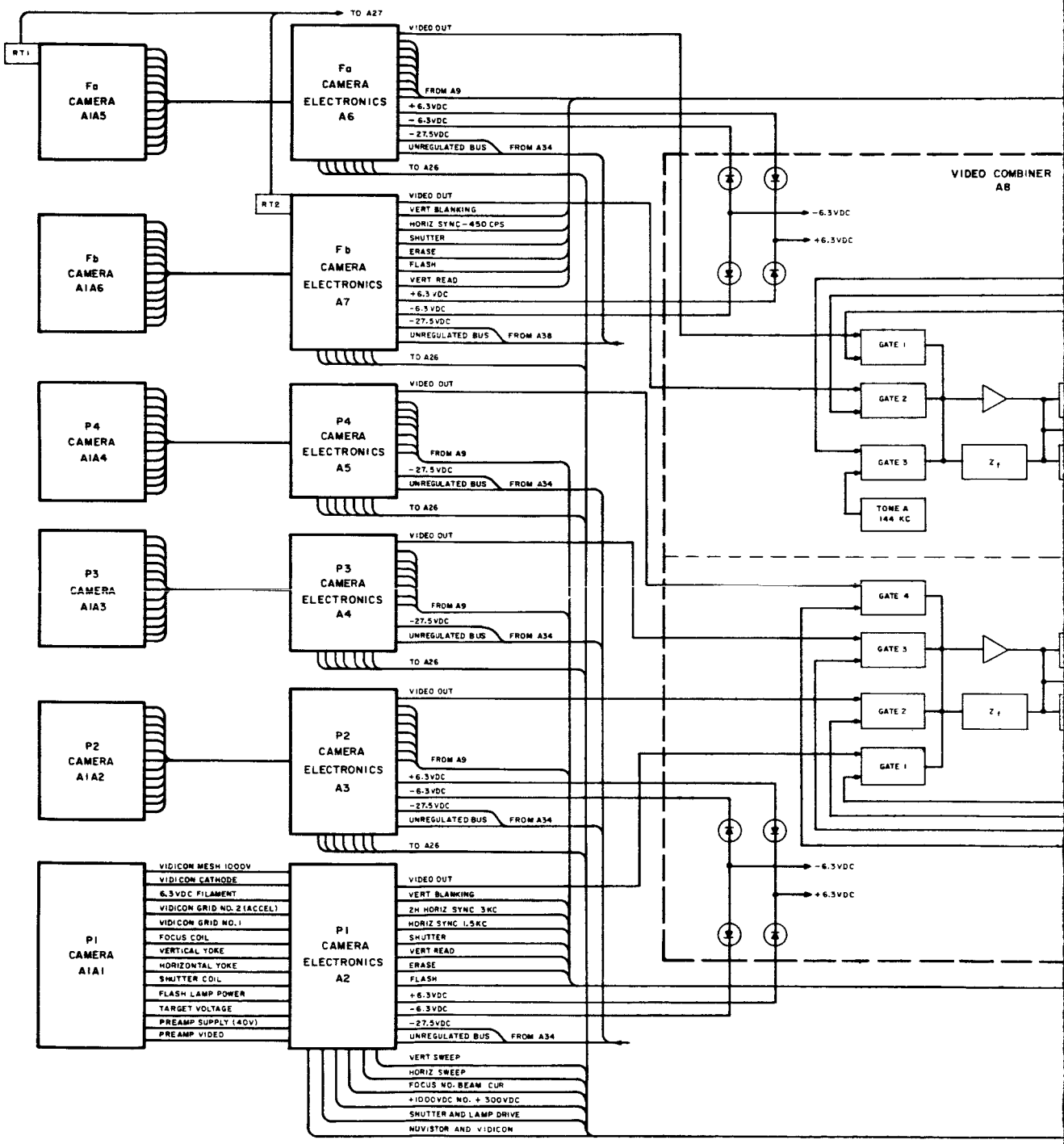
TO A27
RT1
Fa CAMERA A1A5
Fa CAMERA ELECTRONICS A6
VIDEO OUT
FROM A9
+6.3VDC
-6.3VDC
-27.5VDC
UNREGULATED BUS
FROM A34
TO A26
RT2
Fb CAMERA A1A6
Fb CAMERA ELECTRONICS A7
VIDEO OUT
VERT BLANKING
HORIZ SYNC-450 CPS
SHUTTER
ERASE
FLASH
VERT READ
+6.3 VDC
-6.3VDC
-27.5VDC
UNREGULATED BUS
FROM A38
TO A26
P4 CAMERA A1A4
P4 CAMERA ELECTRONICS A5
VIDEO OUT
FROM A9
-27.5VDC
UNREGULATED BUS
FROM A34
TO A26
P3 CAMERA A1A3
P3 CAMERA ELECTRONICS A4
VIDEO OUT
FROM A9
-27.5VDC
UNREGULATED BUS
FROM A34
TO A26
P2 CAMERA A1A2
P2 CAMERA ELECTRONICS A3
VIDEO OUT
FROM A9
+6.3VDC
-6.3VDC
-27.5VDC
UNREGULATED BUS
FROM A34
TO A26
P1 CAMERA A1A1
VIDICON MESH 1000V
VIDICON CATHODE
6.3VDC FILAMENT
VIDICON GRID NO. 2 (ACCEL)
VIDICON GRID NO. 1
FOCUS COIL
VERTICAL YOKE
HORIZONTAL YOKE
SHUTTER COIL
FLASH LAMP POWER
TARGET VOLTAGE
PREAMP SUPPLY (40V)
PREAMP VIDEO
P1 CAMERA ELECTRONICS A2
VIDEO OUT
VERT BLANKING
2H HORIZ SYNC 3KC
HORIZ SYNC 1.5KC
SHUTTER
VERT READ
ERASE
FLASH
+6.3VDC
-6.3VDC
-27.5VDC
UNREGULATED BUS
FROM A34
VERT SWEEP
HORIZ SWEEP
FOCUS NO. BEAM CUR
+1000VDC NO. + 300VDC
SHUTTER AND LAMP DRIVE
NUVISTOR AND VIDICON
VIDEO COMBINER A8
-6.3VDC
+6.3VDC
GATE 1
GATE 2
GATE 3
TONE A 144 KC
GATE 4
GATE 3
GATE 2
GATE 1
-6.3VDC
+6.3VDC

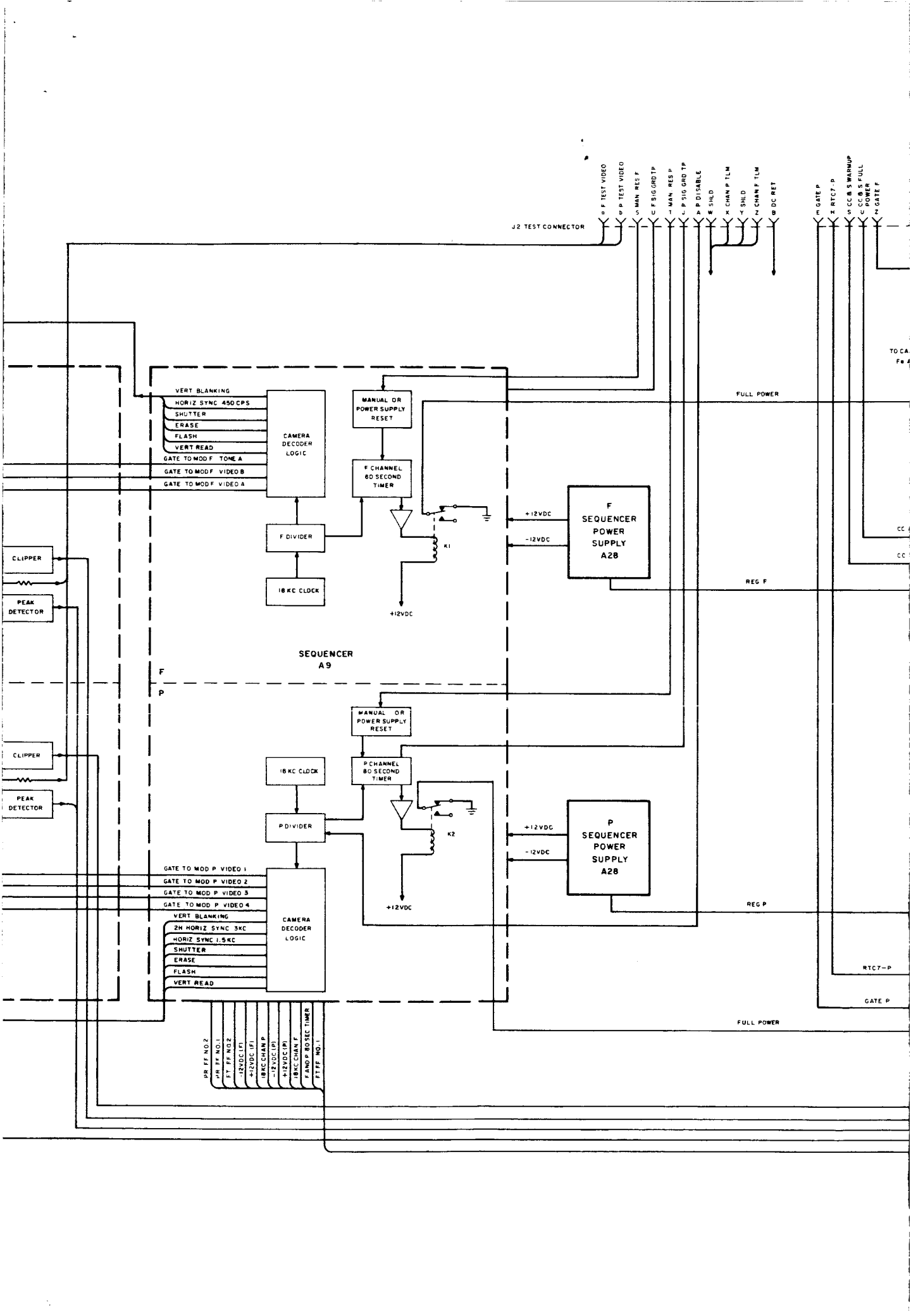
J2 TEST CONNECTOR
a F TEST VIDEO
b P TEST VIDEO
c MAN RES F
d F SIG GRD TP
e MAN RES P
f P SIG GRD TP
g P DISABLE
h SHLD
k CHAN P TLM
l SHLD
n CHAN F TLM
p DC RET
m GATE P
r RTC7-P
s CC & S WARMUP
t CC & S FULL POWER
v GATE F
FULL POWER
VERT BLANKING
HORIZ SYNC 450 CPS
SHUTTER
ERASE
FLASH
VERT READ
GATE TO MOD F TONE A
GATE TO MOD F VIDEO B
GATE TO MOD F VIDEO A
CAMERA DECODER LOGIC
MANUAL OR POWER SUPPLY RESET
F CHANNEL 60 SECOND TIMER
F DIVIDER
18 KC CLOCK
K1
+12VDC
-12VDC
F SEQUENCER POWER SUPPLY A28
REG F
CLIPPER
PEAK DETECTOR
SEQUENCER A9
F
P
MANUAL OR POWER SUPPLY RESET
P CHANNEL 60 SECOND TIMER
P DIVIDER
18 KC CLOCK
K2
+12VDC
-12VDC
P SEQUENCER POWER SUPPLY A28
REG P
GATE TO MOD P VIDEO 1
GATE TO MOD P VIDEO 2
GATE TO MOD P VIDEO 3
GATE TO MOD P VIDEO 4
VERT BLANKING
2H HORIZ SYNC 3KC
HORIZ SYNC 1.5KC
SHUTTER
ERASE
FLASH
VERT READ
CAMERA DECODER LOGIC
RTC7-P
GATE P
FULL POWER
PR FF NO 2
PR FF NO 1
FT FF NO 2
-12VDC (F)
+12VDC (F)
18KC CHAN P
-12VDC (P)
+12VDC (P)
18KC CHAN F
F AND P 60 SEC TIMER
FT FF NO 1

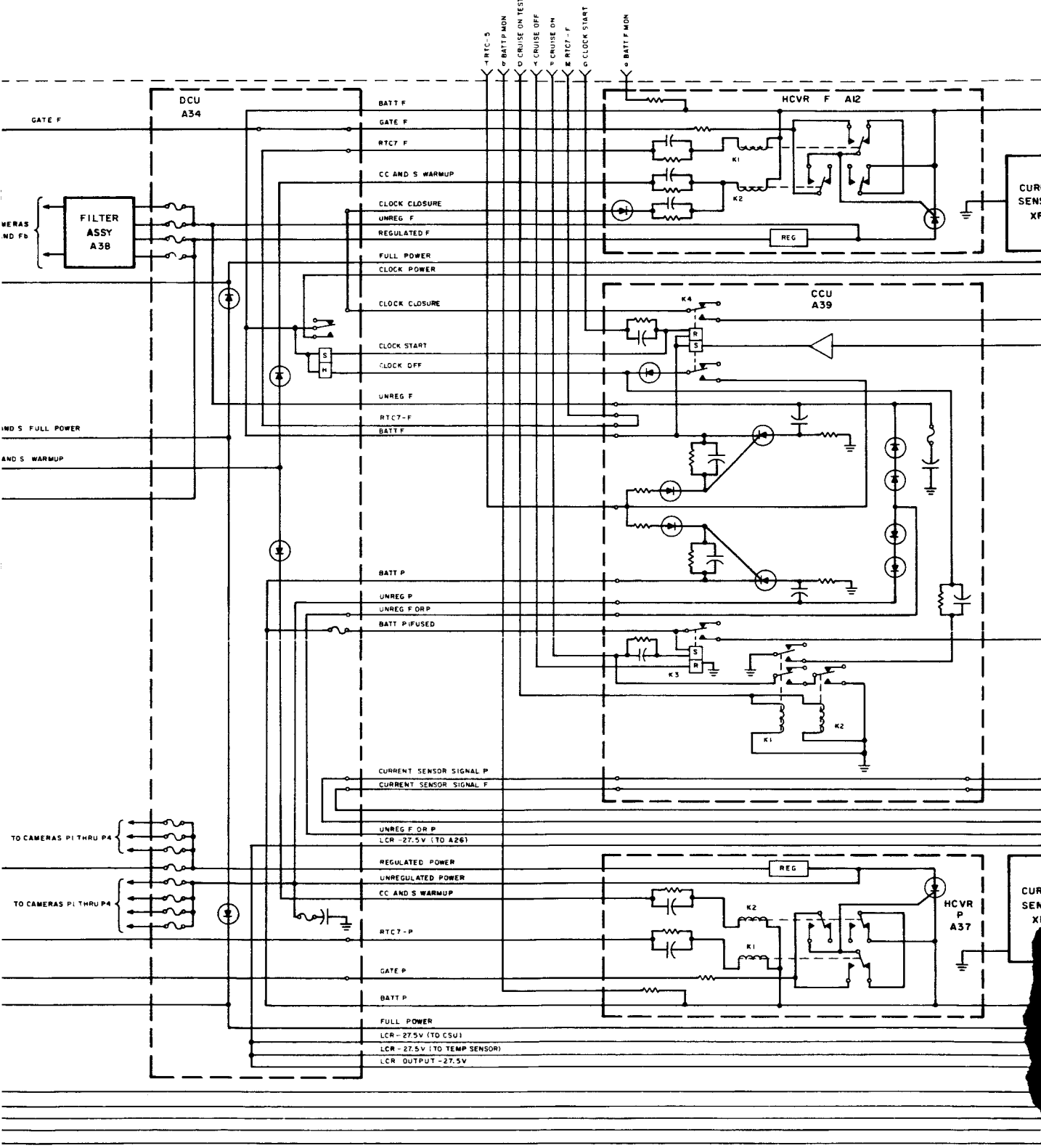
DCU
A34
GATE F
BATT F
GATE F
RTC7 F
CC AND S WARMUP
CLOCK CLOSURE
UNREG F
REGULATED F
FULL POWER
CLOCK POWER
FILTER
ASSY
A38
HCVR F A12
K1
K2
REG
CCU
A39
K4
K3
CLOCK CLOSURE
CLOCK START
CLOCK OFF
UNREG F
RTC7-F
BATT F
BATT P
UNREG P
UNREG F OR P
BATT P (FUSED
CURRENT SENSOR SIGNAL P
CURRENT SENSOR SIGNAL F
UNREG F OR P
LCR -27.5V (TO A26)
REGULATED POWER
UNREGULATED POWER
CC AND S WARMUP
RTC7-P
GATE P
BATT P
FULL POWER
LCR - 27.5V (TO CSU)
LCR - 27.5V (TO TEMP SENSOR)
LCR OUTPUT -27.5V
TO CAMERAS P1 THRU P4
TO CAMERAS P1 THRU P4
HCVR
P
A37
RTC-5
BATT F MON
CRUISE ON TEST
CRUISE OFF
CRUISE ON
RTC7-F
CLOCK START
BATT F MON

SHLD
DC RET
CHAN B TLM
DC RET
RED PWR P
RED PWR F
J1
RCA/JPL INTERFACE CONNECTOR
30J13
F BATTERY A10
30J13
TEMPERATURE SENSOR A27
TEMP TLM
TEMP TLM
+1000 VDC TLM
CATHODE CUR PA
-750V TLM
F TRANSMITTER PWR SUP A16
6.3VDC
K3
REG F
UNREG F
K4
ELECTRONIC CLOCK A35
CLOCK CLOSURE
32 HR SIG
TELEMETRY ASSEMBLY A26
15 PT COM
TLM PWR SUP
K1
K2
3KC VCO
AC AMP
LCVR A17
INPUT
OUTPUT
REG
90 PT COM
225KC VCO F
225KC VCO P
TO 30J2
TO 30J2
+1000VDC TLM
CATHODE CUR PA
-750V TLM
P TRANSMITTER PWR SUP A21
6.3VDC
K3
REG P
UNREG P
K4
FROM A34
F BATT VOLTS TLM
P BATT VOLTS TLM
CURRENT SENSING UNIT A40
VIDEO COMBINER TLM
CAMERA TLM
SEQUENCER TLM
UNREG P TLM
UNREG F TLM
REG P TLM
REG F TLM
FROM A34
30J13
P BATTERY A11
30J13

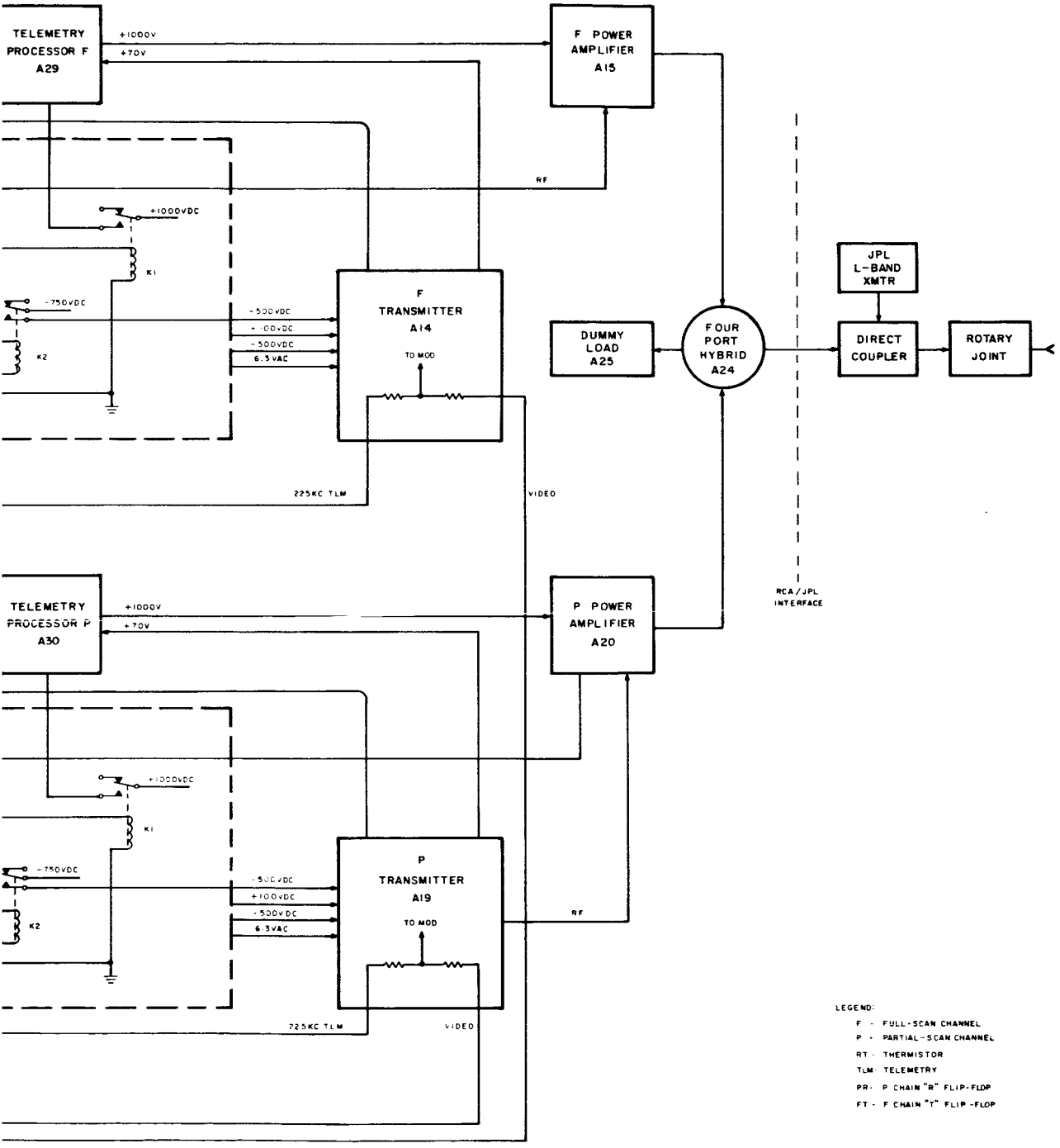

Plate 1. Functional Diagram of Final TV Subsystem Configuration